January 2019

# Diffusion Of Gold Nanoparticles Within Polymer Solutions And Gels

Kavindya Kumari Senanayake R W H
*Wayne State University*, kavindisena@gmail.com

# DIFFUSION OF GOLD NANOPARTICLES WITHIN POLYMER SOLUTIONS AND GELS

by

**KAVINDYA K. SENANAYAKE**

**DISSERTATION**

Submitted to the Graduate School

of Wayne State University,

Detroit, Michigan

in partial fulfillment of the requirements

for the degree of

**DOCTOR OF PHILOSOPHY**

2019

MAJOR: PHYSICS

Approved By:

_____

Advisor Date

_____

_____

_____

_____

## DEDICATION

This thesis is dedicated to my family and especially to my Mother (Thamara Pathiraja), Father (Sriyarathne Bandara), brother (Kasun Senanayake), and husband (Nishantha Jayawardhana) for their invaluable guidance, encouragement and support towards my academic and professional goals.

**ACKNOWLEDGMENTS**

It is my pleasure to thank the countless individuals for their motivation, encouragement and support during my academic career. First, I would like to express my sincere gratefulness towards my dissertation advisor Dr. Ashis Mukhopadhyay for all his valuable guidance and support in my research projects. I surely learned and benefited a lot from his knowledge in the field of soft condensed matter physics, which has been my primary research focus as a graduate student. His guidance during experiments, method of research, comments and feedback in preparation of writing of this thesis, and in manuscripts writing have been of critical importance. I would also like to acknowledge him for all his valuable advice related to my future career beyond Wayne State University. I sincerely appreciate him for all his encouragement and guidance. I would also like to thank Dr. Zhixian Zhou, Dr. Christopher V. Kelly and Dr. Yingxi Elaine Zhu to have graciously agreed to be part of my dissertation committee. They have taken time out of their busy schedule to ensure my thesis meets the standard for publications by providing their valuable questions, feedback and comments. Finally, I would like to thank Dr. Xiang-Qiang Chu for all her valuable advice and guidance during my first few years of graduate studies and acting as a committee member in my dissertation committee until she leaves Wayne State University.

Special thanks must go out to my family for their continuous support and encouragement throughout my all academic pursuits. I wish to thank Namita Shokeen, for her help, assistance and interaction during my research. I really appreciate her for being so supportive and considerate from the very beginning when I joined the lab.

**TABLE OF CONTENTS**

## LIST OF FIGURES

## LIST OF TABLES

# CHAPTER 1 : INTRODUCTION

## 1.1 SOFT MATTER PHYSICS

My research falls in the category of soft matter physics. Here, I will provide a brief introduction to these systems. Soft matter physics is a sub-branch of the condensed matter physics, which studies the colloidal dispersions, liquid crystals, surfactants, emulsions, polymer melts, solutions, gels, and many biological materials. Soft Matter is the study of materials, which are neither liquids and nor solids[4]. Soft materials are widely used in everyday life, such as glues, paint, ketchup, and soap. The length scale of the soft materials is in the range from atomic scale to macroscopic scale[5].

Colloidal dispersions are solid or liquid sub-micrometer particles dispersed in another liquid. An emulsion is a colloidal system, and the liquid colloids are dispersed in a liquid medium. Milk and blood are the best examples for biological emulsions.

Liquid crystals are anisotropic molecules that lead to states with degree of ordering in a phase of matter between crystalline solids and liquids. If the properties of the liquid crystals are temperature dependent the liquid crystals are said to be thermotropic. One of the most common thermotropic liquid crystal phase is “nematic”, where the molecules have no specific positional order, but has a long-range orientational order. Nematic liquid crystals show fluidity similar to isotropic fluids and simultaneously can be aligned by an external field, such as electric or magnetic fields.

Polymers are of high molar mass molecules that are composed of many small structural units connected by covalent bonds[6]. Examples for biopolymers are mucus, DNA, RNA, cellulose,

xanthan, and proteins. Polymer solutions and melts exhibit viscoelasticity, which are significantly different from simple fluids.

Surfactants can be defined as the molecules with two parts: a polar head, which is hydrophilic (water soluble) and the tail, which is hydrophobic. Surfactants are amphiphilic molecules. Therefore, they tend to form a dense film at the air-water interface. At the interface, surfactants align the molecules so that the hydrophilic head is in water and the hydrophobic tail is in the air to minimize the surface tension and the free energy. Surfactants are used in the food industry as wetting agents, in the cosmetic industry, in dishwasher liquids, laundry detergents etc.

Brownian motion is an important aspect in soft matter systems because they are small enough and the typical energies associated with the bonds in these structures are comparable to thermal energy, $k_BT$. Here, $k_B$ is the Boltzmann's constant and T is the absolute temperature. The constituents in a soft matter system can be visualized as in a constant state of random motion. As an example, polymer chains in a solution, always twisting and turning under the influence of Brownian motion. Different categories of soft materials are represented in figure 1.1.1.

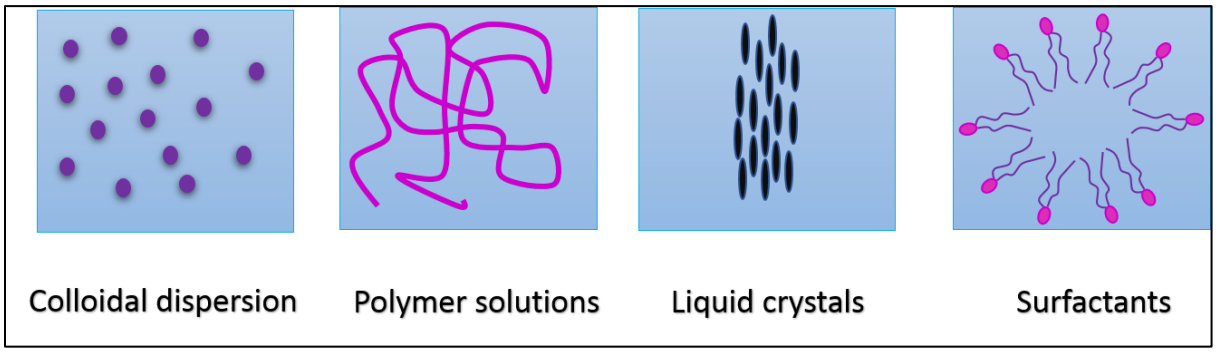


**Figure 1.1.1** Soft materials (Colloidals, polymer solutions, liquid crystals, and surfactants)

My dissertation research work is mainly focused on soft materials, such as polymers and polyelectrolytes, which are discussed in detail below.

## 1.2 POLYMERS

The word “polymer” means “many parts,” and refers to molecules consisting of a repeating structural pattern called “monomers ". The entire polymer structure is generated during the polymerization process, whereby the monomers are covalently linked together. The molar mass (M) of a polymer can be defined as the product of the degree of polymerization (N) and molar mass ($M_{mon}$).

$$M = N M_{mon} \qquad 1.2.1$$

The chemical identity of monomers determines the properties of polymeric systems. Another important factor is the organization of the chain, which is fixed during the polymerization process. Polymer microstructure cannot be changed without breaking covalent bonds. A variety of isomers can be generated by polymerizing the double bond. There are three different categories of isomers: sequence, structural, and stereoisomers. The chains head to head and chains head to tail are two main categories of sequence polymers (Figure 1.2.1). Polymers that contain a double bond in their backbone may exhibit structural isomerism. There are three different structural isomers called cis, trans, and vinyl according to the orientation of atoms (Figure 1.2.2). In stereoisomerism, the carbon atoms connect each other by single bonds and have a tetragonal structure.

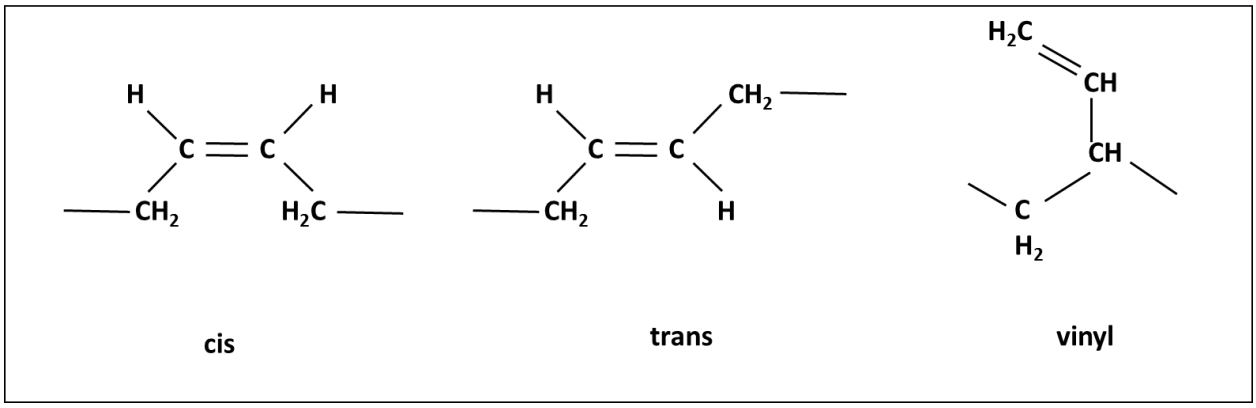


**Figure 1.2.1** Two sequence isomers of polypropylene

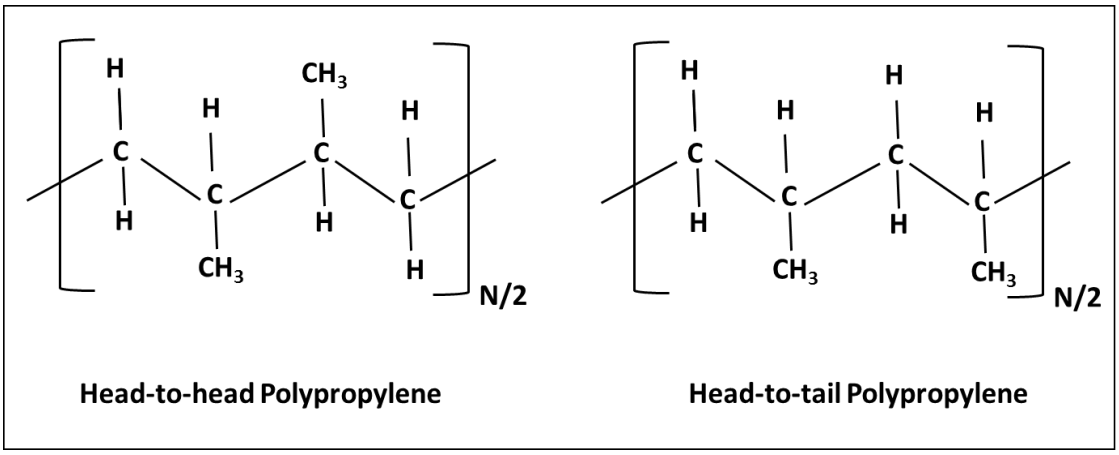


**Figure 1.2.2** Three isomeric structures of polybutadiene (cis, trans, and vinyl)

### 1.2.1 PROPERTIES OF POLYMERS

If a molecule consists of only a small number of monomers it is called an oligomer. Linear polymers contain from 10 up to 20 x $10^9$ monomers. The physical properties of molecules change as monomers are linked together. Boiling point and the melting point of polymeric systems increase rapidly with the number of backbones in the chain. Polymer architecture plays an important role in controlling the properties of polymeric systems. There are several different

types of polymer architectures: linear, ring, star-branched, H-branched, comb, ladder, dendrimer, or randomly branched (Figure 1.2.1.1).

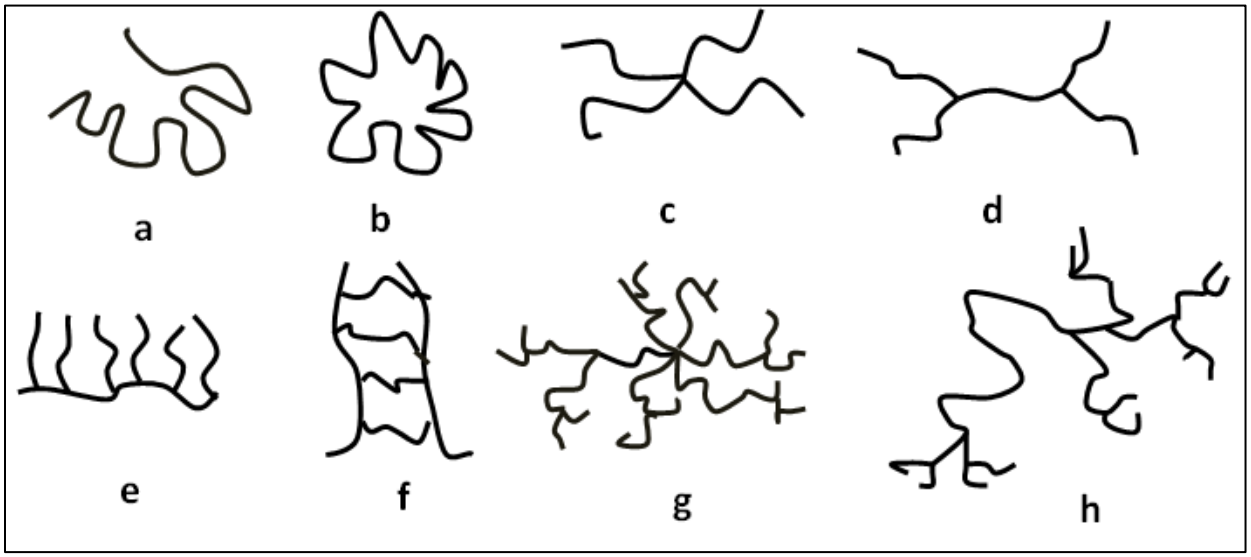


**Figure 1.2.1.1** Examples of polymer architectures: (a) linear; (b) ring; (c) star; (d) H; (e) comb; (f) ladder (g) dendrimers; (h) randomly branched.

### 1.2.2 HOMOPOLYMERS AND HETEROPOLYMERS

Polymers that contain only one type of monomers are called homopolymers. Even though it is made from one polymer, they can differ by their microstructure, the degree of polymerization, or architecture. The combination of several different types of monomer in a single chain leads to a new macromolecule called heteropolymers, with properties that are unique and depend on the composition of the sequence.

### 1.2.3 POLYMER LIQUIDS

There are two types of polymer liquids, called polymer melts and polymer solvents. In order to make a polymer solution, polymers should dissolve in a solvent. Polymer melts can be

obtained by heating the polymer above the glass transition temperature ($T_g$) and the melting point. Polymer solutions can be classified as dilute and semidilute according to the polymer concentration, c, which is the ratio of the total mass of polymer to the total volume of the solution. The volume fraction $\phi$, which is defined in terms of concentration, is the ratio of the volume of the polymer in the solution and the volume of the solution.

$$c = \frac{\text{Mass of the polymer}}{\text{Volume of the solution}} \qquad 1.5.1$$

$$\phi = \frac{Volume\ of\ the\ polymer}{Volume\ of\ the\ solution} \qquad 1.5.2$$

Overlap volume fraction ($\phi^*$) can be used to define transition from dilute to semidilute solutions. The overlap volume fraction is the concentration when macromolecules densely fill and chains are just overlapped.[7]

$$\phi^* = \frac{3M_w}{4\pi N_A R_g^3} \qquad 1.5.3$$

Here, $M_W$ is the molecular weight, $N_A$ is the Avogadro's number, and $R_g$ is the radius of gyration, which is the square root of the average square distance between the monomers in a given conformation and the polymer chain's center of mass.

Solutions are called dilute, at polymer volume fractions below the overlap volume fraction ($\phi<\phi^*$). Polymer coils in dilute solution are far from each other and do not interact. If the volume fraction of the polymer solution is above the overlap volume fraction ($\phi>\phi^*$), the solution is called semidilute (Figure 1.2.3.1).

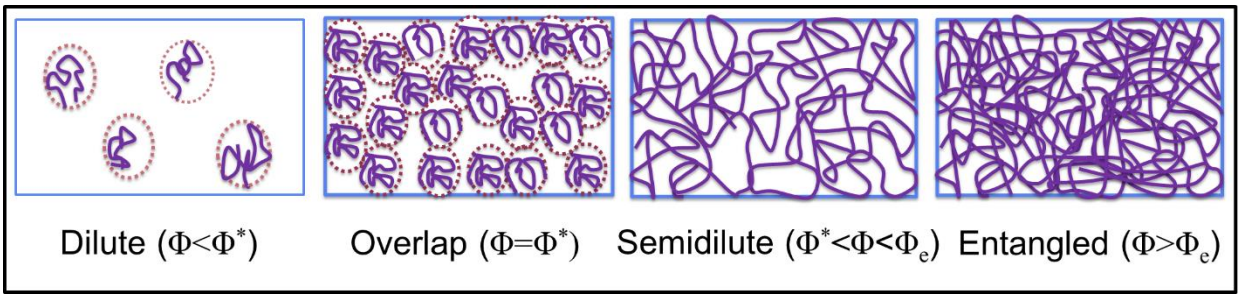


**Figure 1.2.3.1** Schematic diagrams of dilute, overlap, and semidilute polymer solutions

Polymers are examples of viscoelastic materials, which exhibit time-dependent mechanical properties, a combination of viscous flow at long times ($t>\tau_{rel}$), and elastic response at short times.[8] $\tau_{rel}$ is the characteristic relaxation time of the system, which marks the ending of solid-like behavior and beginning of liquid-like behavior. If $t>\tau_{rel}$ the behavior is liquid-like, on the other hand, if $t< \tau_{rel}$ the behavior will be solid-like.

**1.3 POLYELECTROLYTES**

Polyelectrolytes are ionizable polymers, which can get ionized in the polar solvents like water. Polyelectrolytes dissociate in water and get ionized by leaving the charges on polymer backbone and releasing counterions to the solution (Figure 1.3.1).

Most of the biopolymers, such as DNA (Figure 1.6.2), RNA, F-actin, and microtubules are polyelectrolytes. Other examples of polyelectrolytes include, polymethacrylic and polyacrylic acid, polystyrene sulfonate, other polyacids and polybases. Properties of polyelectrolytes in polar solvents vary with solvent quality for polymer backbone, the fraction of dissociated ionic groups, polymer–solvent interactions, and salt concentration. In polyelectrolyte solutions, charges on the

polymer backbone play a vital role, and the electrostatic interaction between charges leads to qualitatively different behavior in contrast to uncharged polymer solutions[9].

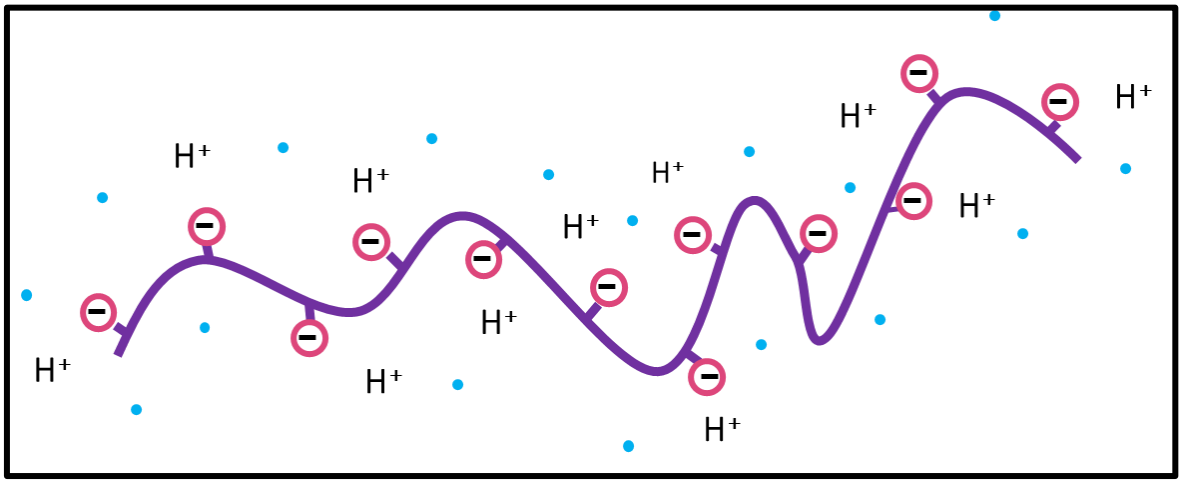


**Figure 1.3.1** Ionized polyelectrolyte in polar solvent

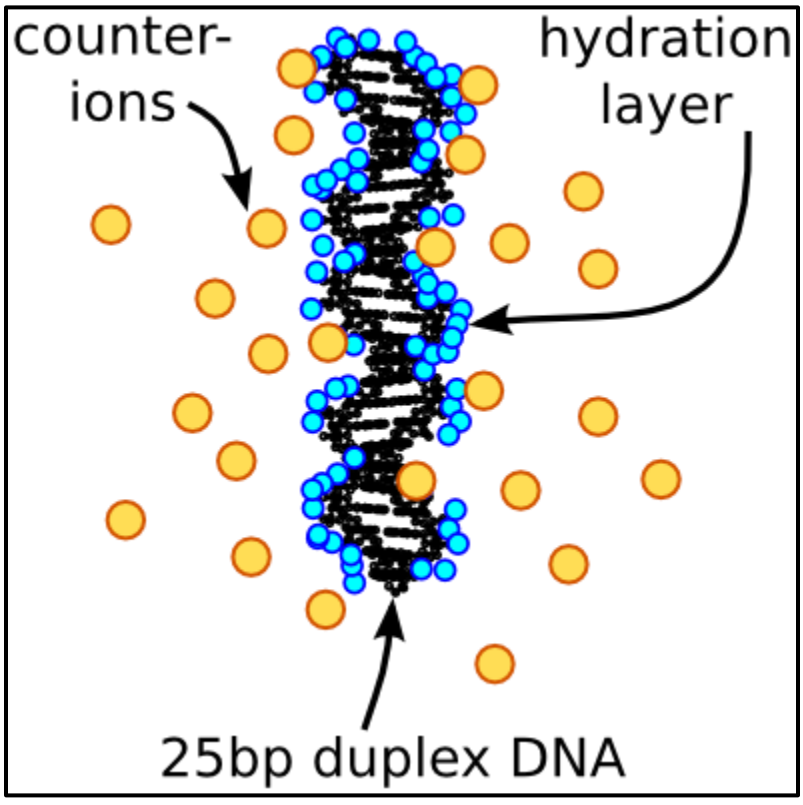


**Figure 1.3.2** Example of polyelectrolyte: DNA is a charged biopolymer which releases positive ions to the medium and negative ions distribute in the polymer backbone Adopted[10]

Unique properties of polyelectrolytes described below,

- Transition from dilute to semidilute regime occurs at much lower concentration compared to neutral polymers with the same molecular weight.
- A prominent peak can be observed in the scattering function of the homogeneous polyelectrolyte solutions, which increases with the polymer concentration with an exponent of ½. This is not observed in neutral polymer solutions.
- The osmotic pressure of salt-free polyelectrolytes is several orders of magnitudes higher in comparison to neutral polymers with the same concentration. Further, the osmotic pressure increases linearly with concentration and remain constant with chain molecular weight for a wide range of polymer concentration. This concludes that the osmotic pressure is mainly due to the counter ions contribution in the solution.
- According to the Fusoss's law, the viscosity of the polyelectrolyte solutions scales as $\eta \sim c^{1/2}$ while it is proportional to polymer concentration for uncharged polymers. Additionally, there is a concentration regime (Fuoss regime), which reduce the reduced viscosity as a function of concentration $\left(\frac{\eta}{c} \sim c^{-1/2}\right)$ in polyelectrolyte solutions. In neutral polymers, no such a regime exists.
- Polyelectrolyte solutions follow unentangle dynamics for a wide range of concentration in comparison to uncharged polymers. In other words, the crossover from semidilute to entanglement occurs further away from the overlap concentration.

**Dilute Solutions of Polyelectrolytes**

In dilute polyelectrolyte solutions, the interactions can be explained as counterions surrounding charged polymer chains in a large unit cell with the size equal to the distance between the chains.[9]

The potential energy of the polyelectrolyte chain U(r)[11] with monomers located at positions $r_1$, $r_2$, $r_3$,……,$r_N$ and corresponding charges of $e$q$_1$, eq$_2$,……,eq$_N$ is,

$$U(\{r\}) = k_B T \left( \frac{3}{2b^2} \sum_{i=1}^{N-1} (r_{i+1} - r_i)^2 + \sum_{i=1}^{N} \sum_{j<i} \frac{l_B q_i q_j}{|r_i - r_j|} \exp\left(-K|r_i - r_j|\right) + \frac{U_{sh}(|r_i - r_j|)}{k_B T} \right) \qquad 1.6.1$$

The first term in the interaction equation explains the entropic elasticity of harmonic bonds, where, b is the length connecting monomers into the polymer chain. The second term in the equation describes the screened Coulomb interaction between charged monomers. Here, $l_B$ is the Bjerrum length that explains the length at which the electrostatic interaction between two charges (e) in the medium with dielectric constant ($\varepsilon$) is equal to the thermal energy $k_B T$ in terms of Boltzmann constant $k_B$ and $T$ in absolute temperature,

$$l_B = \frac{e^2}{\varepsilon k_B T} \qquad 1.6.2$$

The third term describes the short-range interaction between the monomers ($U_{sh}(r)$), which can be typically explained by the Lenard-Johns potential ($U_{LJ}(r)$).

$$U_{LJ}(r) = 4\varepsilon_{LJ} \left( \left(\frac{\sigma}{r}\right)^{12} - \left(\frac{\sigma}{r}\right)^{6} \right) \qquad 1.6.3$$

Here, $\varepsilon_{LJ}$ is the interaction parameter and $\sigma$ is the monomer diameter.

In the chain potential energy equation, the interactions between counterions and salt ions or any other ions are not included, and this effect can be taken into account as a Debye screening length ($r_D = K^{-1}$) as a function of concentration ($c_s$) and the valance $q_s$of ions.

$$K^2 = 4\pi l_B \sum_{l_B} c_s q_s^2 \qquad 1.6.4$$

The electrostatic interaction between ions are exponentially screened on the length scales larger than the Debye screening length. In a dilute solution, the concentration of counterions is very low, so the Debye screening length is larger than the chain size. As a result, ionized groups on a chain interact with each through the unscreened Coulomb potential.

Flory theory describes the free energy of the chain neglecting the interaction between monomers. The theory assumes unidirectional elongation of the chains along the z-axis due to the electrostatic interaction between the chains but unperturbed in x and y-axis. This leads to the ellipsoidal shaped polyelectrolyte chain (Figure 1.3.3) of dimensions of $R_e$ in the longitudinal axis (z-axis) and ideal chain size ($bN^{1/2}$) in the transverse axis (x and y-axis). Two terms contribute to the free energy of the chains, which are the entropy part and the electrostatic part. Entropy decreases with increasing end-to-end distance and hence the free energy increases. On the other hand, the electrostatic term increases with an increase in chain size. Therefore, the optimal chain size $R_e$ corresponds to minimal free energy.

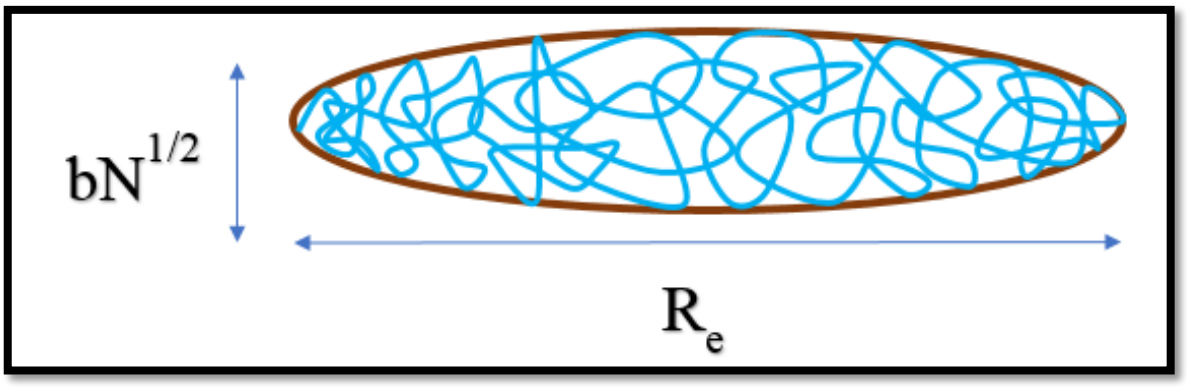


**Figure 1.3.3** Ellipsoidal polyelectrolyte chain

**Scaling Model**

In dilute solutions, the scaling model of polyelectrolyte chain conformation is associated with the assumption of separation of different length scales and the concept of an electrostatic blob, which can be described as the conformation of the chain inside the electrostatic blob are unperturbed due to the electrostatic interactions. All charged monomers inside electrostatic blob have the energy of electrostatic interaction in the order of $k_B T$.

In the length scale larger than the blob size, the electrostatic interaction between blobs leads to the elongation of the polyelectrolyte chain, which arranges into an array of blobs. The size of the chain can be estimated as the product of blob size and the number of blobs per chain[11].

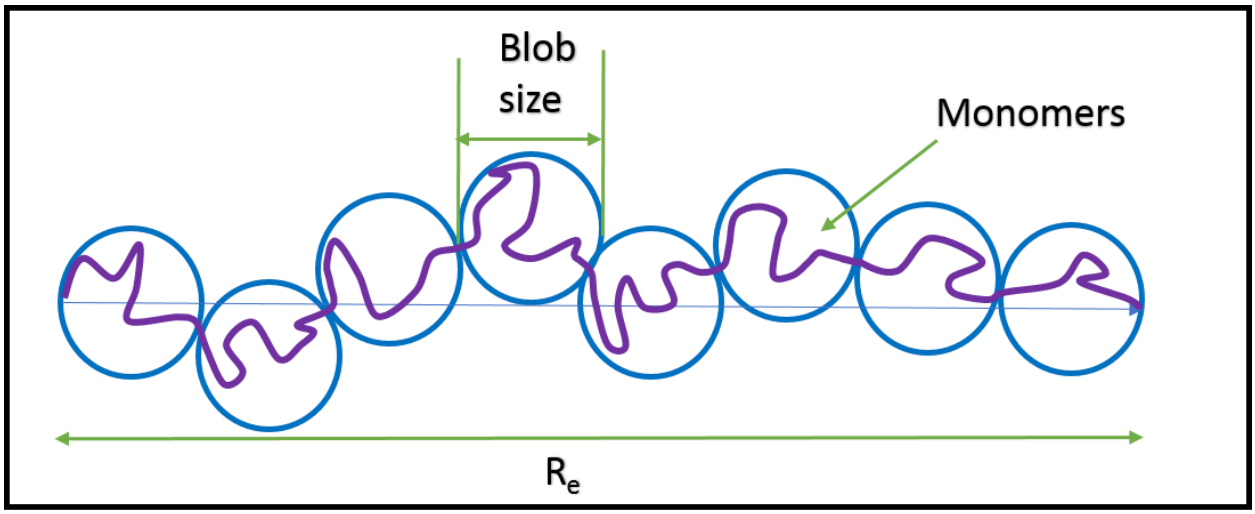


**Figure 1.3.4** Figure of non-uniformly stretched polyelectrolyte chain in a dilute salt-free solution.

My research work is focused on studying polymer solution, weak polyelectrolyte solutions and colloidal particle mixture using gold nanoparticles. In simple liquids, the translational diffusion coefficient, D of isolated spherical particles is given by the Stock-Einstein (SE) relation.

$$D_{SE} = \frac{k_B T}{6\pi\eta R_H} \qquad 1.6.5$$

where $k_B$ is the well-known Boltzmann constant, T is absolute temperature of the ambient, η is the viscosity of the surrounding fluid, and $R_H$ is the hydrodynamic radius of the diffused particle.

In contrast to simple liquids, in case of polymer and polyelectrolyte solutions, where there are probe particles, polymer polyelectrolyte and solvent molecules, various length scales are involved, and the applicability of this relation becomes complicated. This discussion will be revisited in the following chapters.

**1.4 SIGNIFICANCE OF MY RESEARCH**

An understanding of transport properties of nanoparticles through a complex, crowded macromolecular environment will have applications in fields ranging from biophysics and polymer science to drug delivery. The study of the dynamical behavior of metallic nanoparticles of different sizes in polymer, biopolymer liquids, and gels provide information about their mechanical and viscoelastic properties.

Gold nanoparticles exploit their unique physical and chemical properties such as non-toxicities and ease of synthesis for carriers for drug and gene delivery applications[12]. Gold nanoparticles are excellent candidates for biological sensing because the surface plasma absorption band of gold nanoparticles changes significantly with the complex refractive index of the medium and the dielectric properties of the environment[13], which makes them suitable for accurate biological sensing. In addition, surface plasmon-resonance of gold nanoparticles at near-infrared (NIR) absorption results in heating surrounding the cells. Therefore, utilization of this heat is useful in destroying cancer cells as they are more sensitive to heat compared to healthy cells. This cancer therapeutically method is called localized hyperthermia [14, 15].

Biocompatible polymer solutions can be considered as a good model for such a crowded system and provide important information about the mobility of nanoparticles in complex macromolecular fluids, gels, and biological systems. Additionally, from the polymer physics perspective, the studies can give useful information about the structure of the matrix and verify or refine theories of polymer dynamics[16].

This dissertation is organized as follows. Chapter 2 will provide background information relevant to the research work in the thesis with some previous work by the experts in the field. Chapter 3 outlines the experimental techniques used in the research projects. Specifically, fluorescence correlation spectroscopy (FCS), which was used to measure diffusion coefficient of gold nanoparticles is described. Chapter 4-6 include the experimental results of my research. In particular, the chapter 4, "Diffusion of Nanoparticles in Polymer Solutions and Gels", chapter 5 covers the "Nanoparticle Diffusion within Dilute and Semidilute Xanthan solutions, and chapter 6 focuses on the "Diffusion of Gold Nanoparticles in Semidilute Polyelectrolyte Solution".

# CHAPTER 2 : BACKGROUND

## 2.1 INTRODUCTION

The diffusion of colloids and particles in polymer solutions and gels were studied by different techniques, such as fluorescence, dynamic light scattering, gravimetry, radioactive labeling, and membrane permeation.[17] The theoretical models, such as obstruction model, hydrodynamic model, and free volume theory are important understanding the diffusion in polymer solutions and gels. Probe diffusion in polymer is mainly due to the random motion of the molecules, which changes due to the viscosity, probe size, temperature, and microstructure of the medium. The following sections 2.1.1, 2.1.2, 2.1.3, 2.14 of this chapter will cover the results and discussion of former theoretical, experimental and computational studies, which are most relevant to this research and will provide the necessary background for the projects studied in this thesis.

### 2.1.1 THEORIES AND PHYSICAL MODELS OF DIFFUSION

#### 2.1.1.1 Hydrodynamic and obstruction model

Theoretical modeling of diffusion of probe particles in the polymer solution can be classified into two major groups,[18] namely hydrodynamic model[19-24] and obstruction model[25-29]. The hydrodynamic theories are based on the hydrodynamic interactions between the diffusant and the polymer. In the dilute regime, the particles are treated as “hard spheres” if the particle size is smaller than the polymer chain size. Here the particle radius is same as the hydrodynamic radii.[20] In the semidilute regime, the polymer chains are approximated as stationary friction centers consist of monomer beads. Hydrodynamic interaction between the diffused particles and the monomer beads is considered to be screened beyond the length scale of correlation length,

distance from a monomer in one chain to a monomer in another nearest chain,[30] (ξ). Further. the diffusion coefficient follows a stretched exponential function of particle size and the polymer volume fraction.

Obstruction theory relies on the assumption that the polymer chains are motionless relative to the probes, which was first introduced by Fricke in 1924.[31] Additionally, the self-diffusion coefficient of polymer chains is much smaller than that of the probes. The motionless polymer chains in the solution make the increase of the path length of the diffusive probes from one point to the other. Further, in the obstruction model, polymer chains are visualized as a porous network with pore-size determined by the distance between an arbitrary point on the polymer chain and the point on the nearest polymer chain. If the particles are larger than the pore size, the diffusion coefficient can be written as a function of friction of those pores.

**2.1.1.2 SCALING THEORY**

The scaling theory for the dynamics of probe particles in polymer solutions was developed by B-Wyart and de Gennes.[32] The theory was established assuming that the polymer solution as a transient statistical network with the size of correlation length (ξ). According to the theory, the small probe particles ($R< \xi$) feel the solvent viscosity and easily slip through the polymer network. Larger particles, $R>> \xi$, feel the bulk viscosity, and intermediate particles ($R\sim \xi$) feel an effective viscosity, which is in between the solvent viscosity and the bulk viscosity of the medium. This dependence can be explained as a function of the ratio of the particle size to the correlation length. There were many research were done in this field to find the particle size and concentration-dependent viscosity of the polymer solutions.[19, 32-34]

Phillies *et. al.* developed a model to interpret the self-diffusion of macromolecules over a wide range of concentration based on the assumptions of the hydrodynamic model. Their studies suggested a stretched exponential dependence diffusion coefficient of the probes in a polymer solution.[33]

$$D = D_0 \exp(-\beta \Phi^{\nu}) \qquad 2.1.1.2.1$$

Here, D is the diffusion coefficient of particles in the polymer solution, $D_0$ is the diffusion coefficient of particles in the neat solvent, β and ν are adjustable parameters, which depend on the molecular weight of the polymer and probe size. Experiments[35-37] have found that the parameter β and υ changes according to the scaling law of $\beta \sim M^{0.9}$, and $\nu \sim M^{-1/4}$ within the experimental errors for a wide range of molecular weights. Therefore, the generalized Phillies equation can be written as,

In the Phillies model, the hydrodynamic interactions are dominated by the chain-chain interactions; however, the theory did not consider the "reptation" motion of the chains in the entangled regime.

Cukier[19] introduced a model based on hydrodynamic interactions to describe the Brownian motion of spherical particles in semidilute polymer solutions. Cukier considered the semidilute solutions and approximated the solution as a homogeneous solution. Moreover, in the semidilute regime, the polymer chains are motionless compared to the diffusant probes. Diffusant undergo screening due to the overlapped chains, and diffusion coefficient can be explained as,

$$D = D_0 \exp(-\kappa R_h) \qquad 2.1.2$$

Here, κ represent the screening effect due to the hydrodynamic interaction in semidilute solutions, which relates to the resistance between the polymer network, solvent, and diffused

probes. $R_h$ is the hydrodynamic radius of the diffusants. For dilute polymer solutions, the diffusion coefficient can be simplified as,

$$D = D_0(1 - \kappa R_h) \quad 2.1.3$$

The screening parameter $\kappa$ is for a rod-like polymer,

$$\kappa^2 = \frac{\zeta n}{\eta} \quad 2.1.4$$

Here, n is the number density of the rod-like polymer molecules and η is the solvent viscosity. ζ is the frictional coefficient of one rod, which depend on the length (L) and the diameter (b) of the rod.

$$\zeta = \frac{6\pi\eta\left(\frac{L}{2}\right)}{\ln\left(\frac{L}{b}\right)} \quad 2.1.5$$

For coil like polymer,

$$\kappa^2 = \frac{\zeta n^*}{\eta} = 6\pi n^* a \quad 2.1.6$$

Here, $n^*$ is the monomer number density and a is the monomer radius.

In the semidilute regime for small particles, the screening constant follows the scaling relationship with concentration according to, $\kappa \sim c^{\upsilon}$ with υ=0.5 and independent of the polymer geometry. Mel'nichenko *et al.* experimentally studied the diffusion of water in concentrated hydrogel solutions as well as the diffusion of polyacrylamide in silica gels, which were in agreement with the Cukier theory.[38, 39] The limitation of this theory is that this was derived for large diffusant such as polymers and proteins.

All the above theories ignored polymer dynamics. A recent theoretical study by Cai *et al.* suggested a diffusion model by considering the coupling of polymer dynamics with the probe dynamics. They have extended the scaling theory developed by B-Wyart and de Gennes.[32] The

study was developed for 3 regimes of particle sizes, which were the small size (2R<ξ), intermediate size (ξ<2R<a) and Large size (2R> a), where a is the tube diameter, in entangled regime. The correlation length (ξ), distance from a monomer in one chain to a monomer in another nearest chain, can be written in a power law equation,

$$\xi(\Phi) \approx b\Phi^{-\frac{\upsilon}{(3\upsilon-1)}} \qquad 2.17$$

Here, b is the length of the Kuhn monomer segment, υ is the Flory exponent, which depend on the solvent quality. Another important length scale is the entanglement length (tube diameter a), which is a length scale use to determine the dynamics of polymer chains in the entanglement regime[7] and it is typically five times higher than the correlation length.

$$a(\Phi) = a(1)\Phi^{-\frac{\upsilon}{(3\upsilon-1)}} \qquad 2.1.8$$

Here a(1) is the tube diameter in the melt.

(a) Region (i): Small size (2R<ξ) particles: Mobility of particles is not affected by the polymer chains, and the diffusion coefficient is quite similar to that in solvent. Further, the diffusion coefficient of particles is determined by the viscosity of the solvent ($\eta_s$), which is given in the equation below,

$$D_s \approx \frac{k_B T}{2R\eta_s} \qquad 2.1.9$$

$$\text{i.e. } D_s \propto R^{-1} \qquad 2.1.10$$

(b) Region (ii): Intermediate size (ξ<2R<a) particles: Diffusion of particles in this regime is not affected by the entanglement of chains but gets coupled with the polymer dynamics. At shorter time scale in this particle size regime, the motion of the particles is diffusive and feel local viscosity. This diffusive motion last until a time scale $\tau_\xi$

$$\tau_\xi = \tau_0 \left(\frac{\xi}{b}\right)^3 \quad 2.1.11$$

$$\tau_0 = \frac{\eta_s b^3}{k_B T} \quad 2.1.12$$

Here, $\tau_0$ is the relaxation time of the monomers and $\tau_\xi$ is the relaxation time of a correlation blob of size $\xi$. At time scales longer than relaxation time $\tau_\xi$, particles experience sub-diffusive motion as a result of the coupling the with the fluctuation modes of the polymer solutions, and particles feel an effective viscosity ($\eta_{eff}$),

$$\eta_{eff}(t) = \eta_s \left(\frac{t}{\tau_\xi}\right)^{1/2} \quad 2.1.13$$

Therefore, the effective diffusion coefficient,

$$D_{eff}(t) \approx \frac{k_B T}{2R\eta_{eff}(t)} \approx D_s \left(\frac{t}{\tau_\xi}\right)^{-1/2} \quad 2.1.14$$

The sub-diffusive motion continues until the time scale, $\tau_D$, at which the chain size control the viscosity comparable with the particle size.

$$\tau_D = \tau_\xi \left(\frac{2R}{\xi}\right)^4 \quad 2.1.15$$

At this time scale, particle diffuse with the terminal diffusion coefficient,

$$D_t = \frac{k_B T}{2R\eta_{eff}(\tau_D)} = \frac{k_B T \xi^2}{\eta_s (2R)^3} \quad 2.1.16$$

The effective viscosity felt by the particle is proportional to the number of correlation blobs in the polymer chain size comparable to the particle diameter.

(c) Region (ii): Large size (2R>a) particles: At this regime, since particle size is larger than the polymer mesh size, particles are trapped inside the polymer network by the entanglements. At the shorter time scale compared to the entanglement relaxation

time ($\tau_e$), the arrest of the particles motion happens. The entanglement time scale is given as

$$\tau_e = \tau_\xi \left(\frac{a}{\xi}\right)^4 \approx \tau_0 \left(\frac{\xi}{b}\right)^3 \left(\frac{a}{\xi}\right)^4 \qquad 2.1.17$$

At the time scale larger that $\tau_e$ the particle dynamics can be explained using two mechanisms. First, the topological constraints result by the reputation of surrounding polymer chains result at the reputation time ($\tau_{rep}$),

$$\tau_{rep} = \tau_e \left(\frac{N}{N_e}\right)^4 \qquad 2.1.18$$

Here, $N_e$ is the number of monomers per entanglement strand.

The second mechanism is due to the fluctuations of local entanglement mesh, which leads particles to pass through the entanglement gates. This result in a hoping motion[1] of particles from one entanglement cage to the other. The hopping motion of the particles will be discussed in another section.

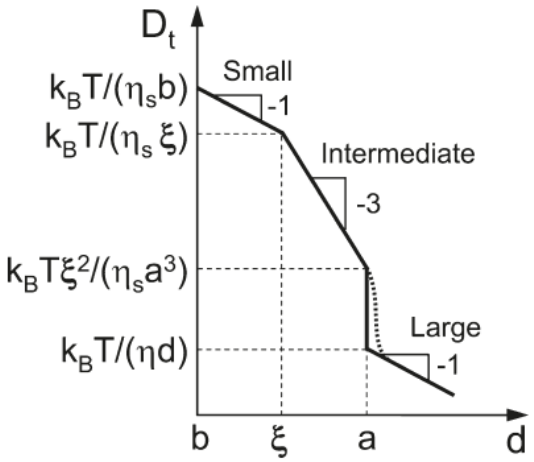


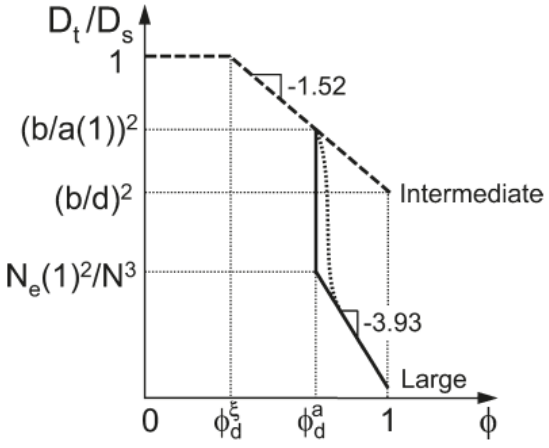

**Figure 2.1.1.1 (a)** Terminal particle diffusion coefficient $D_t$ as a function of particles size (2R=d) in entangled polymer solutions. (b) Normalized terminal diffusion coefficient with the diffusion coefficient at pure solvent as a function of polymer volume fraction in entangled athermal polymer solutions.[18] (Reprinted with permission from Macromolecules 44 (19), 7853-7863. Copyright (2011) American Chemical Society.)

### 2.1.2 PREVIOUS COMPUTATIONAL WORK

Lui *et al.* performed molecular dynamics simulation to study the nanoparticle dynamics in polymer melts.[40] They have studied the effect of polymer concentration, size, the chain length, mass of the particles, and polymer- particle interaction on the particle diffusion coefficient. Their results showed that when the particle size is greater than the radius of gyration, ($2R>R_g$) the diffusion coefficient matches very well with the SE (Stokes-Einstein) value. On the other hand, when the particle size smaller than the radius of gyration ($2R<R_g$), the diffusion coefficient deviated from the SE value, and it is related to the nanoviscosity rather than the bulk viscosity The diffusion coefficient was found to be independent with the mass of the particles and followed a power law relationship with the particle size, $D\sim R^3$.

Ganesan *et al.* had proposed a continuum model for nanoparticle dynamics in polymer metrices.[41] The results suggested that the length scale (L) that controls the transition from colloid to solvent is determined by the radius of gyration ($R_g$) for unentangled. The diffusion coefficient changes with the polymer size ($R_g$) to particle size (R) ratio ($R_g/R$), and strongly depends on the particle size. This study showed that particles feel the macroviscosity in the limit of R>L.

### 2.1.3 PREVIOUS WORK ON HOPPING DIFFUSION

Cai *et. al.* proposed a model for hopping diffusion of large non-sticky nanoparticles subjected to topological constraints in entangled and unentangled polymer networks and gels.[1]

Particles larger than the mesh size, $a_x$, ($2R>a_x$) are confined inside an unentangled network, and the large fluctuation of network strand leads to hopping. The fluctuation of the network cage should be large enough to allow one of the network strands to slip around the particle to occur hopping (Figure 2.1.3.1). In order for a particle to hop from one cage to the neighboring cage, the particle should overcome the free energy barrier, which can be defined as the difference between the maximum and the initial elastic deformation energy of the network stands during a hopping event.

During a single hoping event, the entropic energy barrier involving in the deformation of the loop when it is slipping around the probe can be written as,

$$\Delta U_{hop} \approx k_B T \left(\frac{2R}{a_x}\right)^2 \qquad 2.1.3.1$$

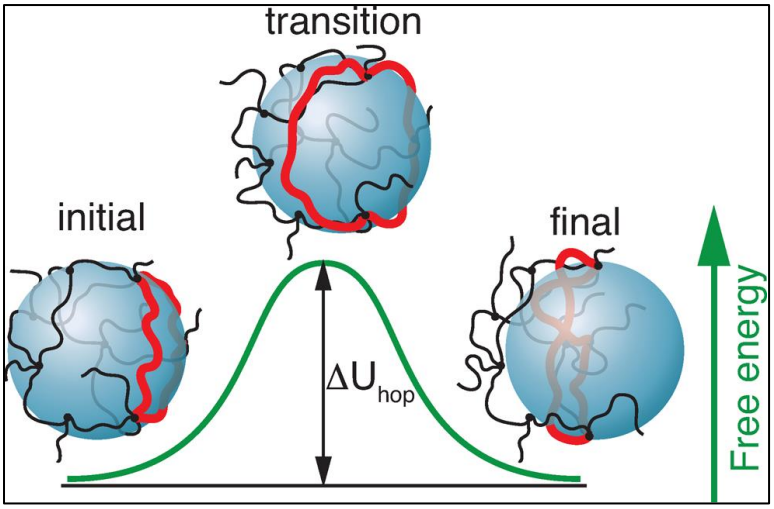


**Figure 2.1.3.1** Figure of a large nanoparticle hops from one network cage to a neighboring cage with a network loop (in red) slipping around the particle. (Adopted[1]) (Reprinted with permission from Macromolecules 48 (3), 847-862. Copyright (2015) American Chemical Society. Further permissions related to the material excerpted should be directed to the ACS)

The hopping barrier measures the probability of the loop fluctuation to a size larger than the particle size 2R. The probability is further proportional to the time waiting for a hoping to occur ($\tau_w$) in unentangled network.

$$\tau_w \cong \tau_x \left(\frac{d}{a_x}\right) exp\left(\frac{d^2}{a_x{}^2}\right) \qquad 2.1.3.2$$

where,

$$\tau_x \cong \tau_0 N_x^2 \qquad 2.1.3.3$$

Here, $\tau_0$ is the monomer relaxation time and $N_x$ is the number of monomers in the network. $\tau_x$ is the Rouse relaxation time, which is the time a network strand attempt to slip around the particle. Even though the loop slips through the particle, hoping motion does not get succeeded until $t>\tau_w$. The probability of the hoping increases with the time for $t> \tau_w$. Further, the diffusion coefficient due to hoping mechanism in unentangled gel,

$$D_{hop} = \left(\frac{b^2}{\tau_x}\right)\left(\frac{a_x}{d}\right) exp\left(-\frac{(2R)^2}{a_x^2}\right) \qquad 2.1.3.4$$

At time scale smaller than the relaxation time $\tau_x$, for large particles (i.e. $2R>a_x$) the diffusion is unaffected by the fluctuations of the network strand and the mobility is similar as in polymer melts. This will be discussed further in Chapter 4.

**2.1.4 PREVIOUS STUDIES ON DEPLETION LAYER EFFECT**

Konderinker *et al.* studied the rotational and translational diffusion of colloidal tracer spheres in semiflexible xanthan solutions.[42] One of their goals was to investigate how the frictional drag coefficient is affected by the hydrodynamic interactions of the tracer particle with the surrounding polymer solution. The Stokes frictional drag of tracer spheres in pure solvent is proportional to the solvent viscosity $\eta_0$. They have observed that modifying the solvent viscosity

by the low shear viscosity makes the effective viscosity experienced by the tracer particles overestimated. According to the phenomenological theory by de Gennes, the hydrodynamic screening length ($\xi_H$) for semiflexible polymers in good solvents is identical to correlation length ($\xi$) within numerical factors (i.e. $\xi_H \cong \xi$).[30] The experimental results by Konderinker *et al.* supports this. Phillies and the coworkers argued that hydrodynamic screening in polymer solution is absent and entanglements in polymer are unimportant for the dynamics of the tracer particles.[33, 35, 36] Further they described that this same mechanism applies to the system with different architectures of the tracer particles, such as rigid spheres and flexible chains. However, this was disproved by an experimental study using different tracer architectures in the same matrix.[43]

Effective medium theory assumes that tracers experience a homogeneous polymer solution, which is Brinkman fluid with the hydrodynamic screening length, $\xi_H$. In real solvents, there are non-adsorbed polymer segments are around the tracer particles, and as a result, this the tracer particles are depleted away a certain distance. The depletion layer thickness will be discussed more in Chapter 5.

**2.1.5 PREVIOUS WORK ON POLYELECTROLYTES**

Poling-Skutvil *et al.* studied the mobility of polystyrene nanoparticles in dilute and semidilute solutions of partially hydrolyzed polyacrylamide.[44] Study found that the particle size to polymer size ratio ($2R_{NP}/\xi$) controls the long-time diffusivity of nanoparticles. The mean squared displacement results show that particle dynamics coupled with the polymer dynamics because polymer undergoes similar crossover between dynamic modes. In the longer time scale, (i.e. $t > \tau_\xi$) polymer chains move as a chain of correlation blobs. Here, $\tau_\xi$ is the relaxation time of a correlation blob written as,

$$\tau_\xi = \frac{\eta_0 \xi^3}{k_B T} \qquad 2.1.5.1$$

$\eta_0$ is the solvent viscosity and is the $\xi$ correlation length. In the opposite limit (i.e. $\tau_\xi < t < \tau_R$) The polymer moves subdiffusively. Here, $\tau_\xi$ is the polymer relaxation time which can be written as follows.

$$\tau_R \approx \tau_\xi \left(\frac{N}{N_\xi}\right)^{2\upsilon+1} \qquad 2.1.5.2$$

where N is the number of monomers in the polymer chain and the $N_\xi$ represents the number of monomers in the correlation blob and $\nu$ is the reciprocal of the fractal dimension of the polymer, which is equal to ½ if the polymer behaves as an ideal string of correlation blobs. The mobility of the polymer chains locally cages the particle until the polymer chain is sufficiently relaxed, and this result in a coupling of dynamics between the particles and polymer. At the time scale of $t > \tau_\xi$, due to the coupling of dynamics, effective viscosity $\eta_{eff}(t)$ felt by the particle increases as,

$$\eta_{eff}(t) \sim \frac{N(t)}{N_\xi} \approx \eta_0 \left(\frac{t}{\tau_\xi}\right)^{1/2} \qquad 2.1.5.3$$

The viscosity continues to increase until the polymer relaxes over the size of the particle at the time, $\tau_R$

$$\tau_R \approx \tau_\xi \left(\frac{2R_{NP}}{\xi}\right)^4 \qquad 2.1.5.4$$

In the time scale $t > \tau_R$, particle polymer dynamics decoupled. Therefore, time scale beyond $t = \tau_R$, particle dynamics depend on the effective viscosity of the medium, $\eta_{eff}$,

$$\eta_{eff} \approx \eta_0 \left(\frac{2R_{NP}}{\xi}\right)^2 \qquad 2.1.5.5$$

The relative diffusivity (D/D0) results have collapsed onto a single curve for small size and follow the predicted scaling relation: $D/D_0 \sim (2R_{NP}/\xi)^{-2}$. However, for larger particles, relative diffusivity somewhat deviates from the curve and they have interpreted their result as particles are large enough to experience the viscoelasticity of bulk solution. This discussion will be continued in Chapter 6.

# CHAPTER 3 : FLUCTUATION CORRELATION SPECTROSCOPY

## 3.1 INTRODUCTION

Fluctuation correlation spectroscopy also called fluorescence correlation spectroscopy (FCS) is a powerful technique to measure the dynamics of molecular processes by using the statistical analysis of fluctuation of fluorescence intensity[8, 45, 46]. FCS was first introduced in the early 1970s by Magde *et. al.* as a compact dynamic light scattering (DLS) system to measure the diffusion and binding of ethidium bromide onto double-stranded DNA. FCS developed further to demonstrate single-molecule detection capabilities in 1993[47]. Fluorescence correlation spectroscopy provides an important methodology in the fields of biophysics, analytical chemistry and cell biology for measuring and probing the mobility, ligand kinetics of biological molecules in cellular environment, the nuclear structure of living cells etc.[48] FCS can be used as a single molecule sensitive spectroscopic technique that can be used to get details about the sample at very low concentration (~pM-nM).

Fluctuations of the fluorescence (Figure 3.1.1) emitted by the biomolecules or dye molecules are useful to obtain the autocorrelation curves (Figure 3.1.2), which carries information such as diffusion coefficient, decay time, etc. The autocorrelation curve can be calculated according to the autocorrelation function as a function of delay time τ. It measures the similarity of the function with itself after a time lag τ.

$$G(\tau) = \frac{<\delta F(t).\delta F(t+\tau)>}{<F(t)>^2} \qquad 3.1.1$$

$\langle F(t)\rangle = \left(\frac{1}{T}\right)\int_0^T F(t)\,dt$ denotes the time average of the fluctuation intensity. $\delta F(t)$ is the fluctuations around the mean value of F(t).

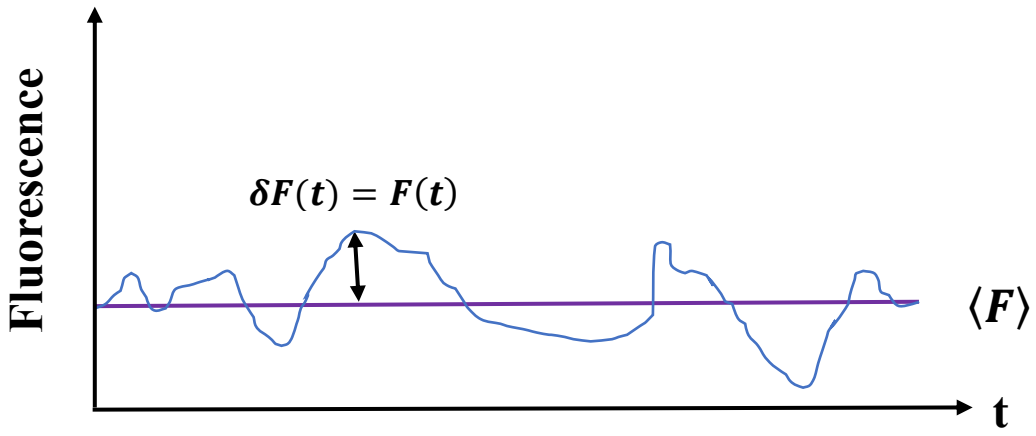


**Figure 3.1.1** Fluctuation of fluorescence particle mobility through the laser focus

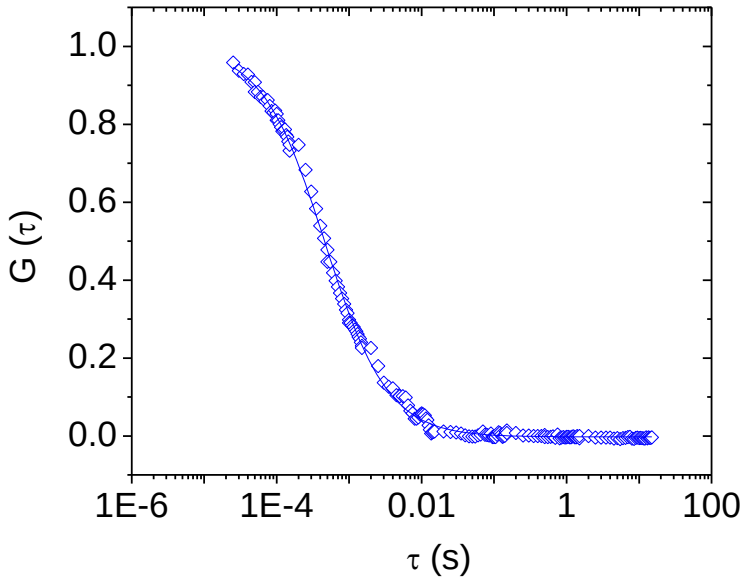


**Figure 3.1.2** Autocorrelation curve as a function of time lag τ Sample: R=5 nm gold nanoparticles in deionized water C= 0.95 nM

The rate of photon emission is proportional to the average number of molecules in the excitation volume (<N>), which according to Poissson statistics implies that relative statistical fluctuation is larger for samples with smaller <N>. The amplitude of the autocorrelation function is inversely

proportional to <N>. Therefore, the signal itself will be stronger for smaller concentration samples.[45]

**3.2 EXPERIMENTAL SETUP**

First, two-photon FCS set up (Berland *et al* 1995) was inspired by the implementation of the two-photon microscopy (Denk et al 1990). Use of non-linear two-photon absorption makes high optical resolution in two-proton FCS set up. The absorption of two photons is a quasi-simultaneous process that happens in a very short time ($10^{-16}$ s), which require two photons with half of the energy that is required for an actual transition(Figure 3.2.1).[49] In a two-photon setup, the fluorescent emission happens only near the laser focus, where the energy density is maximum because the probability of occurring two-photon excitation event is extremely low. Contrary to the use of a pinhole in single photon FCS set up, two-photon FCS has an inherent property to cut off the background fluorescence in the illumination path by spatial filtering.[45] The laser acts as the excitation source for the dye molecules. The efficiency of the photon excitation is greatly increased by using short illumination pulses because of the probability of the two-photon event is directly proportional to the square of the light intensity. Since the excitation intensity is inversely proportional to the square of the distance from the focal plan ($1/d^2$) two-photon FCS excitation is restricted to tiny detection volume (~1 femtoliters) around the laser focus spot. Additionally, the photo damage of the fluorophores is controlled by confining the excitation photons only to the vicinity of the focal spot. These characteristics makes the two-photon FCS more suitable for sensitive studies of biomolecules compared to one photon FCS set up.[49] Another advantage of two-photon FCS is that the wavelength of the excited and the emission photons are significantly different. As a result, the illumination of laser light is well separated according to

the wavelength by introducing a dichroic mirror to the setup. Thus, the emitted fluorescence light can be efficiently filtered out. Commonly used lasers for two-photon FCS set up are the femtosecond and picosecond Ti:sapphire lasers. On the other hand, one photon FCS set up uses continuous laser source.

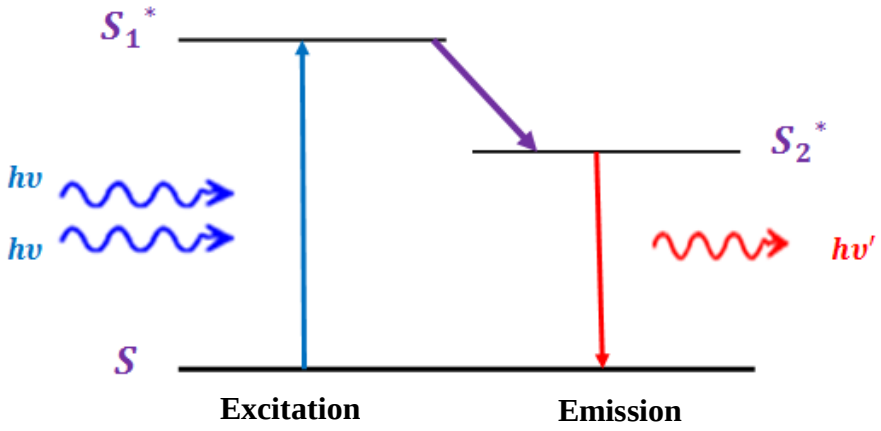


**Figure 3.2.1** Two-photon excitation and emission event. The absorption of two photons with identical energy results in emission of one photon with energy greater than one individual absorbed photon

Femtosecond Ti:sapphire laser (Mai Tai, Spectra-Physics) of near-infrared light (wavelength~800 nm) with the pulse width of 150 fs at a repetition rate of 80 MHz serves as the excitation source for fluorophores in our experiments. Neutral-density filters (NDFs) are used to reduce and select the appropriate power of the laser according to the specific fluorophores used in the experiment. An Axiovert 200, Zeiss inverted microscope act as an experimental platform for the experimental setup. The laser beam passes through the ND filters followed by a beam expander. The beam expander consists of two lenses, which were separated by the distance equal to the addition of their focal lengths. Beam expander expands the laser beam in the size of ~2 mm.

After that, the incoming beam from the beam expander is reflected from a dichroic mirror, which is formed of multiple dielectric coatings. The dichroic mirror is a special mirror that separates the two light paths by reflecting the excitation light into the objective and transmitting the fluorescence emission light from the sample into the detector. The dichroic mirror is responsible of reflecting the light with a wavelength above a certain value called the transition wavelength and transmit under that same wavelength. The transition wavelength of the dichroic mirror should match with the transition wavelength of the fluorophores used in the measurements. The reflected laser beam from the dichroic mirror is focused on the sample through a high numerical aperture (N.A.=1.25,100X) oil immersion objective. At the excitation volume, a nanoparticle or dye molecule absorbs two photons and emits one photon within the short time interval of a few femtoseconds. Since the emitted photon has wavelength less than the absorbed photon, emitted photon transmits back through the same path, first collected by the objective and pass through the dichroic mirror. Incoming photons were collected by the single-photon sensitive photomultiplier tube (PMT) placed after a 50-50 beam splitter. The "afterpulsing" effect of photodetectors distort the autocorrelation curve for lag times shorter than 1 μs, because there is a finite but low probability that single photon generates two electronic pulses instead of one electronic pulse (Figure 3.2.2). The effective solution to reduce the afterpulsing artifact is that splitting the incoming light between two detectors and cross-correlate their outputs. The resultant cross-correlation function is similar to the autocorrelation function and free of afterpulsing in the shorter time lags.

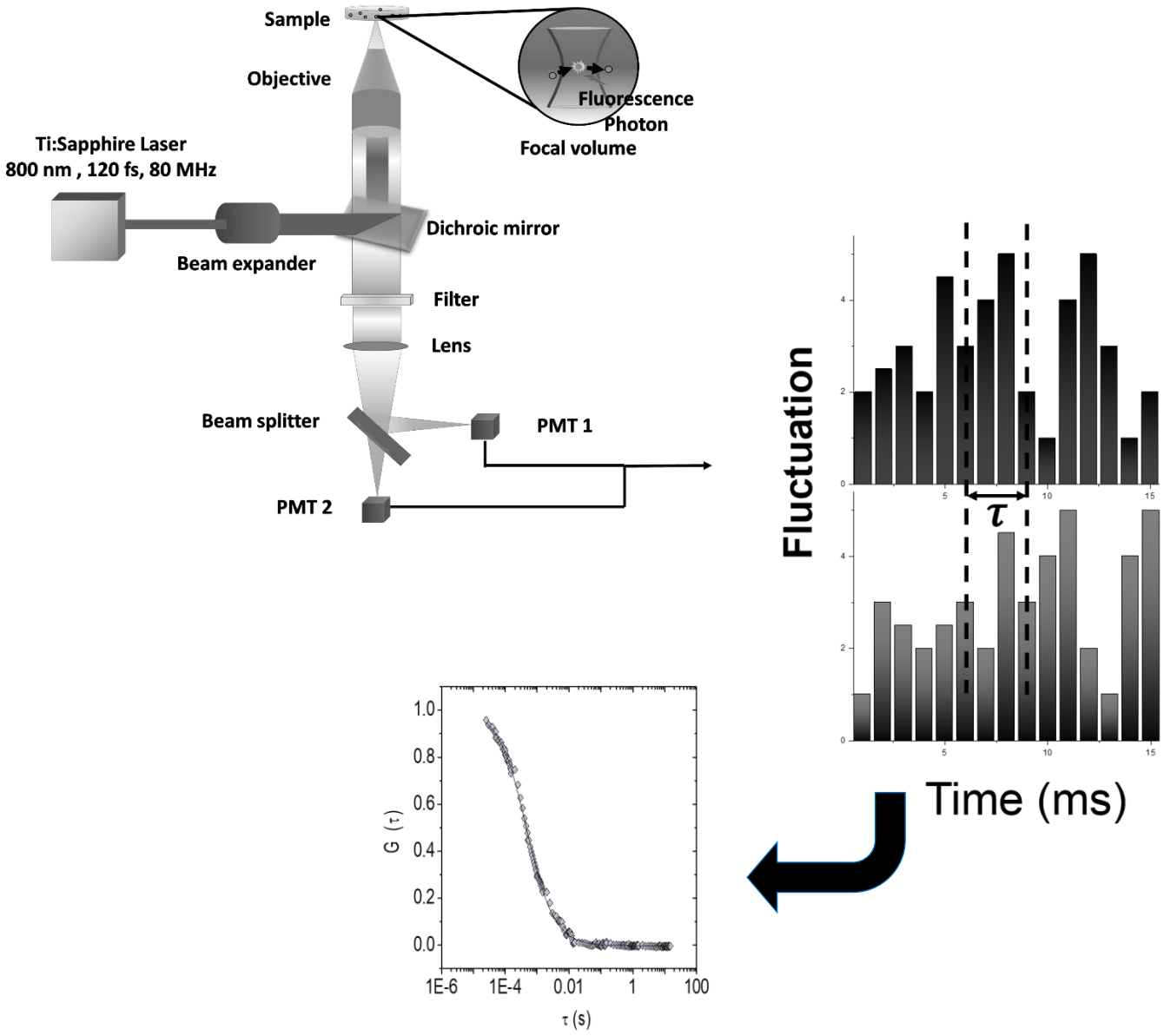


**Figure 3.2.2** Two-photon FCS set up

A polarized signal is required to measure the rotational diffusion of anisotropic particles due to their shape anisotropy. In this situation, a polarized beam splitter is introduced to the set

up before the PMTs to obtain polarized resolve signal. There is a short pass filter that is placed between the dichroic mirror and PMT to prevent any leakage or scattered light entering the PMT. Integrated data acquisition software (ISS, IL) is used to record, organize, and analyze the fluctuations of the fluorescents intensity from the PMT at real time (t). The software provides the autocorrelation curve or cross-correlation curve during the experiment. Autocorrelation function (ACF), G(τ), that is derived from different theoretical models is useful to extract the dynamical information, such as diffusion coefficient of the fluorophores, which measures the similarities of the function itself after a time lag τ.

**3.3 THEORETICAL APPROACH**

Tiny fluctuations in the fluorescence signal from the excited molecules can be quantified by using the autocorrelation function by temporally autocorrelating the recorded intensity signal.[47] FCS autocorrelation curve, G(τ) contains two different types of information. First, the magnitude G(0), measures the number density or characterized molecular aggregates. Second, the rate and the shape of the temporal decay, which provides dynamical information.

The autocorrelation function (ACF) can be defined as,

$$G(\tau) = \frac{\langle \delta F(t-\tau)\delta F(t)\rangle}{\langle F\rangle^2} \qquad 3.3.1$$

The fluctuation of fluorescence intensity $\delta F(t)$ can be written as,

$$\delta F(t) = F(t) - \langle F\rangle \qquad 3.3.2$$

where, $F(t)$ is the measured fluorescence at time t and $\langle F\rangle$ is the average value of the fluctuations measured fluorescence $F(t)$ at time t.

It simplifies to,

$$G(\tau) = \frac{\langle F(t)F(t-\tau)\rangle}{\langle F\rangle^2} - 1 \qquad 3.3.3$$

The autocorrelation function also can be written using a basic algorithm as below.

$$G(i\Delta T) \approx \frac{\left[\frac{\sum_{j=i+1}^{M} n_j n_{j+1}}{M-i}\right]}{\left(\frac{\sum_{j=i}^{M} n_j}{M}\right)^2} - 1 \qquad 3.3.4$$

where, $G(i\Delta T)$ is the autocorrelation function (ACF), M is the total no of acquired data points, $n_j$ is the obtained values, and $\Delta T$ is the sampling time, which ranges from 1 μs to ms.

If only one fluorescent chemical species is present in the sample region,

$$F(t) = kQ \int E(r)C(r,t)dr \qquad 3.3.5$$

where k is a constant, Q is the product of the absorptivity, fluorescence quantum efficiency, and experimental fluorescence collection efficiency of the fluorescence molecules, E(r) is the spatial intensity profile of the excitation light, and C(r.t) is the number density at position r and t.

Then, one can further simplify the fluctuations of fluorescence intensity as,

$$\delta F(t) = F(t) - \langle F\rangle = kQ \int E(r)\delta C(r,t)dr \qquad 3.3.6$$

where $\delta C(r,t) = C(r,t) - \langle C\rangle$

By substituting eq 3.3.3.

$$G(\tau) = \frac{\iint E(r)E(r')\langle \delta C(r,t)\delta C(r',t+\tau)\rangle dr dr'}{(\langle C\rangle \int E(r)dr)^2} \qquad 3.3.7$$

By using the 3D gaussian model for two photon excitation process,

$$E(r) = E(x,y,z) = E_0 exp\left(-\frac{4(x^2+y^2)}{\omega_0^2} - \frac{4z^2}{z_0^2}\right) \qquad 3.3.8$$

where $\omega_0$ is the excitation beam waist and the $z_0$ is the excitation beam height.

For Browninan (translational) diffusion, the fluctuations $\delta C(r,t)$ will have characteristic behavior governed by the diffusion equation which is given below,

$$\frac{\partial \delta C(r,t)}{\partial t} = D\nabla^2 \delta C(r,t) \qquad 3.3.9$$

The solution of above equation is given by

$$\delta C(r,t) = \frac{\langle C \rangle}{4\pi D t^{\frac{3}{2}}} exp\left(-\frac{r^2}{4Dt}\right) \qquad 3.3.10$$

By assuming that the sample is stationary, the probability of finding a diffusive molecule at position $r'$and $t+\tau$, given that the molecule was at position $r$ and time $t$ is,

$$\langle \delta C(r,t)\delta C(r',t+\tau)\rangle = \frac{\langle C \rangle}{(4\pi Dt)^3} exp\left(-\frac{(r-r\prime)^2}{4Dt}\right) \qquad 3.3.11$$

Using the Gaussian model for the two- photon excitation, we can write the autocorrelation function relating the parameters excitation beam waist ($\omega_0$), excitation beam height ($z_0$), sampling concentration (C) and the diffusion coefficient D.

$$G(\tau) = \left(\frac{2\sqrt{2}}{\pi\sqrt{\pi}\omega_0^2 z_0 \langle C \rangle}\right) \frac{1}{\left(1+\frac{8D\tau}{\omega_0^2}\right)\sqrt{1+\frac{8D\tau}{z_0^2}}} \qquad 3.3.12$$

In 3D, the excitation volume can be written as,

$$V = \frac{\pi\sqrt{\pi}\omega_0^2 z_0}{2^3} \qquad 3.3.13$$

The average number of diffusant molecules is related with the concentration as follows,

$$\langle N \rangle = V\langle C \rangle \qquad 3.1.14$$

Therefore,

$$G(\tau) = G(0) \frac{1}{\left(1+\frac{8D\tau}{\omega_0^2}\right)\sqrt{1+\frac{8D\tau}{z_0^2}}} \qquad 3.3.15$$

The number of average diffusant molecules or the concentration can be calculated from the amplitude of the autocorrelation function G(0) using the following equations.

$$\langle N \rangle = \frac{1}{2\sqrt{2}G(0)}, \text{ and } \langle C \rangle = \frac{1}{2\sqrt{2}VG(0)} = \frac{2\sqrt{2}}{\pi\sqrt{\pi}\omega_0^2 z_0 G(0)} \qquad 3.3.16$$

Similarly, 2D autocorelation functio for two-photon excitation process can be written as,

$$G(\tau) = G(0)\frac{1}{\left(1+\frac{8D\tau}{\omega_0^2}\right)} \qquad 3.3.17$$

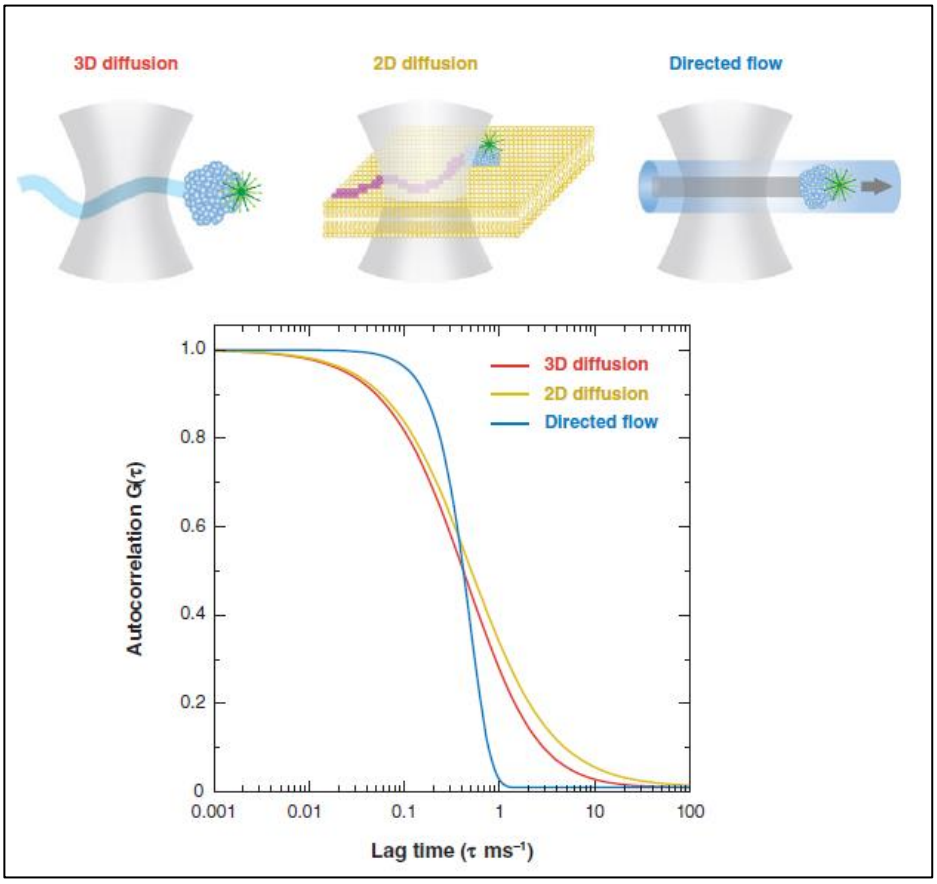


**Figure 3.3.1** Model autocorrelation curves for different kinds of particle motion:free diffusion in three dimensions (red), free diffusion in two dimensions, (yellow) and directed flow (Cyan) (Haustein 2007)[47]

Additionally, The autocorrelation function can be derived when flow present in the sample and it simplify into the following equation,

$$G(\tau) = G(0)\frac{1}{\left(1+\frac{8D\tau}{\omega_0^2}\right)\sqrt{1+\frac{8D\tau}{z_0^2}}}exp\left(-\frac{V_{flow}^2}{\omega_0^2 z_0\left(1+\frac{8D\tau}{\omega_0^2}\right)\sqrt{1+\frac{8D\tau}{z_0^2}}}\right) \quad 3.3.16$$

# CHAPTER 4 : DIFFUSION OF NANOPAERTICLES IN ENTANGLED POLY(VINYL ALCOHOL) SOLUTIONS AND GELS

## 4.1 INTRODUCTION

*The following materials has been originally published in Macromolecules (2019)*[16]

Understanding the diffusion of small molecules, proteins, and nanoparticles within entangled polymer solutions and gels is important for both industrial and medical applications. From polymer physics perspective, the studies can give useful information about the structure of the matrix and verify or refine theories of polymer dynamics.[41, 44, 50-59] Several situations are of interest. Above the overlap concentration ($\phi^*$) in the semidilute solution, the polymer chains form a transient mesh, characterized by correlation length ($\xi$). Beyond a critical entanglement concentration ($\phi_e$), long chain polymer molecules can form an entangled network due to topological constraints.[60] A gel can be formed either by an external cross-linking agent or by the inherent reactivity of a functional group. Physical gels are formed by crosslinking of relatively weaker inter- or intramolecular hydrogen bonding,[61] microcrystallites, or by local helical structures.[62] These are common for many biopolymer systems.[63] As the bond energy is typically only a few times of the thermal energy, the bonds have shorter life time and their location can change with time.[62] The physical gels are reversible, and they can be melted by heating, change of pH, etc. In chemical gels, the network is stabilized by covalent bonds, which are much stronger and thus irreversible.

Dynamic light scattering (DLS),[57, 64, 65] forced Rayleigh scattering (FRS), fluctuation correlation spectroscopy (FCS),[3, 66] and pulse-field gradient spin-echo nuclear magnetic resonance (NMR)[67, 68] techniques had been used to study the diffusion of solvent, small solute molecules like dyes, and probe particles in both synthetic and biopolymer gels. Massaro and Zhu[17] reviewed a majority of the theories and experiments that describe the diffusion of spherical, non-interacting particles and predict reduced

diffusion coefficient, $D/D_o$, as a function of particle size and polymer concentration. Here, D is the diffusion coefficient in the presence of polymer, and $D_o$ is that in the neat solvent. Some assumptions about polymer concentration dependence of the mesh size are needed to use these theories. The free-volume theory by Vrentas-Duda was successfully used to describe the diffusion of particles with size much smaller compared to mesh size.[69] Needing of several parameters for three-component systems (polymer, probe, and solvent), however, limits its application of this theory. More common in this field are hydrodynamic scaling theories and various obstruction-diffusion models. Screened hydrodynamic theories[19] predict a scaling function of the form $f(R/\xi)$ for the reduced diffusion coefficient. Here, R is the particle radius, and $\xi$ is the correlation length in the semidilute solution or mesh size in cross-linked gels. These theories assumed that hydrodynamic interaction between the particle and the polymer, which is screened at the length scale determined by the correlation length ($\xi$) in semidilute solutions, governs the particle dynamics. Obstruction-diffusion models[70] rely on the notion that the volume occupied by the network is inaccessible to the diffusing species, leading to an increased path length between two points. This results in a decrease of the diffusion coefficient compared to that in the solvent. Obstruction models work well when the motion of the network is negligible at the time scale of particle motion and thus more suitable for a rigid network. These models were widely used to investigate the structure of the chemically cross-linked gels from the diffusion data of particles with different sizes.[17]

The above theories make no distinction between the transient networks as formed in the semidilute or entangled polymer solutions vurses permanent cross-links formed in chemically cross-linked gels. In the former case, mesh size depends upon polymer volume fraction ($\phi$), while for the latter it is independent of $\phi$. Rheologically, they can be distinguished by their low-frequency response

in small amplitude oscillatory shear. In the terminal regime, semidilute or entangled solutions exhibit the characteristic of a liquid. However, cross-linked gels show a frequency-independent elastic modulus, which is at least one or two orders of magnitude larger than the viscous modulus.[65]

Recently, scaling theory had been used to contrast size-dependent diffusion of nanoparticles within entangled solution versus cross-linked gels.[1, 18] The theory predicted that if $2R << \xi$, the particles experience mostly the solvent viscosity. Intermediate sized particles, which are characterized by $\xi < 2R < a_e$, experience a length scale dependent nanoviscosity that scales as $(R/\xi)$.[51] Here, $a_e$ is the tube diameter, which depends upon $\phi$. The diffusion coefficient of large particles, $2R > a_e$, is determined by the polymer relaxation time scale, and D varies according to $\phi^{-3.91}/R$ in good solvents.[18] Many aspects of this theory have been verified by recent experiments.[3] An extension of this theory showed that in entangled polymer liquids particles which are slightly larger than the tube diameter can diffuse through barrier hopping.[1] The activation energy for hopping motion is given by $u \approx kT\ (2R/a_e)$, where k is Boltzmann constant and T is the absolute temperature. The diffusion coefficient, therefore, varies according to $D \sim \exp(-2R/a_e)$. According to this theory, the hopping step size is of the order of correlation length. The hopping motion is negligible when $2R >> a_e$, and the only way particles can then move is through entanglement relaxation.[1]

In contrast to entangled solutions, the hopping motion for particles in cross-linked gels had been predicted to have a much stronger dependence on size ratio.[1] For particles slightly larger than the mesh size ($a_x$), the diffusion coefficient $D \sim \exp[-(2R/a_x)^2]$. Here, $a_x$ is the average distance between two permanent cross-links.[1] The particles with size $2R >> a_x$ remain trapped in chemically cross-linked gels.[1] The scaling theories ignore numerical prefactors. If the functional dependence presents as exponential, the missing prefactor can significantly affect quantitative comparison with the data.

A sophisticated force-based microscopic theory has been developed by Yamamoto *et. al.* to describe the diffusion of nanoparticles in entangled and unentangled polymer melts.[71] According to this theory, the particles smaller than the tube diameter experience a length-scale dependent friction coefficient. The particles of size larger than the tube diameter are affected by the entanglement relaxation of the polymer chains. The mobility of the particles was found to decreases dramatically as their size increased relative to the tube diameter. However, unlike scaling theories, a continuous crossover exists between the two regimes as the nanoparticle (NP) motion gets gradually coupled with the polymer relaxation. The theory assumed that the particle motion is entirely determined by the collective relaxation of polymer density fluctuations, which was argued to be a good approximation for larger particles. A later improvement of the theory treated the particle motion and polymer friction self-consistently.[59] The deviation of the modified theory from the earlier one is strongest at the size ratio, $x=2R/a_e$ close to 1. The theory predicts that full recovery to Stokes-Einstein (SE) behavior requires a very high size ratio ($\approx$ 8), which had been verified by experiments.[72]

The two discussed theories assumed that NP dynamics is Gaussian at all times and activated hopping was not directly included. The analysis of hopping motion was performed by using a non-linear Langevin equation.[73] The activation barrier height, average hopping time, and jump distance depend critically on $x-x_c$, where $x_c = (2R/a_e)_c$ is the critical value for localization that depends upon particle size and polymer properties. Except within a small size range between $2R/a_e \sim$ 1.5-2, the contribution to particle mobility due to hopping was found to be significantly smaller compared to contribution from the relaxation of entangled polymer network. This was verified by computer simulation.[55] However, in chemically cross-linked gels or in heavily cross-linked network, the hopping motion can play a role.

The experimental verification of hopping motion and performing quantitative comparison of data with any theory present several challenges: (i) finding a model polymer system, where one can unambiguously determine tube diameter ($a_e$) or mesh size in cross-linked gels ($a_x$) and associate an uncertainty with those measurements; (ii) the small range of size-ratio where the hopping can be important; (iii) the uncertainty with numerical factors in scaling theories;[1] and (iv) limited dynamic range of experimental techniques, which can make detection of hopping difficult if the activation barrier is very high as predicted in force-based approaches.[73]

Experimentally, there is a large volume of literature on probe diffusion within polymer solutions. Phillies *et. al.* have performed many studies with particles of different sizes in various polymer solutions within wide range of concentrations, including semi-dilute and entangled regimes.[74] Among the pertinent experiments, Guo and co-workers have studied the subdiffusive motion of functionalized gold nanoparticles with thiol-terminated polystyrene (PS) chains in high molecular weight polystyrene (PS) solutions using X-ray photon correlation spectroscopy (XPSC).[53] The particle size was chosen to be comparable to length scale of entanglement. They observed subdiffusive motion of the particles, where the anomalous exponent is a function of polymer concentration. They interpreted that the particles experience a heterogeneous microenvironment own higher mobility compared to predictions from microrheology results. They hypothesized that the extra mobility is due to the hopping motion. In contrast to XPCS, our experiments by fluctuation correlation spectroscopy (FCS) measures diffusion coefficient at a very different length scale (~0.5 μm). In addition, the concentration of the polymer in our experiments was chosen to investigate the regime, where the sample behaves as a viscoelastic solid.

The self-diffusion coefficient of fluorescein isothiocyanate (FITC)-labeled dextran and fluorescence labeled polymeric latex was studied in semidilute solutions of hydroxypropyl cellulose (HPC).[75] Most of the diffusion data can be fitted well with the Langevin-Rondelez equation using the assumption that the probes are dense spheres. HPC is a semiflexible polymer, so that the effect of segmental dynamics on probe motion is not significant. The dextran as a probe can change its' size as a function of polymer concentration, which farther complicates data analysis.

In this paper, we studied a polymer solution that has properties intermediate between an entangled network and a permanently cross-linked gel. The concentration of the polymer was chosen such that the entanglement effect cannot be ignored, which is accompanied by transient, relatively loose physically cross-linked structures. We choose a poly(vinyl) alcohol (PVA)-water solution because its physical and rheological properties were well characterized previously.[76] PVA is widely used in industries for applications, such as membranes, films, thickeners, and fibers.[76] Biocompatibility, biodegradability, and water solubility make PVA gels useful in biomedical applications[66] as well, such as for drug delivery and tissue scaffolding. Because of the presence of hydroxyl group in the repeat units, PVA can form both inter- and intramolecular hydrogen bonds.[61] The density of bonds increases with PVA concentration, which can give a relatively stable network.

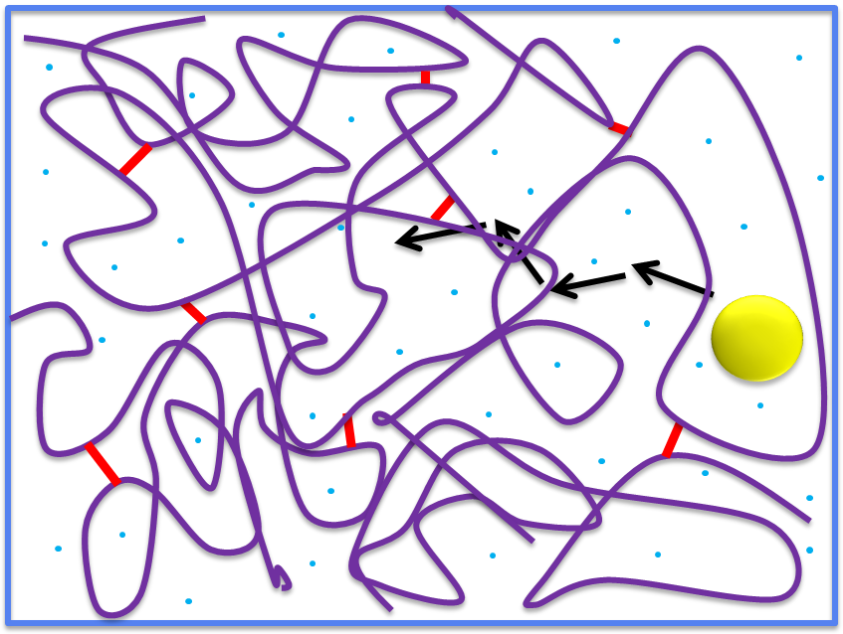

**Figure 4.1.1** Diffusion of gold nanoparticles in physically cross-linked PVA gels

We are aware of a couple of studies of probe diffusion in PVA solutions and chemically cross-linked gels.[61, 66] The diffusion of a small fluorescent dye molecule was studied as a function of PVA concentration and cross-linking densities.[77] At relatively higher concentration, it was shown the chemical cross-linking caused an additional slowing down of the dye diffusion. The difference in time-scale of diffusion between the transient network and cross-linked gel scaled with gel elasticity. In another study, different sized proteins, dextran molecules, and polystyrene latex spheres were used.[66] The reduced diffusion coefficient was found to follow a stretched exponential function. These studies, however, were restricted to semidilute solutions.

In our experiments, we used solid, spherical, and non-interacting particles, which allowed more direct comparison with theories. We vary the particle size systematically from 5 to 30 nm, while not altering the interaction with the matrix. We selected long chain PVA molecules and cover the range of concentrations so that a transition from entangled solutions to physically cross-linked gels can be

studied. We compared our results with the available theories and found potential evidence of hopping motion. We expect that the results presented here will have significance in areas ranging from polymer physics to transport in biological gels.

**4.2 EXPERIMENTAL SECTION**

Poly (vinyl alcohol) powder (MW ≈ 89,000 g/mol, the degree of hydrolysis >98%) was purchased from Sigma-Aldrich. Colloidal gold nanoparticles (AuNPs) of radius (R) = 2.5 , 5, 10, and 15 nm were obtained from Ted Pella, Inc. The concentrations of 2.5, 5, 10 and 15 nm NPs as received in the stock solution were 83, 9.5, 1.09, and 0.35 nM, respectively, which were further diluted to prepare the samples for two-photon fluctuation correlation spectroscopy (FCS) experiments. PVA powder was dissolved in Milli-Q water with the prior addition of AuNPs at 90 $^0$C and stirred to prepare 12 different polymer concentrations of PVA solutions with volume fractions ($\phi$) ranging from 0.078 to 0.22. Dissolution of PVA in aqueous solution above $\phi$=0.22 was found to be difficult; therefore, no experiments were performed beyond this volume fraction. All solutions prepared for our experiments were optically transparent.

Commercially available 8 chambered cover glass of thickness 0.13 - 0.17 mm was used as a liquid cell for two-photon FCS experiments. The final concentrations of 2.5, 5, 10, and 15 nm NPs in PVA samples were 13.8, 1.58, 0.18, and 0.06 nM respectively. The solutions were poured into the sample chamber when those were hot and kept undisturbed for at least 24 h before the FCS experiments to get a homogeneous particle distribution in the bulk.

An Axiovert 200, Zeiss inverted microscope was used as an experimental platform, and the cell was mounted on the mechanical stage of the microscope. Femtosecond Ti:sapphire laser (Mai Tai, Spectra-Physics) of near-infrared light (wavelength=800 nm) with the pulse width of 150 fs at a

repetition rate of 80 MHz was focused on the sample through a high numerical aperture (N.A.=1.25,100x) oil immersion objective. Emitted photons were collected by two photomultiplier tubes (PMTs) having single-photon sensitivity placed after a 50-50 beam splitter. The photon counts were cross-correlated to eliminate the artifacts associated with PMT after-pulsing. The autocorrelation curves, G ($\tau$) were obtained by using ISS (Urbana, IL) integrated data acquisition software. From the fit of G($\tau$) by using known equation for three-dimensional diffusion, translational diffusion coefficient (D) of nanoparticles were determined.[78] Each correlation curve was collected for about 5 minutes and a minimum of six different FCS trials were done for each concentration. By using a common dye rhodamine 6G, whose diffusion coefficient in water is well-known (D=414 $\mu m^2/s$) we determined that the focused laser beam had a half-width, $\omega_0$=0.3 $\mu$m and half-height, $z_0$=1 $\mu$m.

Rheological measurements were performed on TA Instruments DHR3 rheometer with a 20 mm parallel plate with a solvent trap. Small-amplitude oscillatory shear experiments were performed using standard protocols. The linear viscoelastic region was determined by conducting a strain sweeps for samples of different concentrations. Frequency sweeps in the range of 0.1 to 500 rad/s were performed at fixed strain within the linear viscoelastic region of each sample.

**4.3 RESULTS AND DISCUSSION**

Figure 4.3.1 shows autocorrelation curves for four particles at a volume fraction, $\phi$=0.14. We observed normal diffusion in all situations, where the mean-square-displacement (MSD), $\langle r^2 \rangle \propto t$ (Figure 4.3.1 inset). Several studies had reported anomalous diffusion of particles in polymer solutions and gels.[79] These include situations, where the structural length scale of the matrix is comparable to experimental length scale and particles that are constrained within a cage at the time scale of experiment

or if the porous medium is fractal.[80] Agarose gel is an example of the fractal medium. There is no characteristic length scale in these systems and diffusion was found to be anomalous at all time and length scales in both experiments[80] and computer simulations.[81] FCS measured the diffusion coefficient at the time scale of few milliseconds to seconds and length scale ≈ 0.5 μm. The observation of normal Brownian diffusion rules out the possibility of confinement of NPs by the network or presence of any large-scale heterogeneities. The heterogeneity formed by the transient hydrogen bonding is at a few nm length scales, and after the NPs sample through different nano-environment, a single time-averaged diffusion coefficient was obtained.

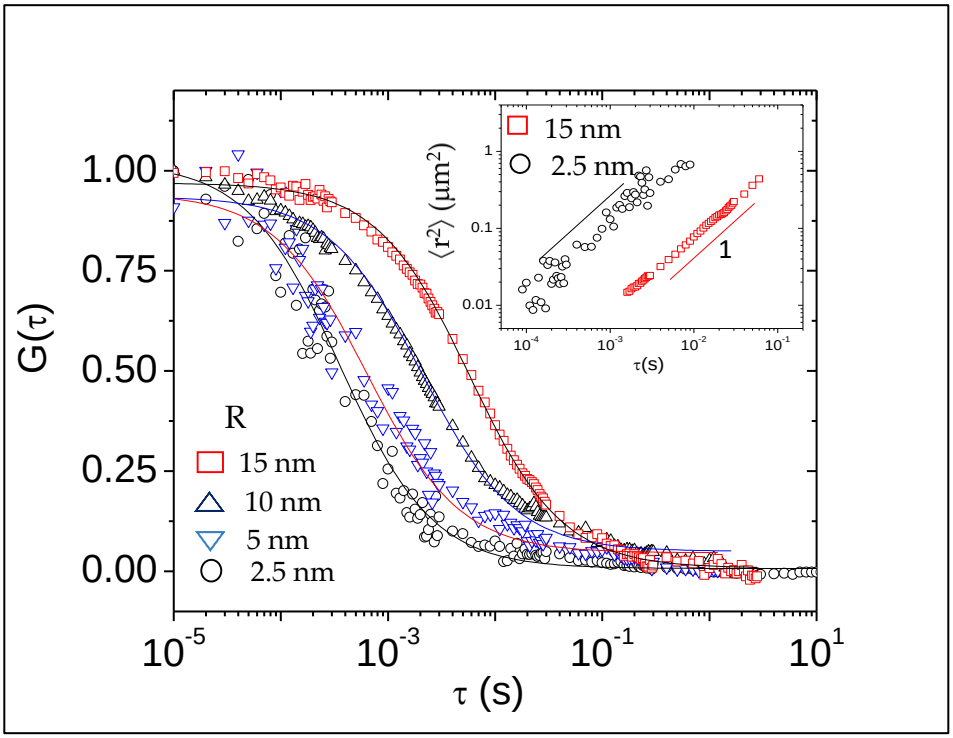


**Figure 4.3.1** Normalized FCS autocorrelation functions for particles within PVA solution of volume fraction, ϕ≈ 0.14. The particle radii are indicated. The solid lines are fits with the 3-dimensional diffusion of normal Brownian motion. The inset showed the mean-square-displacement (MSD) as a function of time in a log-log plot. The straight lines have a slope of 1

We considered the possible association between NPs and the PVA molecules, which will complicate the data analysis. A majority of the theories considered neutral or repulsive interaction between probe and polymer[18]. The interaction has been tested by two different ways. First, we did a time-lapsed measurement of the hydrodynamic radius of NPs in dilute solutions of PVA and did not observe any change. Second, we measured the absorption spectra of gold nanoparticles in water and compared it with a solution containing PVA. Any complexion between NP and polymer will change the position of the peak due to the sensitivity of surface plasmon resonance (SPR) of gold to local nanoenvironment. As shown in figure 4.3.2 SPR showed identical spectra in both solutions ruling out any association between the probe and the polymer.

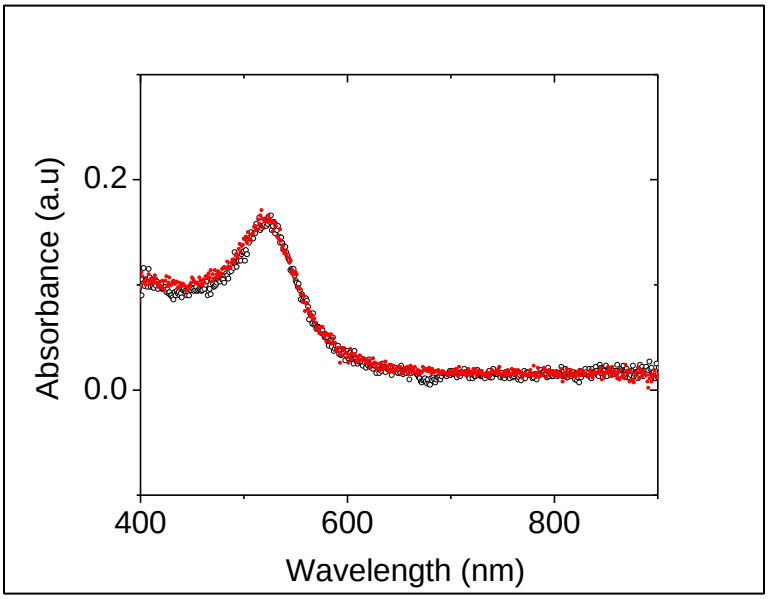


**Figure 4.3.2** Surface plasmon resonance (SPR) absorbance spectra of R=10 nm gold particles in water (closed circles) and in PVA solution (open circles) showed no shift in the peak wavelength indicating no association between the nanoparticles and PVA

PVA-water solutions had been well characterized rheologically by different groups.[76, 82] We performed small amplitude oscillatory shear measurement to probe the equilibrium microstructure.

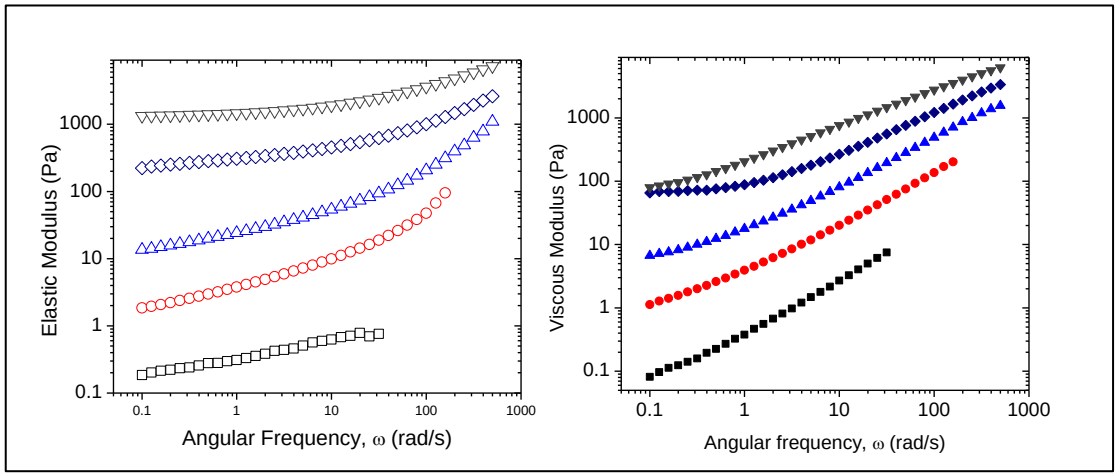


**Figure 4.3.3** Elastic and viscous modulus as a function of small amplitude angular frequency. Both moduli increase as the PVA volume fraction increases. The curves are for different volume fractions. Squares: 0.078; circles: 0.112; up triangles: 0.143; diamonds: 0.17; down triangles: 0.2

We selected five different concentrations, and the results agreed well with previous experiments. In Figure 4.3.3, we showed elastic and viscous modulus, $G'(\omega)$ and $G''(\omega)$ as a function of angular frequency, $\omega$. Both moduli increase with polymer concentration, and for all volume fractions the elastic modulus exceeds the viscous modulus at law oscillation frequencies. For volume fractions above $\phi$=0.14 and at low frequency elastic modulus become almost independent of frequency, larger than the viscus modulus. This kind of rheological response can be contrasted with entangled polymer liquids, where in the terminal regime, $G'(\omega) \sim \omega^2$ and $G''(\omega) \sim \omega^1$ are expected.[76]

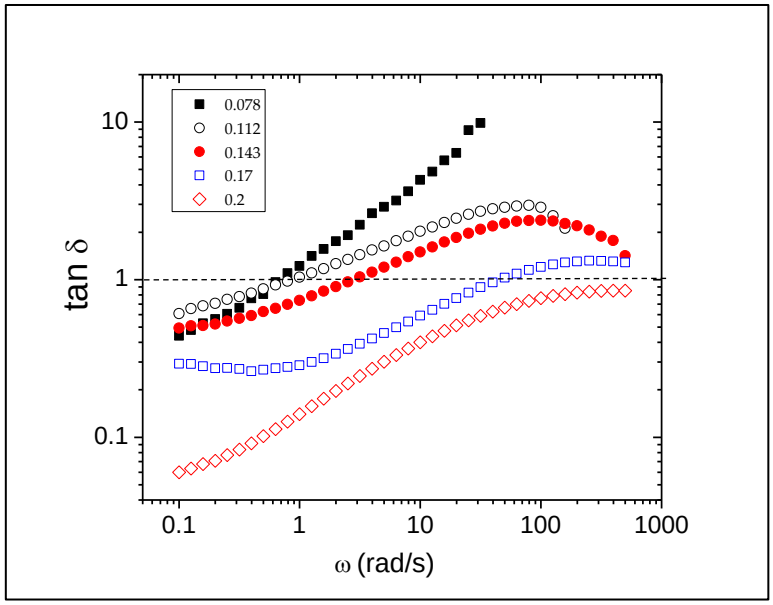


**Figure 4.3.4** Loss tangent tan δ the ratio of viscous to elastic modulus, is shown as a function of small- amplitude oscillation frequency (ω). The dashed horizontal line indicates the crossover from solid-like to a liquidlike response. The data shows predominantly solid-like behavior at long time scales (low frequencies). The volume fraction of PVA in water was indicated in the upper inset

Figure 4.3.4 shows loss tangent, tan δ=G″/G′ as a function of angular frequency. For tan δ > 1, viscous characteristics dominate, while for tan δ < 1 elastic or solid-like characteristics dominate. All samples showed predominantly solid-like behavior at long time scales (low frequencies). Except for ϕ=0.078, all solutions exhibited a peak, which systematically moved to higher frequency with increasing polymer volume fraction. The sample for ϕ=0.2 showed predominantly solid-like behavior at all frequencies examined. These results are similar to previous observations and were interpreted as formation of inter- and intramolecular hydrogen (H) bonding network giving rise to predominately elastic behavior at equilibrium.[76] The cross-linking density increases with polymer concentration as shown by a gradual decrease of tan δ. As the frequency of the oscillation is increased, the network breaks down and the liquidlike behavior begins to emerge. At higher frequency shear-induced local

orientation can favor formation of new intermolecular bonds., which explains the downturn of tan δ at concentrations of 0.112 and 0.143.

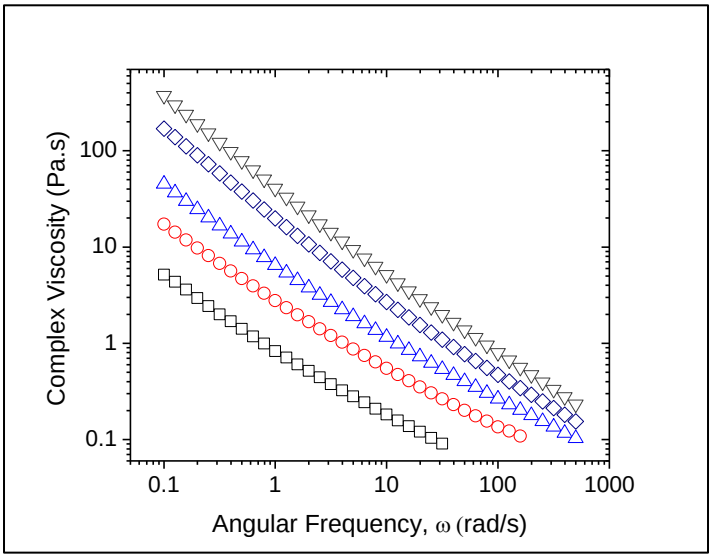


**Figure 4.3.5** Complex viscosity as a function of angular frequency shows shear thinning for all samples. The viscosity decreases due to the breakage of hydrogen bonding. The curves are for different volume fractions. Squares: 0.078; circles: 0.112; up triangles: 0.143; diamonds: 0.17; down triangles: 0.2

Figure 4.3.5 showed complex viscosity as a function of angular frequency. For many polymer solutions, the Cox–Merz rule is often used to infer shear-viscosity behavior from small amplitude oscillatory shear responses.[62, 76, 83] Therefore, fitting the power law model helps parametrize the viscosity at different polymer concentrations. From Table 4.3.1, all samples behave like a shear thinning fluid with flow behavior indexes (n) ranging from 0.2 to 0.7. One possible explanation is that breakage of H-bonds by shear dominates over the formation of new H-bonds during shear thinning, which is commonly related to shear-induced alignment of the polymer chains. Our experiments did not observe the low-frequency $G''(\omega) \propto \omega$ behavior even for the two lowest

concentration samples. In Figure 4.5, we have shown the plot of G"(ω)/ω as a function of ω, which showed strong frequency dependence. At angular frequency of 0.1 rad/s, we obtained G"(ω)/ω is ≈1 and 10 Pa.s for polymer volume fraction of ϕ=0.078 and ϕ=0.112, respectively. These values match well with previous steady shear rheology measurements by a different group.[76]

**Table 4.3.1** Parameterization of complex viscosity graph in Figure 4.3.5. The curves were fitted with a power law model: $\eta=k\boldsymbol{\omega}^{n-1}$, where k is flow consistency index and n is flow behavior index. For shear thinning fluid, n < 1.

| Volume fraction (Φ) | **k** | **n** |
|---|---|---|
| 0.078 | 0.63 | 0.7 |
| 0.112 | 6.3 | 0.63 |
| 0.143 | 34 | 0.58 |
| 0.17 | 340 | 0.33 |
| 0.2 | 1600 | 0.23 |

For the systems studied, gel formation tests by inverting the sample. The gel forms above the concentration of ϕ=0.11. Note that this is not a precise test. As shown in Figure 4.3, the elastic modulus, G′ and viscous modulus G′′ showed some frequency dependence for all samples, Although the frequency dependence of G′(ω) becomes weaker as the volume fraction is increased. A relatively frequency-independent G′ (ω) is obtained at low frequencies for the highest volume fraction sample, ϕ=0.2. Therefore, it is likely that the transition from entangled liquid to gel is gradual. The concentration, ϕ=0.11 is well above the critical entanglement concentration, $\phi_e$=0.02 as found in previous experiment.[84] This suggests that substantial overlappings of the chains are required to form a gel, which corroborates that interaction strength of the individual bond is relatively weak.

For permanently cross-linked gels and classical elastomers, the mean distance between the crosslinks ($a_x$) can be estimated from the terminal elastic modulus (G′) by using rubber elasticity theory,[62] which assumes kT per network chain contribution to G′. Instead of a flat horizontal line as in

a perfect network, we observed that G′(ω) increases slowly with frequency and G′′(ω) is only about an order of magnitude lower compared to G′(ω). The sample with the highest volume fraction of PVA, $\phi$=0.2, showed a relatively flat elastic modulus at low frequencies. By using the relation,[7, 85] $G'=(4/5)kT/a_x^3$. we estimated that $a_x \approx 13$ nm at $\phi$=0.2. There are several uncertainties, which are difficult to estimate with this calculation. The prefactor also depends upon the model of the network[7] e.g., for a phantom network the prefactor depends upon the number of chains connected at a junction. In addition, only the elastically active bonds contribute to the elastic modulus. The contribution from enthalpic interaction was ignored in the above equation.[62] In the situation where a flat elastic modulus was not obtained, one can use the inflection point in the stress relaxation curve and use the relation $G'=\rho RT/M_e$, where $\rho$ is the density, R is the universal gas constant, and $M_e$ is the molecular weight between two points in entanglement. This relation also has some of the similar assumptions as before. Therefore, the determination of $a_e$ or $a_x$ unambiguously or estimating the associated uncertainty is often difficult. This experimental issues needs to be kept in consideration while performing the analysis of the data and comparison with any theory as $a_e$ and $a_x$ enter as an input to the theory.

Some physical properties of PVA,[86] such as degree of polymerization (N) ≈ 2090, the radius of gyration, $R_g \approx 16.5$ nm, entanglement molecular weight, $M_e \approx 5100$ g/mol, and the tube diameter in the melt, $a_e(1) \approx 3$ nm, will be useful for future discussions. The overlap volume fraction, $\phi^*$,which is the onset of semidilute regime is given by: $\phi^*=\frac{3}{4}M_w/(\pi N_A R_g^3) \approx 0.006$. Here, $N_A$ is the Avogadro number. Our experiments were performed with polymer concentration of at least ten times $\phi^*$. Experimentally, the transition between different concentration regimes can be determined by measuring the specific viscosity ($\eta_{sp}$) as a function of polymer volume fraction. Bercea *et. al.* had performed rheology measurements with a series of PVA solutions of different molecular weights.[84] They observed that for

all samples the transition to entanglement regime occurs at a $c^*\eta_{sp}$ =2.05, where c is the polymer concentration in g/dL. For PVA sample of same molecular weight as in our experiments, this gives the crossover at $\phi_e$=0.02. This corroborates that all our samples are above entanglement concentration.

The correlation length ($\xi$) and entanglement tube diameter ($a_e$) in solution vary according to $\xi \approx R_g(\phi/\phi^*)^{-\nu}$, $a_e \approx a_e(1)\phi^{-\nu}$, respectively, where $\nu \approx 0.76$ for good solvents. [7] In our experiments, $\xi(\phi)$ varied from 1 to 2.5 nm and $a_e(\phi)$ varied between ≈ 9-20 nm. The tube diameter is thus an order of magnitude higher compared to the correlation length.

For R=2.5 nm, the particle size (2R) is greater than correlation length, but smaller than tube diameter for all PVA concentrations. According to scaling description, these particles fall in the intermediate size range.[1] In this situation, the frictional force to particle motion originates from the segmental motion of the polymer chains with size comparable to the particle diameter. The volume fraction dependence[1] of D is given as $\xi^2$. As $\xi \sim \phi^{-0.76}$, D is expected to vary according to $\sim\phi^{-1.52}$. In an earlier publication, we showed that the diffusion of gold nanoparticles in semidilute polyethylene glycol (PEG) solutions followed this scaling relation.[3] This scaling relation, however, was not obtained for the present system. The difference is that PEG solution was a viscoelastic liquid, whereas for PVA solutions solidlike behavior dominated at long timescale. At high polymer concentrations, as in these experiments, intra- and intermolecular bond formations can significantly slow down polymer segmental motion. Different hydrodynamic and obstruction theories had been proposed to explain the volume fraction dependence of reduced diffusion coefficient in these systems.[17]

Fig. 4.3.6.a shows D vs. $\phi$ for R=2.5 nm particles in semi-log plot. The hydrodynamic models, such as by Cukier ignores topological constraints and only consider the hydrodynamic interaction (HI) between the polymer and probe.[19] It assumes that HI is screened at the length scale set by the correlation

length and gives a scaling relation of the form: $D/D_o = \exp(-R/\xi)$. By writing, $\phi$-dependence of correlation length as $\xi = b\,\phi^{-\nu}$, the fitting of the data for R=2.5 nm particles was shown with $\nu$ and b as adjustable parameters. We found $\nu \approx 0.76$ consistent with water being a good solvent for PVA at room temperature.[61] The fitting also gives $b \approx 1$ nm, which is comparable to the size of the Kuhn monomer as was reported in a previous AFM experiment.[87]

In contrast to hydrodynamic theories, obstruction models assume that a probe can move, when it finds successive openings greater than its own size, the probability of which decreases with the increasing size. They predict the reduced diffusion coefficient in terms of particle radius, gel network cross-sectional radius ($r_f$), and mesh size ($\xi$). For many biopolymer networks, $r_f$ could be a few nm or larger and cannot be ignored for small probe diffusion. No distinction is made in these models between the pore size in gel and mesh size in the semidilute solution.[17] Amsden model used a Gaussian distribution of pore size at a fixed volume fraction, which had been widely used to analyze protein diffusion in polymer and biopolymer gels.[70] It gives the following expression for the reduced diffusion coefficient: $D/D_o = \exp[-\frac{\pi}{4}(\frac{R+r_f}{\xi+2r_f})^2]$. The radius of the polymer chain, $r_f \approx 0.64$ nm for PVA.[70] Amsden theory also gives a reasonable fit for 2.5 nm radii particles with similar values for the correlation length as a function of polymer concentration as in Cukier theory[19] (Figure 4.3.6). We also tested (not shown) several other theories, including Ogston[26] and Petit models,[17] but concluded that they could not explain our data even qualitatively with any reasonable fitting parameters.

For larger size particles both hydrodynamic and obstruction model by Amsden failed, when the parameters, b and ν were fixed to the values that were obtained for R=2.5 nm particles (Figure 4.3.6 (a) &(b)). These parameters are specific to a polymer-solvent system and should not depend upon the particle size.[70]

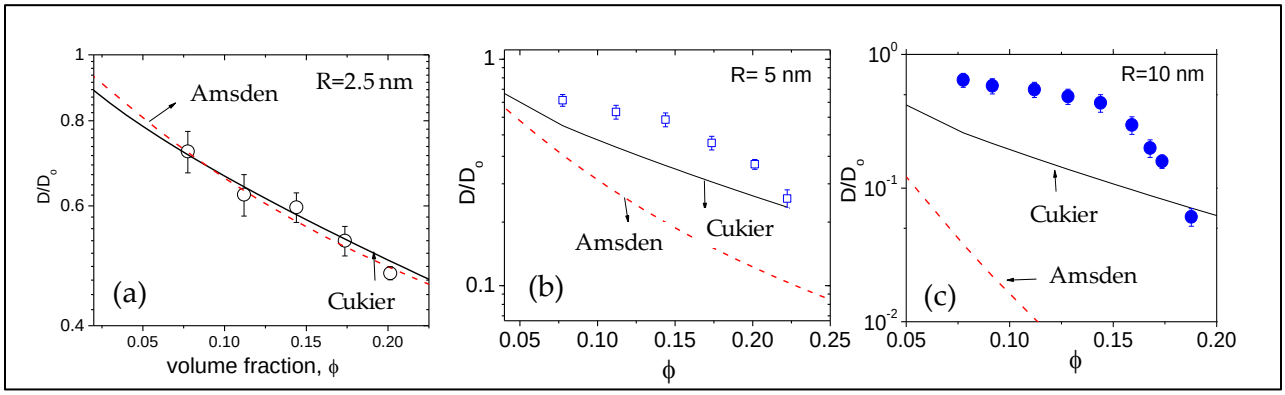


**Figure 4.3.6** Semilog plot of the reduced diffusion coefficient, $D/D_o$ as a function of PVA volume fraction in water for (a) R=2.5 nm, (b) R= 5 nm, and (c) R=10 nm particles. The fittings are with hydrodynamic Cukier theory (solid line) and obstruction diffusion model by Amsden (dashed line). For R= 5 nm and R=10 nm, we kept the solution parameters same as were obtained for R=2.5 nm particles. The poor agreement with the data suggested that the above-mentioned theories are not adequate for describing diffusion for a wide range of particle size and polymer concentrations

Michelman-Ribeiro[66] used a stretched exponential function of the form $D/D_o=\exp(-\alpha\phi^c)$ to fit their diffusion data of probe molecules in the size range of 1-12 nm in semidilute PVA solution. This scaling model is based upon Langevin-Rondelez,[88] which assumed that the semidilute solution is a transient network. They found c=0.73-0.84 for all particles within the volume fraction range of 1-8.6% w/v, which is consistent with good-solvent quality of PVA in water. The prefactor, c increases slightly with the increase of particle size.[66] Our result is consistent with their data for the lowest particle size. For the particle radius of 2.5 nm we obtained good agreement by using the exponent, $\beta\approx0.76$. As shown in Figure 4.3.7), for larger particles and higher concentrations, the fittings

significantly deviate from the data, and unreasonable values for the exponent (c) were obtained as the particle size is increased. The deviation of data from hydrodynamic models is not surprising for the higher concentration samples, as they behaved as viscoelastic solids, where this model is not expected to be valid. An alternative explanation is, therefore, needed to explain the data.

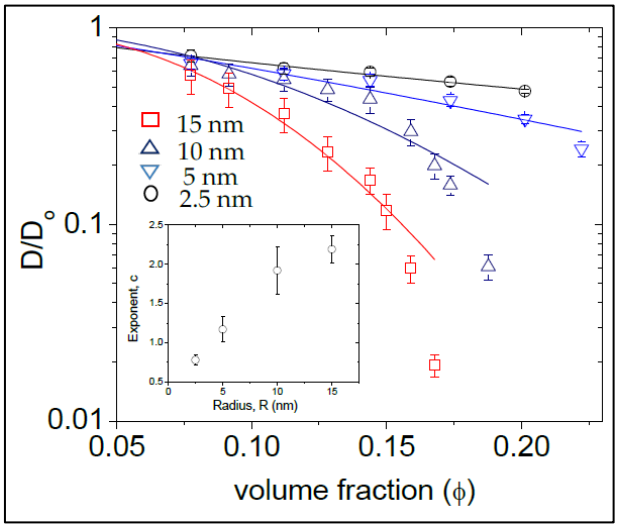


**Figure 4.3.7** Stretched exponential fittings of reduced diffusion coefficient, D/Do vs. volume fraction. The particle sizes are as indicated. The inset shows the exponent (c) as a function of particle radius (R). Except for R=2.5 particles, the exponent for higher particle sizes is not consistent with good-solvent quality of PVA in water

All PVA samples are above the critical entanglement concentration. The entanglement tube diameter, $a_e(1)$ in melt is given by[7]: $a_e(1) \approx bN_e^{1/2}$, where b is the size of Kuhn monomer and $N_e$ is the number of Kuhn monomers per entanglement strand. As determined previously, b≈0.64 nm,[87] $M_e$≈5100 g/mol and the molecular weight of a Kuhn monomer, $M_m$≈300 g/mol, which gives $a_e(1)$ ≈3 nm. The volume fraction dependence of tube diameter is given by,[7] $a_e = a_e(1)\phi^{-0.76}$ in the good solvent. In Figure 4.3.8 we showed semi-log plot of D vs. the size ratio x=2R/$a_e$. We included data for all particles, but only for $x \geq 0.5$. The data can be fitted reasonably well with a straight-line, which is given by the expression $D \approx D_p \exp(-\kappa x)$. The fitting gives, κ≈1.4 and $D_p$≈80 μm²/s. As the particle size is comparable to the tube

diameter within an uncertainty of some numerical factor, we compare the results with the recent theory of activated hopping.[1] In entangled liquids, the theory predicts that $D \approx D_h \exp(-2R/a_e)$, whereas our data indicates a slightly steeper decay of D, though $\kappa$ is close to 1. The scaling theory also gives an expression of the prefactor,[1] $D_h \approx \xi^2/\tau_e$, where the hopping step size is assumed to be of the order of correlation length, $\xi$ and the time scale, $\tau_e \approx \tau_o N_e^2$. Here, $\tau_o$ is associated with the Kuhn monomer relaxation time and is given by, $\tau_o = 6\pi\eta b^3/kT$, where $\eta$ is the solvent (water) viscosity. We estimated that $\tau_o \approx 1$ ns. Ignoring the volume fraction dependence of the correlation length, which varies between 1 to 2.5 nm in the experimental range, we obtained, $D_h \approx 15\ \mu m^2/s$, which is about a factor of 5 lower from the experimental data but nonetheless is within an order of magnitude. As mentioned earlier it was difficult to determine unambiguously $a_e$ or $a_x$ from our rheology data. Because of the exponential dependence of D on the size ratio, this uncertainty can have a very large effect. We note that using $\kappa \approx 1.4$ gives the activation barrier in Figure 4.3.8 to range from 0.7-3.2 $k_BT$. It can be argued that a process is not truly activated unless the barrier is at least greater than 2 $k_BT$. This is important to consider for quantitative comparison with theory.

The experimental points deviated strongly from the straight line in Figure 4.3.8 for both 2R=20 and 30 nm particles, when the size ratio become, $x \approx 1.7$ and $x \approx 2.5$, respectively. For both particles, the ratio corresponds to $a_e \approx 12$ nm with the associated volume fraction of $\phi \approx 0.15$. A power-law fitting of the data for larger particles at volume fractions above 0.15 showed a very high exponent ($\approx 10$). The force-based microscopic theory[59] predicts a continuous, but a very sharp, decrease of diffusion coefficient at $x \approx 1$. For entangled polymer melts, the theory predicts $D/D_{SE}$ as a function of $2R/a_e$ for different degree of entanglement, $M/M_e$. Here, $D_{SE}$ is the diffusion coefficient predicted from Stokes-Einstein relation with full melt viscosity. As $M/M_e$ is increased, the ratio $D/D_{SE}$ decreases more sharply

as the particle motion gets coupled with polymer relaxation. For a small range of $x \approx 1\text{-}2$, $D/D_{SE}$ vs. $2R/a_e$ can exhibit a power law with very high exponent. This theory is for viscoelastic liquids.

The samples above volume fraction $\phi=0.15$ are in the gel phase and the effect of physical cross-linking can no longer be neglected on particle motion. Smaller particles are not affected by the cross-linking as long as they are much smaller than the distance between two cross-linking points, but larger particles experienced an additional resistance to the motion. In Figure 4.3.8 (inset) we showed separately the data which deviated from the straight line in Fig. 4. For both particle size, the data can be fitted with an exponential function, $D \sim \exp(-\kappa x)$, however, with a much larger prefactor $\kappa \approx 7.5$. The hoping model proposed by Dell *et. al*[73] found that activation barrier for hopping is very large and average hopping time varies exponentially according to $\tau_{hop} \sim \exp(-16x)$. The prefactor to the exponential depends upon a dimensionless confinement ratio, $x_c$ at the onset of localization, which is a polymer-specific number. A very high exponent, such as $\kappa=16$, however, will be very difficult to observe experimentally for a wide range of size ratios due to limited dynamic range of experiments.

Any uncertainty in $a_e$ or $a_x$ can significantly affect any quantitative comparison with the theory because of the exponential dependence of D on the size ratio. We used the size of Kuhn monomer, $b=0.64$ nm as obtained for PVA in a previous experiment.[87] The fitting of our data in Fig. 3a gives $b \approx 1$ nm. This changes the value of $\kappa$ from 1.4 to 2.2 for the slower exponential process and from 7.5 to 11.7 for the faster decay. We can associate this range of $\kappa$ values as uncertainty originating from determination of $a_e$. These numbers may need revision if more accurate experimental determination of tube diameter or mesh size becomes possible by complementary experimental methods.

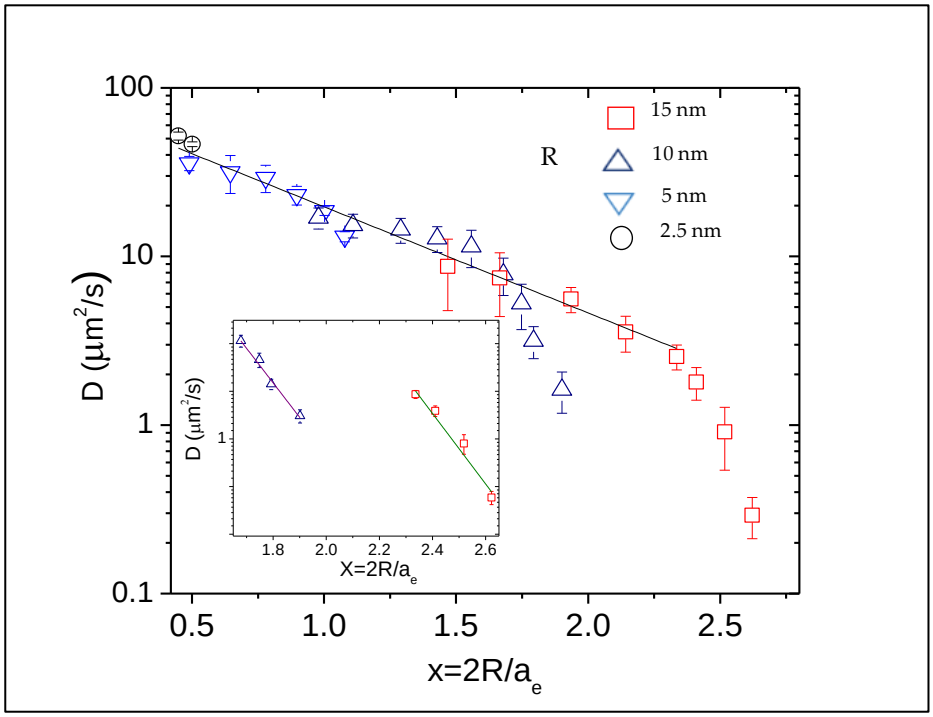


Figure 4.3.8 Semilog plot of D vs size ratio (x); i.e., particle size/tube diameter is plotted for 0.5 < x < 2.5. The solid line is according to D ~ exp (-κx), where κ≈1.4. The particle radii are as indicated. For particles with radius 10 nm and 15 nm the data deviated from the straight line at volume fraction above ϕ≈0.15. Inset: A second exponential process can be observed for particle raddi 10 and 15 nm above ϕ≈0.15 with an exponent κ≈7.5

Qualitatively different models of fluid flow, the shoving model for example, connects activation energy with the shear modus.[89] In this model the activation energy is dominated by the work done to shove around the surrounding isotropically in an elastic solid. The friction coefficient is expected to follow the exponential function, $\zeta \sim \exp(VG_e/kT)$, where V is the volume of the particle and $G_e$ is the terminal elastic modulus. In glasses and supercooled liquids, this model predicts a linear relationship between the glass transition temperature ($T_g$) and elastic modulus. To determine the effect of elastic modulus on diffusion coefficient, we assumed that friction to the nanoparticle diffusion is additive. The additive assumption was previously used to

explain the diffusion of small dye molecules in chemically cross-linked gels.[77, 90] It was observed that when a semidilute solution was cross-linked by the addition of an external moiety, diffusion slows down significantly.[90] For our system, we assumed that in addition to constraint imposed due to the presence of polymer entanglement there is an additional slowing down due to physical cross-linking. We determined the extra friction factor by calculating $\zeta = kT(1/D_{exp} - 1/D_{ent})$, where $D_{exp}$ is the experimentally measured diffusion coefficient and $D_{ent}$ is the diffusion coefficient as expected from the straight-line fitting. In Figure 4.3.9, we plotted $\zeta$ as a function of the elastic modulus (G'). Even though limited amount of data is available, they showed that $\zeta$ increases monotonically with G' and is a strong function of the particle size. For the same elastic modulus, the friction factor is enhanced by about two orders of magnitude when the particle size is increased by a modest factor of 1.5. The transition from entangled solution to cross-linked gel, thus has a significant effect on nanoparticle diffusion. However, as shown in Figure 4.3.9, the variation of friction coefficient is not exponential with elastic modulus and verification of volume dependence will require a few more particle sizes.

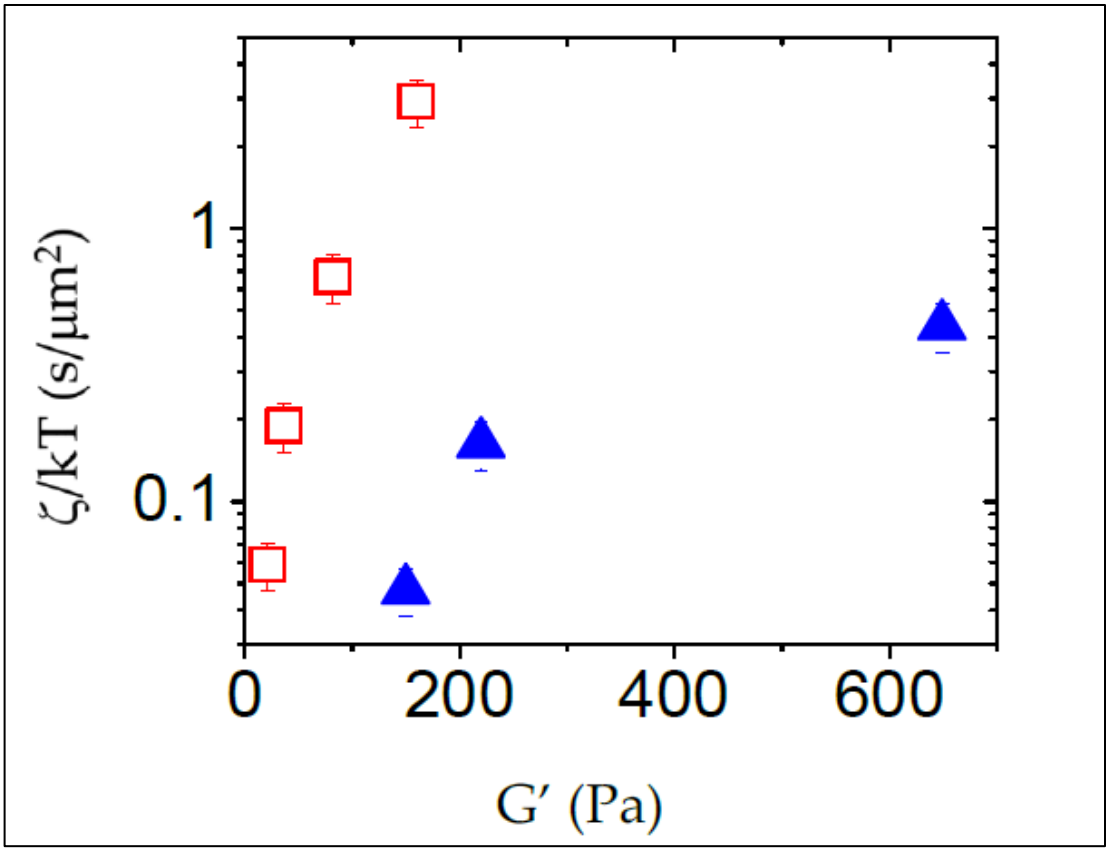


**Figure 4.3.9** The friction factor associated with the additional slowing down normalized by thermal energy is plotted as a function of terminal elastic modulus for R=10 nm (filled triangles) and 15 nm (squares)

**4.4 CONCLUSION**

We studied the diffusion of gold nanoparticles in poly(vinyl alcohol) entangled solutions and gels. The nanoparticle diameter was varied from 5 to 30 nm and PVA concentrations were selected so that the transition from entangled solution to gel can be studied. We determined that for a wide range of size ratio, $x=2R/a_e$, where R is the particle radius and $a_e$ is the tube diameter, diffusion coefficient follows a simple exponential scaling relation given by $D\sim \exp(-\kappa x)$, where $\kappa$ is of the order of unity. This functional form is similar to a recent theoretical result of activated hopping in entangled solutions. For larger particles, an additional sharp slowing down of D was observed beyond a critical volume fraction. The diffusion coefficient of this second process also follows an exponential function, but with a much

larger $\kappa \approx 7.5$. This can be compared with the theoretical prediction of $\kappa = 16$ from the force-based non linear Langevin theory. The quantitative comparison with any theory should be taken with caution. The scaling theory ignores numerical prefactors, which is an issue. The force-based theory predicts that the activation barrier is very high and hopping is negligible except for highly cross-linked gels and size ratios between 1.5 and to 2. The limited dynamic range of experimental techniques can make it difficult to verify this theory. Our rheology data did not show a pronounced terminal elastic modulus. It was difficult to accurately calculate tube diameter or gel mesh size from this data and estimate their uncertainty. As theories of hopping motion predict an exponential dependence of diffusion coefficient on the size ratio, any uncertainty with those measurements could significantly affect the value of $\kappa$. A revisit of the presented analysis thus may be needed if the polymer parameters can be determined with less uncertainties in the future. The synthesis of well-characterized cross-linked polymer solutions and gels, where tube diameter or mesh size can be varied controllably and measured unambiguously, will significantly aid any comparison with the theories. We expect that the results presented here will help to understand the size-dependent nanoparticle and molecular diffusion in polymer network and motivate farther theoretical work in polymer physics. As gels formed by many biopolymer networks are by physical cross-links, our result will also be important in the area of biological transport.

# CHAPTER 5 : NANOPARTICLE DIFFUSION WITHIN DILUTE AND SEMIDILUTE XANTHAN SOLUTIONS

## 5.1 INTRODUCTION

*The following materials have been originally published in Langmuir (2019)*[91]

The active and passive transport of nanoparticles within biopolymer solutions or gels are of significant contemporary interest.[74, 92, 93] Xanthan gum and cellulose are two polysaccharides that are widely used in various applications, including pharmaceutical, food, cosmetic, and petroleum industries due to their safety, biocompatibility, biodegradability, and unique rheological properties.[94] Xanthan gum is secreted from Gramnegative bacterium Xanthomonas campestris at the cell wall surface by a complex enzymatic process. Synthetic gums are produced by a complex fermentation process and were determined to have almost identical structure and composition to naturally occurring gums.[42, 95] The primary structure consisted of five repeated sugar units: two glucose, two mannose, and one glucuronic acid. The backbone of xanthan has the same composition as in cellulose but differ by their side-chain conformation.[95]

Due to the presence of glucuronic acid in the side chain, xanthan in water behaves as an anionic polyelectrolyte.[95] Solution studies had shown that xanthan behaves as a semiflexible polymer with short segments of single- or double-stranded helices.[42] In salt-free condition, the xanthan is stiffer and possessed more disordered conformation compared to ionic solutions. Above a certain temperature, which depends upon the ionic condition of the solution, xanthan gum undergoes a helix to random coil conformational change. This transition was shown to be reversible and accompanied by a change in viscosity.[95]

Xanthan solutions exhibit interesting rheological properties, which had been studied by several groups.[2, 42, 96-98] Steady and oscillatory shear measurements by Wyatt et al. demonstrated

that xanthan in salt-free solutions behaves as a semiflexible polyelectrolyte. The dilute solution prevails up to a concentration of $c^* \approx 70$ ppm, and the onset of entanglement effect occurs at $c_e \approx$ 400 ppm. All solutions, beyond a concentration of 20 ppm, showed shear-thinning behavior-an initial high zero shear rate viscosity decreases with increasing shear rate. The extent of shear thinning and the zero shear rate viscosity increase as the polymer concentration is increased. The onset of shear thinning moves to lower shear rate as the concentration is increased in the dilute regime and reaches a peak value at the overlap concentration, $c^*$. The dependence of viscosity can be well described by the Cross model. The shear thinning behavior was shown to follow a power law, $\eta \propto \dot{\gamma}^{-n}$, where the exponent (n) increases from 0.34 at c = 50 ppm to n = 0.58 at c = 200 ppm. The viscosity vs shear rate graph can be fitted with a power law in the shear-thinning regime and a best fit straight line in the Newtonian plateau. The inverse of the shear rate, where the two lines intersect, can be identified with the mesh relaxation time ($\tau_R$).[2] The concentration dependence of the relaxation time and zero shear rate viscosity of xanthan was found to be consistent with polyelectrolyte solutions in these experiments.

Koenderink et al. performed measurements of tracer diffusion in an ionic (0.1 M aqueous NaCl) semidilute solution of xanthan of high molecular weight ($M_w = 4 \times 10^6$ g/mol) at concentrations up to $30c^*$. They used optically anisotropic fluorocarbon spheres of diameter 190 nm and measured translation and rotational diffusion coefficients using depolarized dynamic light scattering (DDLS) technique.[42] Both translational and rotational diffusion were slowed down by the same factor as the polymer concentration was increased. Additionally, the authors performed sedimentation measurements, which showed that the sedimentation rate has a much stronger dependence of polymer concentration. They concluded that transport processes, such as

diffusion and sedimentation, differed from each other due to the time- and length-scale dependence of friction coefficient (ζ). An effective medium theory, which treats the polymer solution as a homogeneous Brinkmann fluid with hydrodynamic screening length the same as the concentration-dependent static correlation length (ξ), can explain the concentration dependence of the rotational diffusion coefficient and sedimentation rate. In contrast, the translation diffusion coefficient was best explained by assuming the presence of an inhomogeneous depletion layer around the particles. Diffusion of particles was found to be much faster compared to the expectation based from the Stokes−Einstein (SE) relation using the zero shear rate viscosity. This is expected as the polymer relaxation occurred at a much longer time scale compared to particle motion. Though the experiments extended well into the entangled regime, the authors did not distinguish between transient mesh as formed in semidilute solution vs the topological constraints as presented by entanglement in more concentrated solutions.[18] The experiments were also performed in size regimes where the particle size is greater than the correlation length in the semidilute solution.[42]

In the present paper we used particles which are much smaller than the correlation length. In combination with previous rheology measurements as performed on the same system, we showed that our experiments probed the short-time diffusion coefficient, i.e., the time scale of particle diffusion ($\tau_D$) is faster compared to the polymer mesh relaxation time scale ($\tau_R$). This means that although FCS experiments gave a single diffusion coefficient with mean square displacement (MSD) proportional to time, the diffusion time as measured is much faster compared to the matrix relaxation time. We showed that within dilute polymer solutions the diffusion coefficients of d = 5 and 10 nm particles were governed by obstruction effects presented

by the presence of relatively extended stiff rods. At semidilute solutions, an additional hydrodynamic interaction between the particle and the polymer as given by Darcy flow[42] through porous medium became operative. For larger particles (d = 30 nm), the presence of depletion around the particles could not be ignored. We used the scaling results of a recently developed self-consistent mean-field theory[99] of depletion of rods around a spherical particle to qualitatively explain the diffusion coefficient vs volume fraction results. Analysis of the data is presented by using a minimal set of adjustable parameters.

**5.2 EXPERIMENTAL SECTION**

Xanthan gum powder of molecular weight Mw ≈ $2 \times 10^6$ g/mol was donated by CP Kelco. The powder was used for sample preparation without further purification since the manufacturer certified the high purity, which is according to the standards used in the industry.[2] Tannic acid-stabilized gold nanoparticles of size 5, 10, and 30 nm were purchased from Ted Pella, Inc. We previously measured the size and polydispersity of the particles by TEM measurements. The typical polydispersity of the particles is about 15%, and their size matched well with the manufacturer-supplied information.[72] Concentrations of stock solutions of these particles were 83, 9.5, and 0.35 nM, respectively, which were further diluted in xanthan gum solutions for two-photon fluctuation correlation spectroscopy (FCS) experiments. The xanthan gum solutions (concentration ranges from 10 to 300 ppm) were prepared by dissolving the powder in deionized water followed by magnetic stirring for 1 h at room temperature. The xanthan solutions were kept undisturbed for 24 h and then mixed with nanoparticles using a vortex mixture at a speed of 50 rpm to get a homogeneous distribution of particles. The mixture was additionally kept for 4 h undisturbed for equilibration before performing FCS experiments. We performed control

experiments with FCS and a viscometer, where instead of vortex mixing the sample was only gently stirred for a longer time. We used 200 ppm polymer sample as a reference. The measured diffusion coefficient of 5 nm particles and viscosity of xanthan solution were in excellent agreement within experimental errors for samples with and without vortex mixing.

The diffusion coefficient of nanoparticles was measured using fluctuation correlation spectroscopy (FCS).[16] Femtosecond Ti:sapphire laser (Mai Tai, Spectra-Physics) was used as the excitation source, which generates 100 fs width near-infrared laser pulses of the wavelength 800 nm at a frequency of 80 MHz. A Zeiss inverted microscope (Axiovert 200) was used as the experimental platform. The laser beam was focused onto the sample through a high numerical aperture (N.A.= 1.25, 100×) oil immersion objective. The emitted photons were collected using two photomultiplier tubes (PMTs). The counts were cross-correlated to avoid artifacts from after pulsing. The autocorrelation curve was averaged for a few minutes. The well-known diffusion coefficient of rhodamine 6G in water (D = 414 $\mu m^2/s$) was used to calibrate the FCS focal volume, which gives the calibration parameters.[78] We determined that the halfwidth of the laser beam $\omega_0$ ≈ 0.3 μm and the half-height $z_0$ ≈ 1 μm. Each sample was measured six times by FCS, from which the average D and the standard deviation were calculated. The error bars in the figures where reported are statistical error from the repeated measurements. The absorption spectra of d = 30 nm gold nanoparticles were collected using a USB-650RED TIDE spectrometer in deionized water and in dilute xanthan gum solution.

## 5.3 RESULTS AND DISCUSSION

Figure 5.3.1 shows normalized autocorrelation functions with the fitting using the model of 3d diffusion with normal Brownian motion. In normal diffusion, the mean-square-displacement (MSD) is proportional to time, i.e., $\langle r^2(t) \rangle \approx t^{\alpha}$, where $\alpha = 1$. Keeping the exponent $\alpha$ as a free parameter did not improve the quality of fitting. From the fitting we can extract the diffusion coefficient (D) of the nanoparticles. Koenderink et al. observed that the translational diffusion coefficient of 190 nm particles was reduced by about 10% and 50% at a volume fraction of $10^{-4}$ ($3c^*$) and $10^{-3}$ ($\sim 30c^*$), respectively, compared to neat solvent.[42]

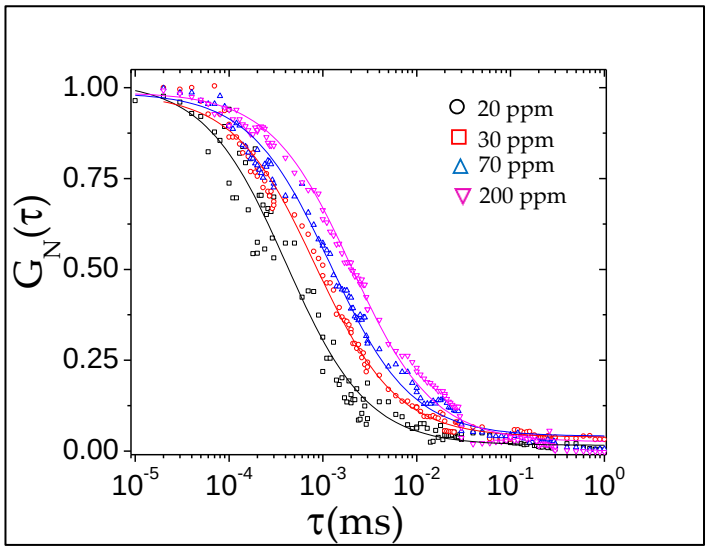


**Figure 5.3.1** Normalized autocorrelation functions for 10 nm diameter particles diffusing in xanthan solutions of different concentrations, which are indicated. The curves have been normalized so that the increase of the diffusion time with concentration becomes clear. The solid lines are fitting with 3-dimensional model of normal diffusion. Diffusion coefficients (D) were obtained from these fittings

A comparison with our data showed a much more dramatic decrease of D for all three particles studied. The measured D can be related to a characteristic diffusion time of the particles

through the laser focus $\tau_D = w_0^2/8D$, which is approximately the time, where the autocorrelation function decays to one-half of its short-time magnitude. As shown in Figure 5.3.2.a for 10 nm particles, $\tau_D$ increases from 0.43 to 3.46 ms as the polymer concentration was increased from 10 to 300 ppm. This time scale can be compared to the collective relaxation time of polymer mesh ($\tau_R$) as obtained previously by rheology measurements.[2] In Figure 5.3.2.b we plotted the relaxation time scale as a function of polymer concentration up to c = 300 ppm.

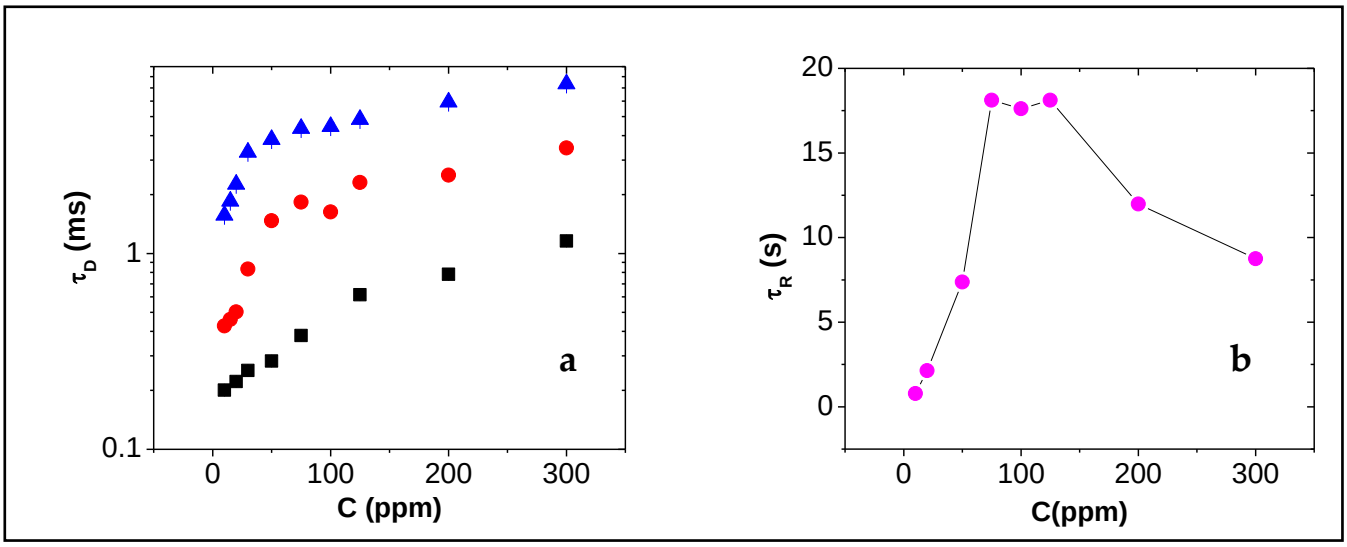


**Figure 5.3.2** (a) Diffusive time scales of particles with d=5 nm (black squares), d=10 nm (red circles), and d=30 nm (blue triangles) as a function of xanthan concentration. Error bars are indicated, but in some cases, they were smaller than the size of the symbol. (b) polymer mesh relaxation time scale ($\tau_R$) for xanthan as was determined from Ref.[2]

The relaxation time increases from 1 s at c = 10 ppm to 20 s at $c^*$ = 70 ppm and then decreases to 10 s at c = 300 ppm. The local peak near the overlap concentration is in contrast to neutral polymer solutions, where the relaxation time increases monotonically with polymer concentration.[7] However, these experimental data compared well with the theory of polyelectrolytes in salt-free solutions.[100]

In Figure 5.3.3 we plotted the ratio $\tau_D/\tau_R$ vs polymer concentration, which indicates that $\tau_D \ll \tau_R$ with a minimum close to the overlap concentration.

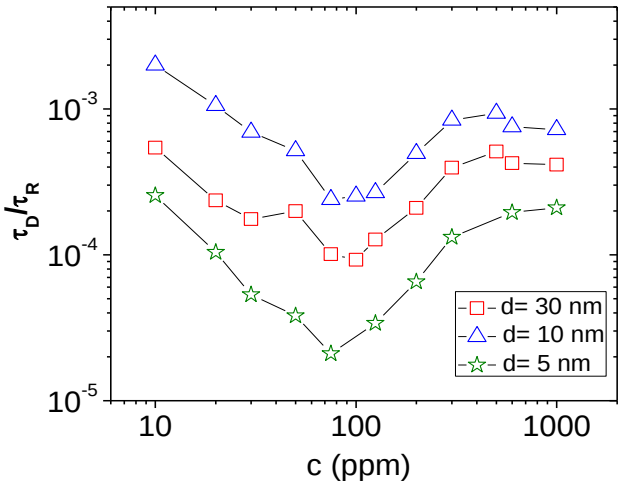


**Figure 5.3.3** The ratio of particle diffusive time scale ($\tau_D$) to xanthan network relaxation time scale ($\tau_R$). $\tau_D$ was obtained from the FCS data and $\tau_R$ was obtained from the steady state rheology data in Ref.[2] The ratio is much less than unity at all concentrations indicating that the polymer can be viewed essentially static at the time scale of particle motion

The graph showed that the diffusion time scale of nanoparticles is much smaller compared to the network relaxation time scale. Thus, the mesh remains almost static at the time scale of the particle motion, and the particle motion is not coupled to the polymer relaxation time. In this situation, the particle diffusion coefficient (D) is expected to be much faster compared to the expectation based on the Stokes−Einstein ($D_{SE}$) relation using the zero shear rate viscosity. Therefore, instead of analyzing the ratio $D/D_{SE}$, it is more appropriate to study the concentration dependence of the reduced diffusion coefficient $D/D_o$, where $D_o$ is the diffusion coefficient of the nanoparticles in neat solvent. As xanthan molecules are much larger compared to NPs, even a temporary attachment with a segment of the polymer chain will dramatically slow down the particle diffusion coefficient, which was not observed experimentally. We, therefore, rule out the

adsorption, which was further verified by noting identical absorption spectra of gold nanoparticles in water and within a solution containing xanthan (Figure 5.3.4). However, we cannot rule out transient bonding between the particles and the polymer segment at a time scale much shorter compared to the experimental time scale. The polydispersity of xanthan is another issue, which previous experiments did not address. We believe that as the particle size is much smaller compared to the polymer, the particles only feel the local polymer segments and not the effect of the whole chain, which is affected by polydispersity. The effect of polymer dispersity on the nanoparticle mobility by FCS is not systematically studied to the best of our knowledge.

Some important properties of xanthan solutions will be important for future discussion. The overlap concentration for transition from dilute to semidilute solution, where the chains begin to overlap, is $c^* \approx 70$ ppm. The transition from semidilute to entanglement concentration occurs at a concentration of $c_e \approx 400$ ppm.[2] The maximum concentration used in our experiment of 300 ppm was thus below the entanglement concentration. This concentration is also sufficiently low so that some of the complications as reported in the literature, such as aggregation, phase separation, or existence of nematic ordering, can be avoided.[42] The persistence length ($L_P$) of xanthan in ionic solutions had been reported to be ~50 nm for single helix[97] and ~120 nm for double helix.[42, 97]

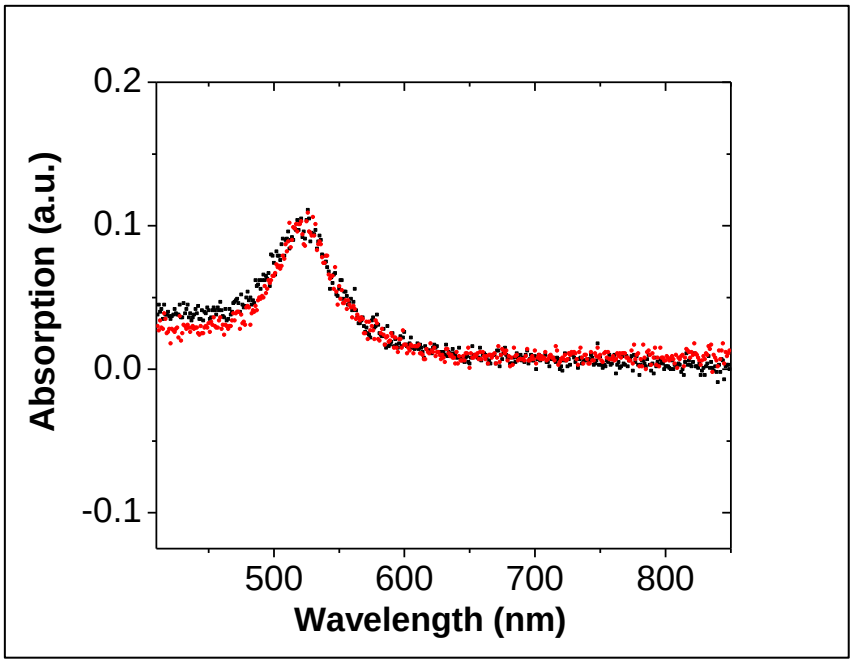


**Figure 5.3.4** Absorption spectrum of d=30 nm gold particles in water (red circles) and in 10 ppm xanthan gum (black squares) showed no shift in the absorption peak indicating no association between the gold nanoparticles and xanthan

In salt-free solutions, a good estimate of $L_p$ was not available, but it was noted that xanthan retained a high degree of rigidity.[97] The thickness of xanthan chain had been reported to be $2r_f$ = 2.4 nm, which cannot be ignored for smaller nanoparticles.[42] Each monomer of xanthan ($C_{35}H_{49}O_{29}$) has a molecular weight $M_o$ = 723 g/mol corresponding to about 2500 repeat units for Mw ≈ 2 × $10^6$ g/mol. The contour length ($L_c$) of xanthan was estimated[101] to be ~1 μm using the relation that molar mass per unit contour length is 1940 g $mol^{-1}$ $nm^{-1}$. In the isotropic state, the mesh size, or the static correlation length of the xanthan network follows the scaling relation $\xi_c = \xi_o(c/c^*)^{-0.75}$, where the power-law exponent corresponds to good solvent condition. The correlation length amplitude ($\xi_o$) for the worm-like chain model can be calculated by using the theory of Doi,[102] which gives $\xi_o \approx 70$ nm. Only at the highest concentration considered here, the mesh size ($\xi_c \approx 23$ nm) is comparable to the diameter of the biggest gold particles (d = 30 nm) (Figure 5.3.5).

The picture of polymer mesh with the static correlation length as the most important length scale is valid in the semidilute, unentangled solutions.[103] Our experiments also spanned the dilute regime. One expects a significant difference in the structure of the polymer network on

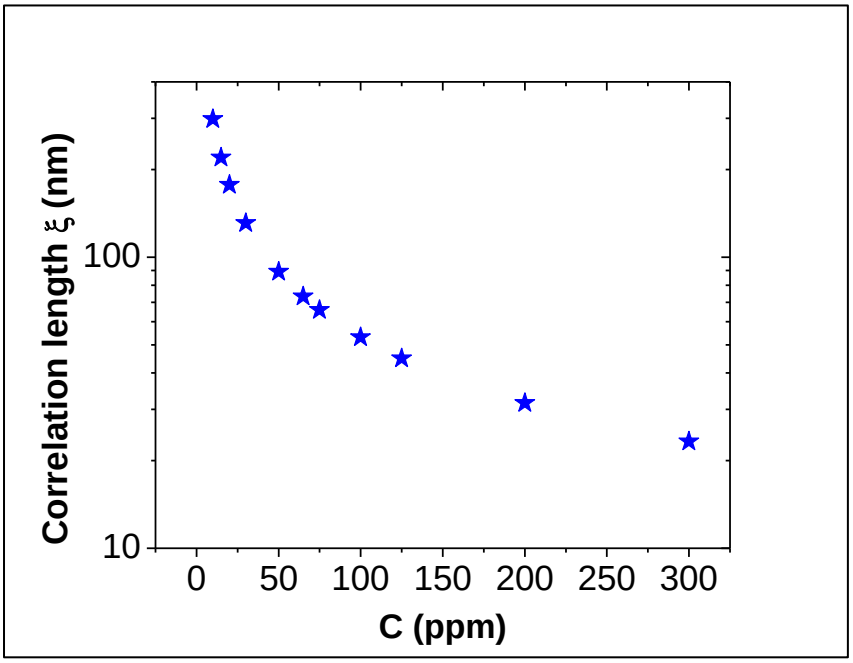


**Figure 5.3.5** Correlation length as a function of the concentration of the xanthan solution. The correlation length decreases with polymer concentration

crossing from dilute to semidilute solution. Scaling theories by de Gennes[32] and Rubinstein[18] showed the importance of different size ratios, e.g., particle size/correlation length or particle size/entanglement tube diameter in controlling the particle mobility. There are several experiments in recent years, which investigated the effect of different length scales on the diffusion coefficient,[3, 16] time dependence of mean square displacement,[56, 104, 105] and crossover among different size ratios.[72, 78, 106] According to the language used by de Gennes and Rubinstein, the particles in our experiments fall in the category of the "small" particle. The scaling theory is not applicable in this regime. As the particle size is smaller compared to the persistence length

and as concluded from Figure 5.3.3, polymer can be considered static on the time scale of particle motion; we hypothesize that particle diffusion is akin to in an environment of isotropic suspension of the thin rods.[17] We, therefore, used theories of sphere diffusion in a network of rod-like obstacles. An obstruction−diffusion theory, which ignores the hydrodynamic interaction between the particle and the rods, was proposed by Ogston.[107] The theory assumed that the solution is formed by long, thin straight fibers and that diffusion is obstructed only when the particle encounters the polymer chain. The theory gives a functional form of the reduced diffused coefficient as $D/Do = \exp(-(d + 2r_f)/\chi_m)$, where $\chi_m$ is the average spacing in a uniform random suspension of chains, $\chi_m = kL^{-1/2}$. Here, L is the length of the chain per unit volume with unit of $nm^{-2}$, which is proportional to the volume fraction of xanthan, and k is a numerical constant, whose value depends upon the geometric model used to describe the network.[17, 108] The functional form has the advantage that it depends upon a minimum number of adjustable parameters. The gold nanoparticles in our experiments are tannic acid stabilized. We need to add the thickness of this organic layer, which is ~1 nm.[78]

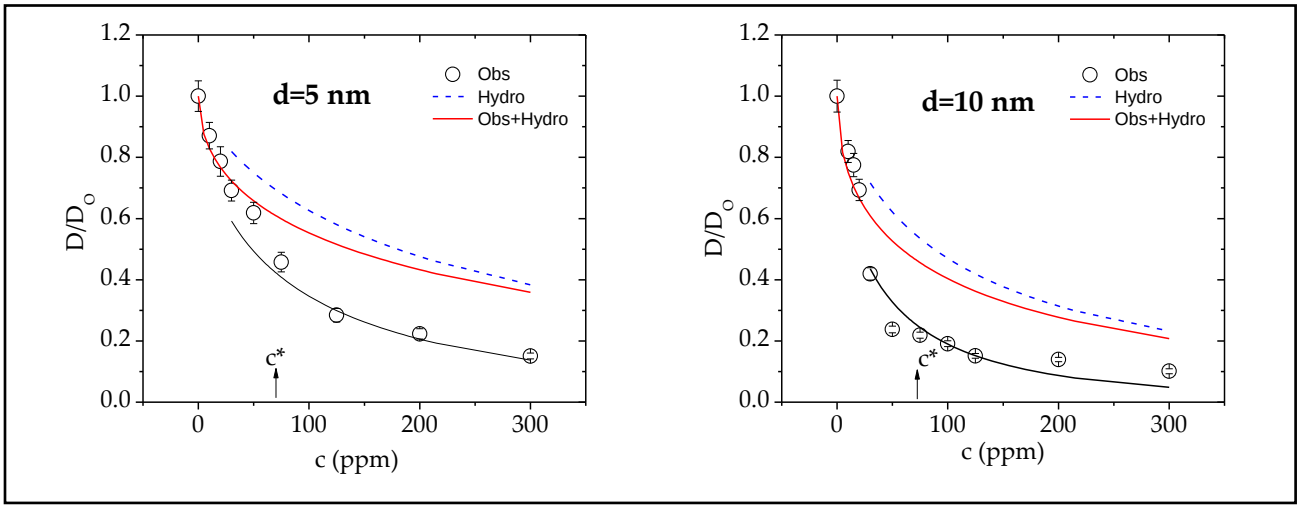

**Figure 5.3.6** The reduced diffusion coefficient, $D/D_o$, plotted against xanthan concentration, c (ppm). 1 ppm=1 mg/L. $D_o$ is the diffusion coefficient of the nanoparticles in pure water. The overlap concentration as determined from previous rheology measurements was indicated, $c^* \approx 70$ ppm. The obstruction model by Ogston is shown by the red solid line and the hydrodynamic Darcy flow is the blue dotted line. As both effects are expected to be present in the semidilute polymer solutions their combination is shown by the black solid line. The model parameters are kept same for both particle sizes, d= 5 nm and d=10 nm. The models ignore semiflexible nature of xanthan, dynamics of the network, the effect of particle diffusion in polymer motion, interaction between particles and polymer segment. These can cause deviation from the experimental data

As shown in Figure 5.3.6, for concentrations less than the overlap concentration, $c^* \approx 70$ ppm, the Ogston model can explain the reduced diffusion coefficient for 5 and 10 nm particles with $k \approx 10$. For a random network of thin, straight fibers, Ogston[107] obtained a mean value of $\langle k \rangle \approx 3$ and modal value $k_m \approx 4$. The value of k in this theory was determined without considering the thickness of the fiber and flexibility of the chain, so a perfect agreement cannot be expected.[17] For higher concentrations and in the semidilute regime the obstruction model significantly underestimates the reduction of diffusion coefficient.

The excess reduction of the particle mobility can be explained by considering that polymer chains act not only as obstacles but also as a source of hydrodynamic resistance. The solvent molecules slowed down near almost stationary polymer chains. This increases the friction drag on the probe particles and reduces the diffusion coefficient compared to the obstruction effect alone.[42] For 5 and 10 nm particles, the particle size is much smaller compared to the static correlation length. The theory developed by Dhont *et al.* considered this case, where the spheres can easily slip through the network.[109] The distortion of the microstructure due to the motion of the tracer particles is neglected in this situation. The friction coefficient is determined by the hydrodynamic interaction between the particle and the polymer. However, the theory cannot

predict a screening length, which is an adjustable parameter obtained by fitting of the experimental data.[110]

The effective medium theory, which assumed that the polymer chain consists of randomly distributed immobile scattering centers, had been put forward by several researchers. Altenberger et al. determined that the reduced diffusion coefficient depends upon the obstacle volume fraction and hydrodynamic interaction coupling constant.[111] The latter is determined by the ratio of the obstacle size to the distance of the closest approach. The authors claimed that the validity of their theory improved with decreasing coupling strength ($\ll 1$) or in the limit of point obstacles. The reduced diffusion coefficient varies as $\phi^{-1/2}$ at low volume fraction and $\phi^{-n}$ at higher volume fraction ($\phi$), which is similar to theory developed by Phillies.[74] The value of n can range from 0.5 to 0.75 depending upon the chain stiffness and solvent quality. The reduced diffusion coefficient, according to their theory, does not depend upon the size of the particle. The effect of particle size, which comes from indirect interaction of the obstacles with the mobile particle, was not considered in their theory. This specific feature of this theory, however, contradicts our experimental result, where we observed that the reduced diffusion coefficient is a function of the particle size at a fixed polymer concentration. In addition, as shown in Figure 5.3.7, the concentration dependence of the reduced mobility does not follow the power-law behavior with exponent −0.5 as predicted in the low-concentration regime.

An explicit probe size dependence of the reduced diffusion coefficient was obtained by the hydrodynamic theory proposed by Cukier, which also assumed that rods be fixed on the time scale of the sphere diffusion.[19] The scattering of hydrodynamic waves from the sphere motion interacts with the rods, which slows down the sphere motion. In dilute polymer solution, Cukier

obtained an exact result of the form $D/Do = (1 + d/\kappa + ...)^{-1}$, where $\kappa$ is the screening length and is given by $\kappa = (\eta/\zeta_n)^{0.5}$. Here, $\eta$ is the viscosity of the neat solvent, $\zeta$ is the friction coefficient of the

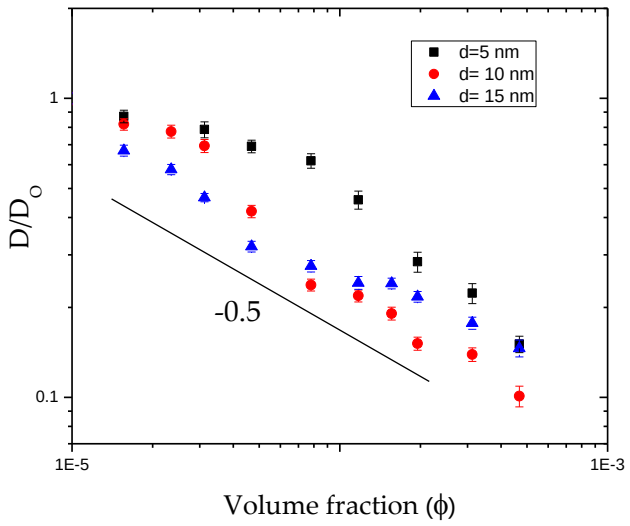


**Figure 5.3.7** The reduced diffusion coefficient is compared with prediction of model by Altenberger *et. al.* The theory predicts $D/Do \sim \phi^{1/2}$, which was not observed in our experiments. The symbols have the same meaning as in Figure 5.3.2.a

rods, and n is the number density of the rods. According to their theory, $\kappa \approx \phi^{-1/2}$, where $\phi$ is the polymer volume fraction. The friction coefficient of rods is given by $\zeta = 3\pi L\eta/\ln(L/b)$, where each molecule is modeled as a prolate ellipsoid with the major and minor axis, L and b, respectively ($L \gg b$). The above expression of $D/D_o$ is exact for dilute polymer concentrations.[17] At semidilute concentration, an ansatz was used by Cukier to obtain $D/D_o = \exp(-d/\kappa)$, which reduces to exact functional form for $d/\kappa \ll 1$. The exponential function was shown to explain the concentration dependence of the reduced coefficient data well for many polymer systems. Specific to xanthan solutions, experiments by Jamieson[112, 113] with microspheres of radius 1.1 μm diffusing in xanthan solution of $M_w = 2 \times 10^6$ g/mol (L = 1.5 μm, b = 2 nm) at a concentration of 0.1% (w/v) the

experimental value of reduced diffusion coefficient 75 matches well with Cukier theory prediction of 84. The functional dependence of $D/D_o$ on concentration, however, was not verified in those experiments. Note that the functional form as given by Cukier is similar to the obstruction theory developed by Ogston et al., which is purely geometric and does not rely on hydrodynamic screening. The exponential dependence of $D/D_o$ is given by the same functional form $\alpha R\phi^{1/2}$, where the prefactor ($\alpha$) depends upon the model used.[17]

Alternate models exist on the assumption that spherical particles embedded in a homogeneous porous medium consist of fixed frictional obstacles. The flow through the porous medium is described by a modification of Darcy's equation. Phillips *et al.* used a different approach than Altenberg et al. to calculate the friction coefficient using Brinkman's equation, which combines Darcy's law for flow in a porous medium with the usual low Reynold numbers approximation of the Navier−Stokes equation.[108] The ratio of the mobility in Brinkmann fluid to neat solvent is given by $D/D_o = [1 + (d/\kappa) + 1/3(d/\kappa)^2]^{-1}$, where $\kappa^2$ is the hydrodynamic (Darcy) permeability of the porous medium and it measures the resistance of the polymer network to a fluid flow.

According to the scaling theory developed by de Gennes, a semidilute solution can be viewed as a transient network, where the hydrodynamic interaction gets screened at a length scale determined by the correlation length ($\xi$).[103] The correlation length varies with concentration according to $\xi \approx c^{-0.75}$, the exponent corresponding to good solvent condition.[7] Koenderink et al. identified $\kappa$ with the static correlation length ($\xi_c$).[42] However, there is disagreement in the literature about the difference between the static ($\xi_c$) and hydrodynamic ($\xi_H$) screening lengths. Though some experiments suggested that they are almost identical within a numerical factor,

other theories and experiments observed a significant difference between them.[114-117] Wiltzius et al. experimentally observed that the ratio $\xi_c/\xi_H$ increased from 1 to 4 and the ratio $\xi_H/R_H$ decreased by a factor of 10 as the polymer concentration is increased in the semidilute solution.[116] $R_H$ is the hydrodynamic radius of the polymer.

Analysis of the hydrodynamic effect neglected the effect of "obstacles" presented by the polymer chain. Conversely, the obstruction models ignore the hydrodynamic resistance to the solvent flow presented due to the presence of the nearimmobile chains. As in most systems both obstruction and hydrodynamic effects can be assumed to be both present, it was proposed that effects of obstruction and hydrodynamics are multiplicative so that the reduced diffusion coefficient is a product of the two $D/D_o = (D/D_o)_{hydro}(D/D_o)_{obst}$.

In Figure 5.3.6 we have shown the result, where both effects were considered. A reasonably good agreement with experimental results was obtained with the hydrodynamic screening length in Darcy flow varying according to $\kappa \approx 25c^{-0.75}$ for both 5 and 10 nm particles. The amplitude of $\kappa$, however, is smaller compared to $\xi_o$, which is ~70 nm. However, as noted earlier, there is disagreement whether the correlation length and the hydrodynamic screening length are strictly equal. The qualitative agreement is satisfactory as the models used considered only static rods and do not consider the effect of rod mobility on probe diffusion.[102] It had been established both experimentally[3] and theoretically[18, 71] that the mobility of the particles can also affect polymer dynamics. These two effects need to be considered in a self-consistent manner.[59] Though there had been progress for flexible polymers, currently no theories exist for NP diffusion in semiflexible polyelectrolyte solutions.

For the largest size particles (d = 30 nm), our data is consistent with the obstruction model in the low concentration regime with the same value of κ as was used for other particle sizes, but it overestimates the reduction of the diffusion coefficient in the semidilute solution (Figure 5.3.8). We interpret this as an indication that polymer segments are depleted near the particle surface.

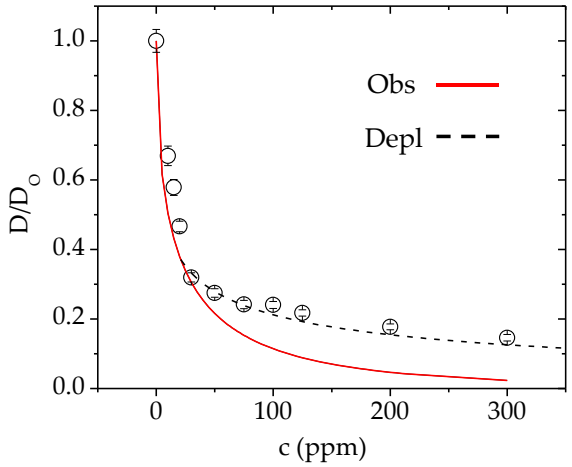


**Figure 5.3.8** $D/D_o$ plotted against xanthan concentration, c (ppm) for d=30 nm particles. The fitting with the obstruction model of Ogston is shown by the red solid line using the same model parameters as in Figure 5.3.6 The fitting overestimates the reduction of the diffusion coefficient in the semidilute solution. The dashed line is a fitting with the depletion theory, where we assumed that depletion layer thickness follows a scaling relation with exponent $\nu \approx 0.42$

In general, one can expect a gradual change of the polymer segmental density, being zero at the particle surface to the average bulk value of polymer concentration far away from the surface.[42, 109] For particles, which are much smaller compared to polymer persistence length, the free energy cost to insert the particle is high, so a depletion effect can be neglected. In this case, the insertion free energy is dominated by the interfacial term, which originates from the energy penalty to create an inhomogeneous distribution of polymer density near the particle.[99] However, for d = 30 nm particles, the depletion effect can be important. Tuinier et al. considered a simple

model where the polymer density is zero within the depletion layer and the particles feel solvent viscosity, while at the outside of it the segmental density is equal to the bulk value and the particle feels full bulk viscosity.[109] The imposed viscosity gradient generates a slip effect. They assumed that the relaxation of the polymer is fast so that the particle motion does not deform the depletion layer. By using Stokes' stream function theory, they derived an analytical form of the frictional force. The theory gives an algebraic expression of the reduced diffusion coefficient as a function of dimensionless parameters, $\varepsilon = 2\delta/d$ and $\lambda = \eta_s/\eta_m$ which is given as $D/Do = Z(\varepsilon,\lambda)/Q(\varepsilon,\lambda)$. Here, $Z(\varepsilon,\lambda) = 2(2 + 3\lambda)(1 + \varepsilon)^6 - 9(1 - \lambda/3 - 2\lambda^2/3)(1 + \varepsilon)^5 + 10(1 - \lambda)(1 + \varepsilon)^3 - 9(1 - \lambda)(1 + \varepsilon) + 4(1 - \lambda^2)^2$ and $Q(\varepsilon,\lambda) = 2(2 + 3\lambda)(1 + \varepsilon)^6 - 4(1 - \lambda)(1 + \varepsilon)$. Here, $\eta_m$ is the bulk viscosity, $\eta_s$ is the solvent viscosity, and $\delta$ is the thickness of the depletion layer. The theory correctly predicts two limiting cases. In situations where the particle is much bigger than the depletion layer, i.e., $\varepsilon \ll 1$, the particles feel closer to bulk viscosity, and where it is much smaller than the depletion layer ($\varepsilon \gg 1$), the particles feel solvent viscosity. Intermediate-sized particles feel an effective viscosity, which is between the solvent and the medium viscosity and is a complex function of $\varepsilon$ and $\lambda$ as given by the above expression. These calculations are for flexible polymers.

For semiflexible and rod-like polymers near spherical particles, Ganesan *et al.* developed a self-consistent mean field theory, which can be used for a wide range of polymer concentration.[99] The theory gives the thickness of the depletion layer ($\delta$) as a function of particle size, static correlation length in the semidilute solution ($\xi_c$), and persistence length ($L_p$) of the chain. In the situation where $\xi_c > L_p$, the correlation length determines the thickness of the depletion layer. In the opposite limit, the polymer segmental density near the particle is a complex function of $\xi_c$ and $L_p$. Their calculation showed that $\delta$ follows a complex scaling law determined

by the concentration of the polymer and size of the nanoparticles. For particle size smaller than the persistence length, as for our system, Ganesan *et al.* observed a scaling relation of the form $\delta/d \approx (d/\xi)^{-\nu}$, where $\nu$ is an exponent with a value less than 1. The value of the exponent decreases gradually as the ratio $d/L_p$ decreases.[99]

In Figure 5.3.6 we have shown the experimental result in the semidilute solution for d = 30 nm particles. For the static correlation length we used the scaling form[7] $\xi = \xi_o(c/c^*)^{-0.75}$. Within the small range of polymer concentration, our result indicates that the exponent $\nu \approx 0.42$. The exponent is 1 for a flat surface, where the thickness of the depletion layer follows the static correlation length. The much smaller value for the exponent $\nu$ indicates a strong effect of the surface curvature in the depletion layer thickness. Assuming the persistence length of 120 nm for xanthan, $R/L_p \approx 0.125$. The mean-field results[99] suggested a decrease of $\nu$ from 0.89 to 0.73 as the ratio $R/L_p$ decreases from 2 to 0.04. The lower experimental value of $\nu$ in our experiment, however, requires further verification as the results were obtained for a single-sized particle and a limited range of concentration. Additionally, in our situation, the structural relaxation of the polymer is slower compared to the particle motion. Thus, deformation of the polymer due to the motion of the particle is not equilibrated to form a symmetric depletion layer. The particles feel an inhomogeneous depletion layer, which changes as the particles move. The theoretical result for this situation with a semiflexible polymer, however, is currently unavailable.

**5.4 CONCLUSION**

Diffusion of nanoparticles in a semiflexible polymer is governed by an obstruction effect in the dilute solution. A model proposed by Ogston, which approximated the chain as thin long straight fibers, can explain the concentration dependence of the reduced diffusion coefficient in

this regime. Hydrodynamic interaction between the polymer and the particle makes a significant contribution to particle mobility in the semidilute regime. The concentration dependence of the screening length follows the same power law as the static correlation length. For a larger sized particle, the depletion effect is important. We found a scaling form for the depletion layer thickness that varies as (correlation length) 0.42. It is different than the flat surface, where the thickness is proportional to the correlation length. The smaller exponent demonstrates the effect of surface curvature on polymer density profile near a nanoparticle. As many biopolymers (e.g., DNA, actin, etc.) are semiflexible, the results presented here will be important to understand how semiflexible or rod-like polymers interact with spherical nanoparticles.

# CHAPTER 6: DIFFUSION OF SMALL CHARGED NANOPARTICLES WITHIN A SEMIDILUTE POLYELECTROLYTE SOLUTION

## 6.1 INTRODUCTION

In the recent years, there is a growing interest to understand the passive and active transport of particles and biomolecules in complex fluids, including polymer solutions and gels, cytoplasm, and biological networks. Diffusion is the most important passive transport process driven solely by thermal energy, $k_BT$ where $k_B$ is the Boltzmann constant and T is the absolute temperature. The theories developed by Langevin, Einstein, and Smoluchowski considered situations where a large particle moves within a continuum fluid.

In particular, for spherical particles much celebrated Stokes-Einstein (SE) equation relates the diffusion coefficient with the particle radius (R) and the bulk viscosity ($\eta_o$) of the medium. The predicted diffusion coefficient from SE relation using the zero shear bulk viscosity matches well with experimentally measured quantity and is a standard method to determine the particle size by measuring its' diffusion coefficient within a small molecule solvent of known viscosity. An underlying assumption of SE relation in equilibrium systems is large separation of time scales between solvent motion and the particle dynamics. For a micrometer sized particle diffusing in water this condition is easily met. The typical solvent motion occurs in the picosecond time scale, where the Brownian time scale ($\tau_B$) is of the order of a microsecond for a particle of size 1 μm.

If the size of the particle approached to the solvent molecules itself, deviation from continuum theories is expected and many-body correlation comes into play. An example of this situation, which has drawn a lot of interest within the last few years is the diffusion of nanoparticles (NPs) within polymer solutions and melts. Sophisticated theories, including scaling theory[18, 32] force-based statistical dynamical theory,[71] mode-coupling theory[41, 51, 118] have been

developed, and molecular dynamics simulations have been performed.[40, 55] In semidilute polymer solutions, experiments found that the diffusion of NPs can be 2-3 orders of magnitude faster compared to the expectation based upon SE relation if the particle size is smaller than the radius of gyration of the polymer chain ($R_g$).[3, 50] The deviation from SE relation increases as the ratio $R/R_g$ decreases.[119] A transition from subdiffusive to a diffusive behavior had also been observed by some research groups, which can explained in terms of a depletion layer around the particles[119] The scaling theory also predicts a time-dependent viscosity, which gives subdiffusive motion of nanoparticles, which crosses over to diffusive motion at a longer time scale.[18] Fewer studies in heavily entangled polymer solutions and melts discuss where topological constraints created by the entanglement of the chains control the flow of the bulk[53] The available theories and experiments indicated that the tube diameter ($d_t$) is the important length scale and if the particle size is below the tube diameter, significantly enhanced diffusion was observed[120] The deviation from SE relation is a strong function of $R/d_t$ and SE relation is obeyed when the ratio $R/d_t$ approaches a factor of 8-10.[71, 72] However, these results have been primarily studied with neutral polymers.

The studies of nanoparticle diffusion within charged polymers or polyelectrolytes are limited. The dynamics and rheological properties of polyelectrolytes are interesting and rich as noted in pioneering theoretical studies by Colby,[11] Rubinstein,[7, 9, 100] and MuthuKumar,[121] among others.[122-126] In polar solvents, such as in water, the polymer chain becomes charged with free counterions diffusing freely in the solution in the dilute limit. In salt-free solution, the Debye length (approximately 0.5 μm) is typically larger than the size of the polymer for moderate molecular weight ($M_w$) chains.[9] Therefore, monomers of the chain interact with each other

through an unscreened Coulomb interaction. Due to electrostatic repulsion among the monomers along the backbone, the polyelectrolytes adopt an elongated ellipsoidal conformation.[9] This makes the transition from dilute to semidilute concentration regimes to occur at a lower concentration compared to linear polymer of similar $M_w$.[11] Theoretical and experimental work suggest that semidilute regime persists for a wide range of polymer concentrations.[2, 11] The entanglement dynamics comes into play only at a much higher concentration, which can be orders of magnitude larger than the overlap concentration[11, 44, 127] in neutral polymers.[127]

The most important length scale in semidilute polymer solution is the correlation length ($\xi$),[9, 11] which sets the range of Coulomb, hydrodynamics, and excluded volume interactions.[127] The correlation length is highest at the overlap concentration, but decreases with increasing polymer concentration following a power law.[127] In good solvents, for neutral polymers, $\xi \sim \phi^{-0.76}$ and for polyelectrolytes $\xi \sim \phi^{-0.5}$, where $\phi$ is the polymer volume fraction. Experimentally, Lin *et. al.* measured diffusion coefficient of polystyrene (PS) particles of size 38 nm by using quasielastic light scattering within a solution of poly(acrylic acid) (PAA) of molecular weight, $M_w = 3 \times 10^5$ g/mol in water. They observed a non-monotonic change of D as a function of PAA concentrations, which they interpreted as a change of the apparent hydrodynamic size of the particles. The analysis of data was complicated, as in the light scattering experiments both polymer and particle can contribute to scattering, which become worse as the polymer concentration increases.[128] More recently, Poling-Skutvik *et. al.* used a semidilute solution of partially hydrolyzed polyacrylamide and PS particles in the size range of 300 nm to 2 μm.[44] The experiments covered the size ratio of $2R/\xi \approx 0.5\text{-}150$, where they observed that reduced diffusivity ($D/D_o$) follow a power law with $2R/\xi$ with exponent of -2. The authors compared the ratio, $D/D_{SE}$, which is always greater than 1 and

depends upon the ratio of $R_g/R_o$ and polyelectrolyte concentration. $D/D_{SE}$ increases as the ratio $R_g/R_o$ decreases and the polymer concentration increases.[44] The latter results were in accord with neutral polymer solutions.[3] Sozanski *et. al*. used molecular probes of size ranging from ~0.5 nm (rhodamine dye) to 7 nm (dextran) in high salt solution.[119] Under the experimental conditions, the Debye screening length was much smaller than the correlation length and therefore chains interact through screened Coulomb interaction. At the large length scales, the diffusion of the particles followed a scaling relation, which is not much different compared to that of neutral uncharged polymer.

A distinguishing aspect of this article is the use of much smaller nanoparticles (size range=5 nm to 40 nm), which complements the earlier experimental studies. The size ratio, $2R/\xi$ in our experiments ranges from 0.05 to 0.85, which thus corresponds to small particle size-range according to the definition of scaling theory.[18] The size of the particles is also similar to the average size of many proteins, biomolecules, and viruses. The particles also carry a net electric charge, similar to many biomolecules in their in vivo state. The results presented here will be important to understand how nanoparticles move through a charged and crowded macromolecular environment, which will have ramifications in fields ranging from biophysics and polymer science to drug delivery.

**6.2 EXPERIMENTAL METHODS**

Poly acrylic acid (PAA) powder ($M_W$ ~ $10^6$ g/mol) was purchased from Polyscience Inc, Tannic acid stabilized (radius, R =2.5 nm, 10 nm, 20 nm) gold nanoparticles (NPs) were obtained from Ted Pella, Inc. The concentration of 2.5 nm, 10 nm, and 20 nm NPs as received in the stock solution in water were 83 nM, 0.8 nM, and 0.13 nM respectively, which were further diluted in

distilled deionized water for two-photon fluctuation correlation spectroscopy (FCS) experiments. The nanoparticle concentration was adjusted such that a good signal-to-background ratio was obtained. PAA powder was dissolved in 90 $^0$C in a temperature bath to prepare four different concentrations with volume fractions, $\phi$= 0.37x10$^{-3}$, 0.72x10$^{-3}$, 1.09x10$^{-3}$, and 1.48x10$^{-3}$. We reported concentrations in terms of volume fraction as this is a common practice for neutral polymers. Different scaling relations are also expressed in terms of volume fractions. The conversions among volume fraction, weight fraction, and mg/ml are given in Table 6.2.1.

**Table 6.2.1** Concentration calculations for PAA samples

| **Weight fraction (w/w)** | **C (kg/m$^3$)** | **Volume fraction (v/v)** |
|---:|---:|---:|
| 0.00042 | 0.42 | 0.00037 |
| 0.00083 | 0.83 | 0.00072 |
| 0.00125 | 1.25 | 0.00109 |
| 0.0017 | 1.72 | 0.00148 |

The conversion requires the density of PAA, which we took as 1.150 g/ml at 25 $^0$C as reported by Lin *et. al*.[128] PAA samples were ultrasonicated for 30 minutes after adding nanoparticles to make a homogeneous polymer solution. We performed viscosity measurements, both before and after the nanoparticles added to ensure that sample preparation method did not degrade the polymer. The measurements yielded nearly identical results. The sample preparation was done using distilled deionized water (18 MΩ-cm Millipore), but the presence of $H^+$ ions from the dissociation of PAA and the absorption of atmospheric $CO_2$ makes the solution acidic with the pH ranging from 4.2 (for $\phi$=0.37x10$^{-3}$) to 3.4 (for $\phi$=1.48x10$^{-3}$) measured using Orion 3 Star pH meter (Thermo Scientific, Inc.). Commercially available (Fisher Scientific) 8 chambered cover

glass of thickness 0.13 - 0.17 mm was used as a liquid cell for FCS experiments. An Axiovert 200, Zeiss inverted microscope served as an experimental platform, and the cell was mounted on the mechanical stage of the microscope. Femtosecond Ti:sapphire laser (Mai Tai, Spectra-Physics) of near infrared light (wavelength=800 nm) with the pulse width of 150 fs at a repetition rate of 80 MHz was focused on the sample through a high numerical aperture (N.A.=1.25, 100x) oil immersion objective.[78] The power at the sample stage was kept below 1 mW. The emission is collected with two single-photon counting modules placed after a 50-50 beam splitter. The counts are cross-correlated, which eliminates the artifacts associated with photomultiplier tube (PMT) after-pulsing. From calibration, we determined that the half-width of the focused laser beam, $\omega_0$=0.3 μm and the half-height, $z_0$=1 μm by using a common dye rhodamine 6G, whose diffusion coefficient in water is well-known (D=414 μm$^2$/s). Each correlation curves were collected for about 15 minutes and were repeated for at least six times from which the average D and its standard deviation were determined.

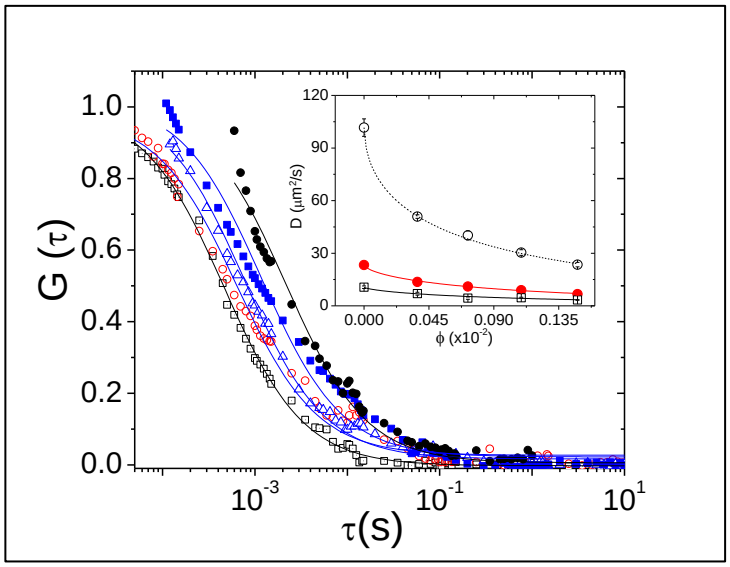

**Figure 6.2.1** Normalized autocorrelation functions are shown for four different concentrations of poly acrylic acid (PAA) in water: (squares) 0%, (circles) $3.7x10^{-4}$, (triangles) $7.2 \times 10^{-4}$, (filled squares) $1.09x\ 10^{-3}$, (filled circles) $1.48 \times 10^{-3}$. The measurements were for gold nanoparticles of radius 10 nm. The solid lines are fittings with autocorrelation function as described in the experimental techniques section. Diffusion coefficients (D) as determined from the fittings were listed in Table 6.2.2. The inset shows the average D as a function of volume fraction for all three particle radii: (circles) 2.5 nm, (filled circles) 10 nm, (squares) 20 nm. The error bars are standard deviation from at least 6 measurements. The fitting in the inset is according to stretched exponential function. Fitting parameters are listed in Table 6.2.3.

**Table 6.2.2** Experimental diffusion coefficients D of AuNPs (in $\mu m^2/s$) as measured by fluctuation correlation spectroscopy (FCS)

| | R=2.5 nm | | R=10 nm | | R=20 nm | |
|---|---|---|---|---|---|---|
| **Φ ($x10^{-3}$)** | **D** | **δD** | **D** | **δD** | **D** | **δD** |
| 0 | 102 | 5 | 23 | 1 | 11 | 1 |
| 0.37 | 51 | 1 | 14 | 1 | 7 | 1 |
| 0.72 | 40 | 3 | 11 | 1 | 4 | 1 |
| 1.09 | 30 | 2 | 9 | 0.4 | 5 | 0.3 |
| 1.48 | 23 | 1 | 7 | 1 | 3 | 0.2 |

**Table 6.2.3** Fitting parameters β and υ using Phillies equation: $D=Do\ exp(-\beta\phi^{\upsilon})$

| R (nm) | υ | β |
|---|---|---|
| 2.5 | 0.53 | 4.00 |
| 10 | 0.64 | 4.10 |
| 20 | 0.68 | 4.41 |

In Figure 6.2.1 we showed the correlation functions with fittings for R=10 nm particles in four different PAA concentrations and the inset shows D as a function of volume fraction. Rheological measurements were performed on TA Instruments DHR3 rheometer with a 20 mm parallel plate with a solvent trap. Steady state flow and small-amplitude oscillatory shear experiments were performed using standard protocols.[98] Linear viscoelastic region was determined by conducting a strain sweep at 1 Hz. Frequency sweeps were performed at fixed strain within linear viscoelastic region.

DLS experiments were performed with an ALV compact goniometer system (Model ALV/SP-125, Germany) equipped with an avalanche photodiode detector and a digital correlator to determine the hydrodynamic size of PAA. Rheology measurements were performed without any nanoparticles added. As the concentration of NPs in FCS experiments was much less than nM, we expect no perturbation of the system with the particles. Control experiments ruled out any adsorption of polymers on the particles. The hydrodynamic size of the particles (as measured by FCS) did not change as a function of time when they were kept for several hours in the solution. This is also expected as both particles and polymers are similarly charged and there is a repulsive interaction between them.

**6.3 RESULTS AND DISCUSSION**

PAA is a weak polyelectrolyte. In water PAA acquires a negative charge, where the degree of ionization depends sensitively upon the pH of the solution. For example, about half of the PAA units gets charged at pH=6.5.[129] Under our experimental conditions where the pH of the solution was ranging from 3.4 to 4.2, previous studies had determined that ionization is between 7-10%.[129] The corresponding Debye screening length ranges between ≈23 nm to 55 nm (Table 6.3.1), which is shorter compared to the size of the polymer. So the charge repulsion among the monomers cannot be ignored and it plays a role on the conformation of the PAA in dilute solution. The picture that emerges is a weak polyelectrolyte interacting with its monomers through a long-range electrostatic repulsion. In this situation, the chain adopts a somewhat elongated conformation similar to directed random walk, where the length along the chain axis depends upon the number of monomers and the strength of electrostatic interaction, while in the perpendicular directions the chain adopts a random walk.[11]

**Table 6.3.1** Calculated Debye screening length

| Volume fraction $\Phi$ ($x10^{-3}$) | pH | $[H^+]$ ($mol/m^3$) | Debye screening length, $\kappa^{-1}$ (nm) |
|---|---|---|---|
| 0.37 | 4.20 | 0.063 | 54.6 |
| 0.72 | 4.10 | 0.080 | 48.7 |
| 1.09 | 3.61 | 0.25 | 27.7 |
| 1.48 | 3.43 | 0.37 | 22.5 |

DLS provides an orientation-averaged hydrodynamic size of the polymer. With a dilute concentration of PAA (a factor of 10 below the overlap concentration), we observed a single exponential relaxation at a scattering angle of $25^0$, which gives the hydrodynamic radius of PAA, $R_h \approx 78$ nm (Figure 6.3.1). We used the relation, $R_g/R_h=1.45$[130] to determine the radius of gyration, $R_g \approx 113$ nm. An alternate, and sometimes claimed to be more accurate determination of $R_g$ is through intrinsic viscosity ([η]) measurements, which is a measure of polymer's contribution to the viscosity at a very dilute solution (in the limit of $\phi \rightarrow 0$). We used a falling ball viscometer and using well-known relation, $[\eta] = \left(\frac{5}{2}\right)\left(\frac{4\pi N_{av} {R_g}^3}{3M_w}\right)$, we determined, $R_g \approx$ 105 nm. This is similar (within a few percent) of the value obtained from DLS measurements and was used to calculate the overlap concentration and correlation lengths at different concentrations.

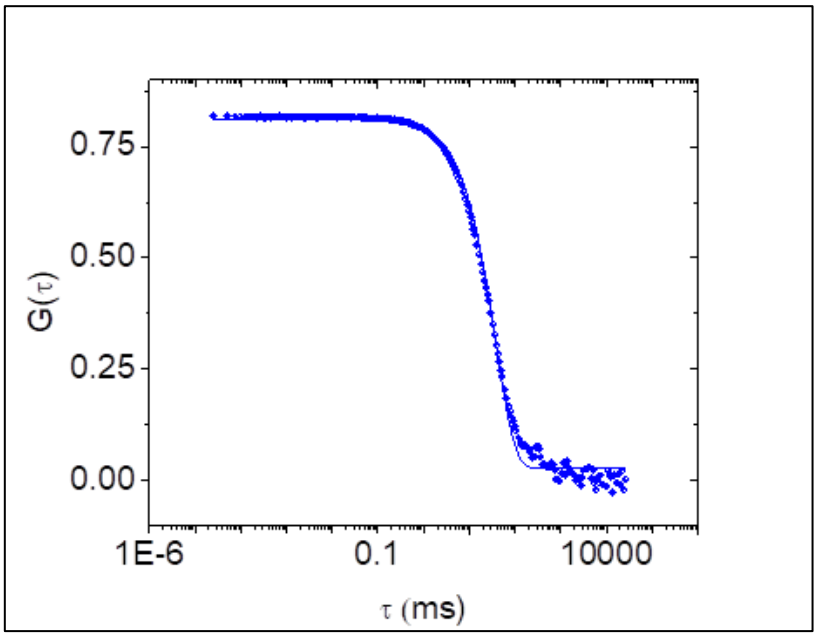


**Figure 6.3.1** Autocorrelation function for PAA at volume fraction of $8.7\times10^{-6}$. The measurement was taken at $25^0$ scattering angle. The fitting (solid line) is with a single exponential function.

The transition from dilute to semidilute concentration occurs when the chains begin to overlap.[106] Because of the extended chain conformation for polyelectrolytes, the transition occurs at a much lower concentration compared to neutral polymers.[11] The overlap concentration was determined by using the relation, $c^*=M_w/(\frac{4}{3}\pi R_g^3 N_A)$, where $M_w$ is the molecular weight and $N_A$ is the Avogadro number. By using $R_g$ as obtained from the intrinsic viscosity measurements, we calculated $c^*\approx0.34\times10^{-3}$ g/ml, corresponding to a volume fraction, $\phi^*\approx2.9\times10^{-4}$. So all our measurements were performed in the semidilute regime and volume fraction ranges from $1.3\phi^*$ to $5\phi^*$. The entanglement concentration ($c_e$) for polyelectrolytes is a few orders of magnitude higher than c* and has not been investigated in this study.[11, 44, 127]

The correlation length ($\xi$) is the most important length scale in semidilute solution, which is a measure of average distance of a monomer of one chain to the monomer of the next chain.[9]

For neutral polymers in good solvent, $\xi \sim \phi^{-0.76}$, but for polyelectrolytes, the correlation length scales as[11] $\phi^{-0.5}$. The calculation of correlation length was shown in Table 6.3.2, which varies from 95 nm ($\phi$=0.37x10$^{-3}$) to 47 nm ($\phi$=1.48x10$^{-3}$).

**Table 6.3.2** Calculated correlation length for each concentration

| **Volume fraction (v/v)** | **$\xi$ (nm)** |
|---|---|
| 0.00037 | 95 |
| 0.00072 | 68 |
| 0.00109 | 55 |
| 0.00148 | 47 |

The hydrodynamic interaction, excluded volume interaction, and electrostatic interaction all get screened beyond correlation length.[127] The comparison of correlation length with the Debye screening length as a function of concentration will thus indicate a significant conformation change of the polyelectrolyte as the volume fraction increases. The ratio of the nanoparticle size to correlation length ($2R/\xi$) is important to understand the dynamics. A majority of the studies focused on diffusion of particles within electrically neutral polymer solutions. For size ratio $2R/\xi \ll 1$, the particles experience mostly the solvent viscosity,[119] which is slightly enhanced by the presence of the monomers and dissolved counterions in the solution. Hydrodynamic interaction between the particle and the polymer is also important at these length scales.[127] At length scales larger than correlation length ($2R > \xi$), hydrodynamic interaction gets screened,[44] but the motion of the polymer can significantly contribute to the NP dynamics.[18] In our experiments we covered

the size ratio of ~0.05 to ~0.85, which provides the opportunity to study the small-size and near transition to intermediate size regime.

Rheology measurements (Figure 6.3.2) showed viscosity as a function of shear rate for all four concentrations. All samples showed strong shear thinning and a zero-shear viscosity. It was noted before that in contrast to neutral polymers, the relaxation time of semidilute polyelectrolyte solution increases as the concentration is lowered and the longest relaxation time corresponds to overlap volume fraction.[127] With the limited concentration range studied in our experiments, we were unable to verify this aspect of the theory. We, however, showed that Cox-Merz rule,[131] which states that viscosity from steady shear measurements is equal to oscillatory measurements, i.e., $\eta(\dot{\gamma}) = \eta^*(\omega)$ with $\dot{\gamma} = \omega$ is obeyed, indicating that the system is rheologically simple.

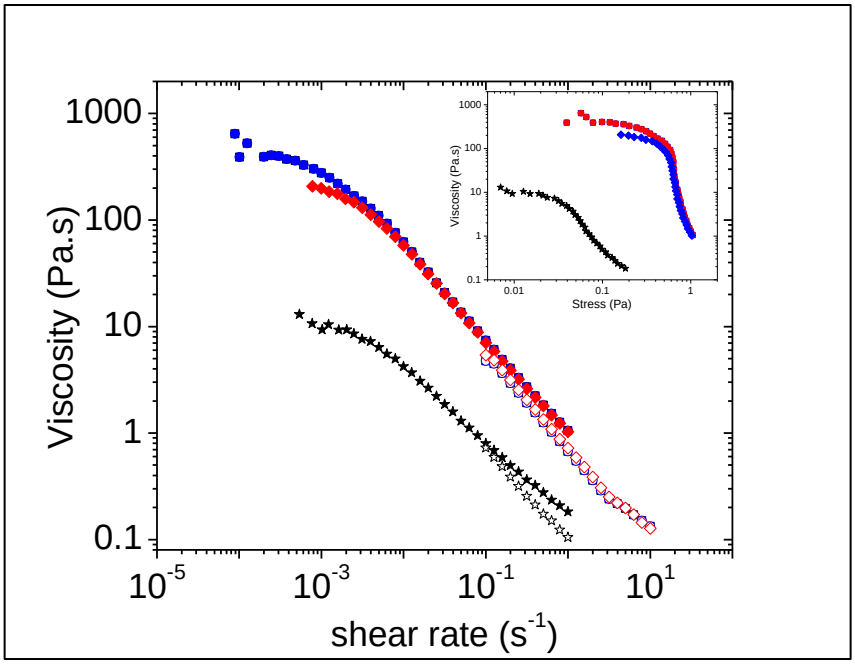


**Figure 6.3.2** Viscosity as a function of shear rate as measured by a parallel plate rheometer. Solid symbols are viscosity from steady shear measurements and open symbols are complex viscosity as measured by oscillatory shear measurements. Their overlap indicates PAA solutions are rheologically simple fluids. The results showed shear thinning in PAA solutions.

Symbols are for four different volume fractions, $\phi$: (stars, black): $0.37 \times 10^{-3}$, (diamonds, red) $0.72 \times 10^{-3}$, (circles, blue) $1.09 \times 10^{-3}$, (squares, black) $1.48 \times 10^{-3}$. Measurement temperature was 20 $^{0}$C. (Inset) Viscosity as a function of stress. The graphs showed small stress of less than 1 Pa can cause a large change of viscosity.

The mechanism of relaxation from steady shear is same as from oscillatory shear.[42] This also rules out formation of gel like network in the system.[97] Plotting the rheology data in terms of viscosity as a function of stress shows a very small amount of stress (≤1 Pa) is needed to reduce the viscosity by two orders of magnitude (Figure 6.3.2 inset). This implies formation of weak structures, which easily breaks down with the application of small amount of stress. i.e., yield stress is small and inconsequential. Viscosity of PAA solutions was measured by several researchers, including Flory *et. al*.[128] Those experiments were limited to much higher shear rate of the order of 1000 $s^{-1}$ and thus most likely probed the shear thinning regime.[132]

de Gennes had proposed that when the particle size is much smaller than the correlation length ($2R << \xi$), the particles slip easily through the polymer mesh and they only feel the solvent viscosity.[95] In the opposite limit ($2R >> \xi$), they feel the macroscopic zero shear viscosity ($\eta_0$) of the solution.[3] In the transition region, the particles feel a local viscosity which is between the solvent and bulk viscosity, and is given by a scaling function depended only upon the polymer concentration through correlation length, but independent of polymer molecular weight.[3] Many models have been put forth for this function and most of them give a stretched exponential form in terms of volume fraction. Some models are based upon the hydrodynamic interactions between particles and polymers, where the interaction is screened at the length scale of correlation length. For example, Cuckier gave a functional form: $D=D_o \exp(-\kappa R/\xi)$, where $\kappa$ is a screening constant,

and $D_o$ is the diffusion coefficient in neat solvent.[19] Some models are mostly phenomenological, such as Phillies equation: $D=D_o \exp(-\beta\phi^{\nu})$, where $\beta$ and $\nu$ are adjustable parameters.[128] A similar functional form was obtained by Dhont *et. al* by considering the effect of depletion layer around the particles.[23] In Figure 6.2.1 (inset) we showed the fitting with stretched exponential form. The exponent $\nu$ is expected to lie between 0.5 and 1. Our fitting parameters are included in table 6.2.3). We obtained $\nu$=0.54 for R=2.5 nm particles, which increases to $\nu$=0.68 for R=20 nm particles. Similar trend was observed for NP diffusion in neutral polymer (polyethylene glycol solutions)[78] But as the adjustable parameters $\beta$ and $\nu$ cannot be predicted, these fittings do not have much physical meaning[52]

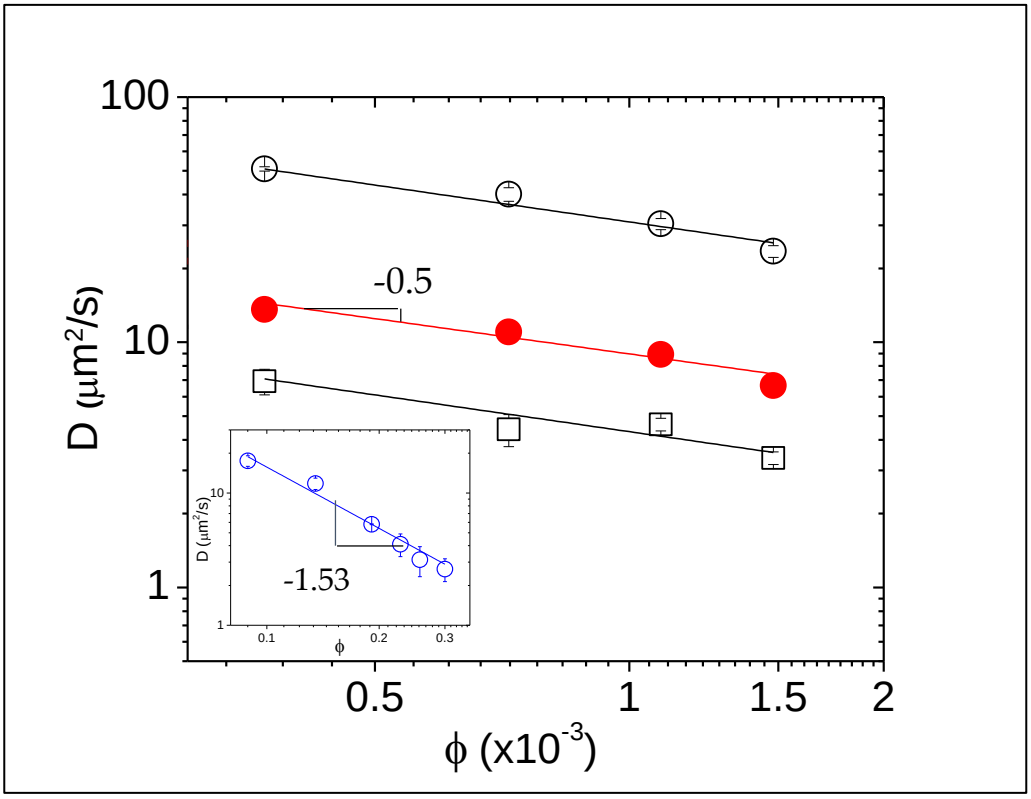


**Figure 6.3.3** D vs. $\phi$ in log-log plot showing the scaling behavior of $D \sim \phi^{-0.5}$ for all three particle sizes at four different PAA concentrations. (circles) 2.5 nm, (filled circles) 10 nm, (squares) 20 nm. All particles are in the small size range ($2R < \xi$). (Inset) Comparison is shown for nanoparticle diffusion in neutral semidilute polymer solutions, which showed a much stronger

dependence on volume fraction with scaling ponent -1.53 (Ref. [3]). These experiments are for intermediate size particles ($2R > \xi$).

In neutral polymer solutions, Rubinstein *et. al*. have identified several regimes of particle diffusion, where they considered fluctuation of the network in the semidilute concentration and the effect of entanglement in the concentrated solution.[18] The analysis is useful for situations, when the particle size is greater than the correlation length. In a previous publication, we showed that our experiments can be well described by their theory, which gives the volume fraction dependence of D that follows a power law[3] Specifically, in the semidilute solutions, where correlation length is the most important length scale, the theory predicts[18] $D(\phi)\sim\xi^2/R^3$ if $2R > \xi$.

This dependence comes from the arguing that particles experience an effective viscosity as if it is within a polymer liquid composed of chains with similar size as of the particles. As $\xi\sim\phi^{-0.76}$ for uncharged polymers in good solvent, we expect $D(\phi)\sim\phi^{-1.52}$, which matches closely with the observed exponent 1.53 (Figure 6.3.3, inset).[11] In Figure 6.3.3 we plotted D as a function of $\phi$ in log-log plot for NP diffusion in PAA solution. In all cases the data fits well with a power law with exponent -0.5. Admittedly, there is some uncertainty in determination of the correlation length, which can change the size ratio ($2R/\xi$) as given in SI8. Similarly, the calculation of overlap volume fraction assumes a random walk conformation for the chain, while the actual conformation is ore like a directed random walk. All these, however, do not affect the data presented in Figure 6.3.3.

To obtain the NP size-dependence of diffusion coefficients, we plotted in Fig. 4 (inset a), D vs. 1/R. The graphs can be well fitted with a straight line passing through the origin. Therefore, D varies inversely with particle radius as in Stokes friction for spherical particles in liquids according to $\zeta=6\pi\eta_{eff}R$, where $\eta_{eff}$ is the effective viscosity experienced by the particles. From the slopes of the graphs, we got $\eta_{eff}$ for all four particle concentrations as shown in Figure 6.3.4 (inset

b). The figure also plots zero shear viscosity ($\eta_0$) as a function of polymer concentration as obtained from rheology measurements. The increase of $\eta_0$ is about five orders of magnitude compared to pure water viscosity for the highest PAA concentration studied. This is not unexpected, because as the particle size is smaller than the correlation length, they mostly experience the solvent viscosity that is slightly enhanced due to the presence of the polymers. Figure 6.3.4 (main) summarizes the data for three particle sizes and four different concentrations. The log-log plot of diffusion coefficient vs. the size ratio ($2R/\xi$) falls on a single curve with the slope of -1. According to scaling theory,[18] the probe diffusion coefficient is inversely proportional to the particle size in the probe size range of $b < 2R < \xi$, where b is the Kuhn length. Our experiment is in agreement with this prediction. For the volume fraction dependence, the theory predicts that D is independent of $\phi$ in the concentration range of $0 < \phi < \phi^{\xi}$, where $\phi^{\xi}=\phi^*(R_g/2R_o)^x$. The exponent, $x=(3\nu-1)/\nu$, where $\nu$ is the excluded volume parameter. With $\nu=0.588$ in athermal solvent, $x=1.32$. For polyelectrolytes, using $\nu=1$, $\phi^{\xi}$ ranges from 0.128 (for 2R=5 nm) to 0.002 (for 2R=40 nm). Our experiments were, therefore, performed in the volume fraction, $\phi < \phi^{\xi}$. An argument can be made that for a weak polyelectrolyte, such as PAA with only about 7% ionization, using $\nu=1$ is not justified. Earlier experiments had obtained for a different polyelectrolyte system $\nu=0.7$-$0.8$ in salt-free solutions.[133] We calculated $\phi^{\xi}$ using $\nu=0.7$, which still showed $\phi \leq \phi^{\xi}$. We are not aware of any theory, which showed scaling behavior of small ($2R < \xi$) particles within semidilute solutions. Compared to intermediate sized particles ($2R > \xi$) in neutral polymer solutions, the volume fraction dependence is weak (Figure 6.3.3) for small particles. However, our data clearly points to a scaling relation.

Both particles and the polymers are negatively charged under the experimental conditions. We measured the zeta potential of PAA as -20.1 mV. For 20 nm gold NPs, the zeta potential was -39.3 mV. As both of them are negatively charged, we expect particles to experience a repulsive force, which prevents them to come into contact with the charged monomers. Within Debye-Hückel approximation, the surface potential can be related to the total charge of a spherical colloid.[134] For nanocolloids, it gives total charge, Q=-3.8 x $10^{-18}$ C. For polymers, ions can penetrate inside and unlike solid particles, it is soft and flexible.

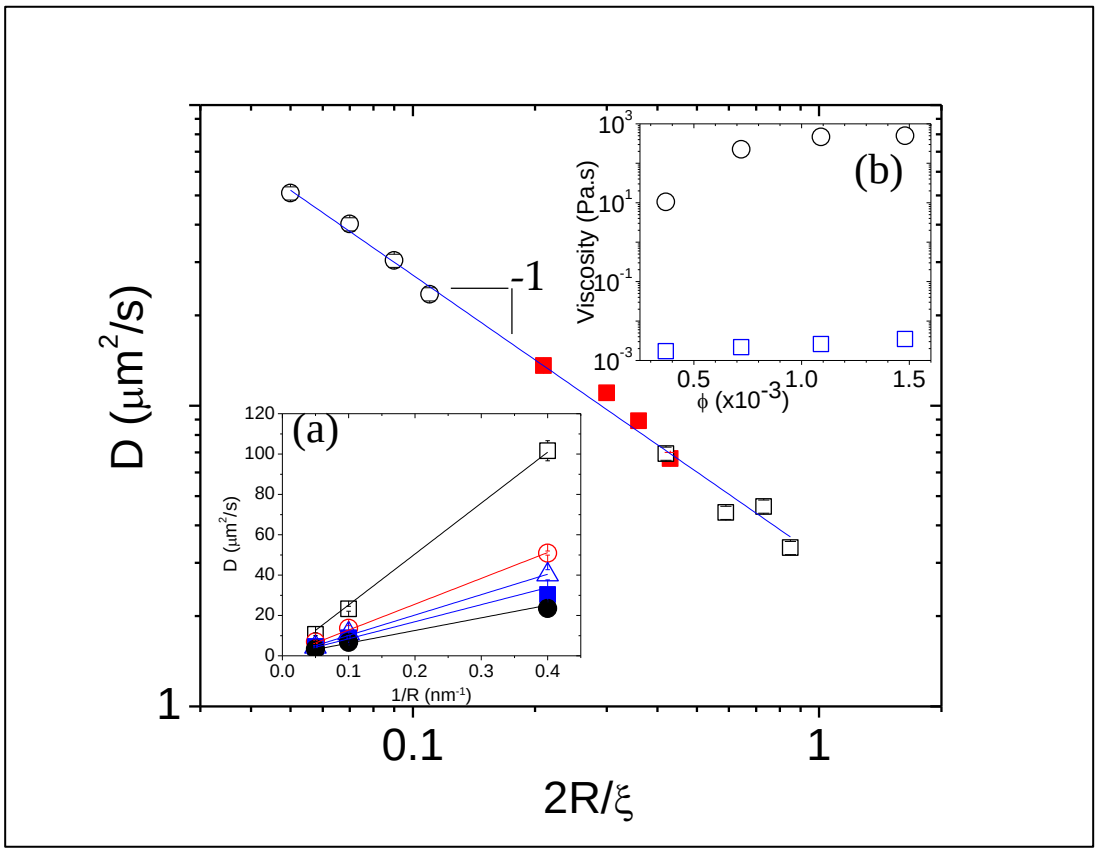


**Figure 6.3.4** Inset (a) 1/R dependence of diffusion coefficient, from which an effective viscosity ($\eta_{eff}$) can be deduced. Inset (b) Comparison of viscosity results. (Circles): Zero shear viscosity, (squares): effective viscosity ($\eta_{eff}$) derived from diffusion coefficient measurements by FCS, which is closer to the solvent viscosity as expected for small particle size. Symbols are for four

different volume fractions, $\phi$: (open squares): 0, (open circles): $0.37\times10^{-3}$, (open triangles): $0.72\times10^{-3}$, (filled squares): $1.09\times10^{-3}$, (filled circles): $1.48\times10^{-3}$. (Main figure) Diffusion coefficient vs. size ratio shows a scaling behavior with exponent -1. Data for all concentrations and particle sizes fall on a single curve. (circles): 2.5 nm, (filled squares): 10 nm, (open squares): 20 nm.

There is a large amount of studies on finding the interaction potential between two charged solid bodies under different ionic conditions. Here, we are interested in calculating the repulsive electrostatic potential energy that NPs experience with the chain size comparable to correlation length as the correlation length is the only relevant length scale in the semidilute solution.[9] A general expression for constant potential boundary condition valid for both large and small $\kappa a$ is given by Bell *et. al*,[135] $\emptyset_R = \frac{4\pi R(r-R)\varepsilon_0\varepsilon_r\varphi_0^2}{r} ln\left[1+\frac{\mathrm{R}}{(\mathrm{r}-\mathrm{R})}\exp(-\kappa a)\right]$, $r=(a+2R)$, Here $\kappa^{-1}$ is the Debye screening length and $a$ is the surface to surface separation of the particles, and $\varphi_0$ is the Zeta potential. We determined that the interaction energy is about a factor of two times the thermal energy of the particles at contact. So, we expect that there is some depletion of polymers near the particle surface, but the rubbing of the polymers against the particle surface also cannot be totally ignored. Due to relatively large size of laser focus (≈0.5 μm), FCS is not sensitive to the motion of the NPs within the depletion region. Assuming, a depletion layer of thickness $\approx R_g$, the time-scale of particle motion within the depletion region corresponds to ≈0.1 ms. Therefore, we measured the long-time diffusion, where the matrix surrounding the particles has enough time to relax. The dependence of D on $\phi^{-0.5}$ or $\xi^{1}$ is still a puzzle, even though this dependence is much weak compared to diffusion of NPs in semidilute neutral polymer solutions in the intermediate size range. It is possible that the size-ratio in the experiments was in the transition regime, so a non-negligible volume fraction dependence was observed. We expect that our results will stimulate more theoretical studies of charged NP diffusion within polyelectrolyte solution.

## 6.4 CONCLUSION

We have shown that diffusion coefficient of small nanoparticles in weakly charged semidilute polyelectrolyte solution scales inversely with particle size and depends upon volume fraction as a power-law with an exponent of -0.5. The diffusion coefficients fall on a master curve when plotted against the size ratio, $2R/\xi$ with an exponent of -1. Rheology measurements showed shear thinning and compared to zero shear rate viscosity, the particles experience much smaller local viscosity and slightly enhanced solvent viscosity. As most biopolymers are charged, our results will help to understand diffusion of charged particles or macromolecules inside biopolymer solutions.

# CHAPTER 7 : CONCLUSION

The experiments comprising my dissertation have focused on investigating the nanoparticle dynamics in polymers, polyelectrolyte solutions, and gels. Understanding the dynamical properties of nanoparticles in macromolecular solutions, such as polymer, biopolymers, and polyelectrolytes are significant for several interdisciplinary fields of studies as well as relevant for many technological applications. By using FCS, we investigated these systems studied, which gave the opportunity to understand the structural and dynamical information about them at nanometer to micrometer length scale. Important results and findings of these experiments have been reported in chapters 4 through 6.

First, we studied the diffusion of gold nanoparticles within entangled solutions and gels formed by high molecular weight poly(vinyl alcohol) (PVA) in water. We found that existing hydrodynamic and obstruction models are inadequate to describe the size dependence of the particle diffusion coefficient (D). For size ratios $x = 2R/a_e \approx 0.5-2.5$, our results suggested a functional form for $D \sim \exp(-\kappa x)$, where 2R is the particle diameter, $a_e$ is the entanglement tube diameter and $\kappa \approx 1$. This result qualitatively agrees with the scaling theory prediction of hopping motion for particles within entangled polymer solutions. For larger particles within higher volume fractions of polymer, an additional sharp slowing down of the particle motion was observed, which also exhibited an exponential dependence on the size ratio, but with a much higher value of $\kappa$. Such a rare hopping process can be explained qualitatively by recently developed force-based nonlinear Langevin theory.

Second, we measured the translation diffusion coefficient (D) of nanoparticles within dilute and semidilute solutions of a semiflexible polymer, xanthan. Our results showed that for

particle diameters (d) of 5 and 10 nm, the obstruction theory can explain the concentration dependence of D in the dilute regime. Diffusion in semidilute solutions is better explained by additionally considering the modified Darcy flow with the hydrodynamic screening length. The depletion effect is operative for larger particles (d = 30 nm) within semidilute solutions. We interpret our result with a scaling relation for the depletion layer thickness, $\delta \approx \xi^{\upsilon}$, where is the correlation length and the exponent =0.42 Our results showed that when the polymer network relaxation is much slower compared to the diffusive time-scale of particles, multiple theories needed to explain the full picture.

Third, we have studied the translational diffusion coefficient of nanoparticles in semidilute unentangled polyelectrolyte solutions. The measured diffusion coefficients (D) showed a scaling relation, $D\sim(R/\xi)^{-1}$ in the range of $2R/\xi$ between 0.05 and 0.85, where R is the particle radius and $\xi$ is the correlation length. Additionally, rheology measurements showed a zero-shear rate viscosity and shear thinning, which are typical of high molecular weight polyelectrolytes. The local viscosity experienced by the particles is slightly (a factor of 3-4) more compared to solvent viscosity and significantly smaller compared to zero shear rate viscosity.

As most of the biopolymers are charged and uncharged polymers, our results are significantly suitable for understanding the transport properties of nanoparticles and macromolecules in biopolymer environment.

## REFERENCES


1. L.-H. Cai, S. Panyukov and M. Rubinstein, Macromolecules 48 (3), 847-862 (2015).

2. N. B. Wyatt and M. W. Liberatore, J. App. Polym. Sci. **114** (6), 4076-4084 (2009).

3. I. Kohli and A. Mukhopadhyay, Macromolecules **45** (15), 6143-6149 (2012).

4. R. A. Jones, *Soft condensed matter*. (Oxford University Press, 2002).

5. P.-G. De Gennes, Reviews of modern physics **64** (3), 645 (1992).

6. M. Kleman and O. D. Laverntovich, *Soft matter physics: an introduction*. (Springer Science & Business Media, 2007).

7. M. Rubinstein and R. H. P. Colby, *Polymer Physics; Oxford University Press New York*. (2003).

8. K. Koynov and H.-J. Butt, Curr. Opin. Colloid Interface Sci **17** (6), 377-387 (2012).

9. A. V. Dobrynin and M. Rubinstein, Prog. Polym. Sci. **30** (11), 1049-1118 (2005).

10. (2016), Vol. 2019.

11. R. H. Colby, Rheologica Acta **49** (5), 425-442 (2010).

12. P. Ghosh, G. Han, M. De, C. K. Kim and V. M. Rotello, Adv. Drug Deliv. Rev. **60** (11), 1307-1315 (2008).

13. J. Pérez-Juste, I. Pastoriza-Santos, L. M. Liz-Marzán and P. Mulvaney, Coordina. Chem. Rew. **249** (17-18), 1870-1901 (2005).

14. H. Liao and J. H. Hafner, Chem. Mater. **17** (18), 4636-4641 (2005).

15. T. B. Huff, L. Tong, Y. Zhao, M. N. Hansen, J.-X. Cheng and A. Wei, Nanomedicine (2007).

16. K. K. Senanayake, E. A. Fakhrabadi, M. W. Liberatore and A. Mukhopadhyay, Macromolecules **52** (3), 787-795 (2019).

17. L. Masaro and X. X. Zhu, Prog. Polym. Sci. **24** (5), 731-775 (1999).

18. L.-H. Cai, S. Panyukov and M. Rubinstein, Macromolecules **44** (19), 7853-7863 (2011).

19. R. Cukier, Macromolecules **17**, 252–255 (1984).

20. M. Krüger and M. Rauscher, J. Chem. Phys. **131** (9), 094902 (2009).

21. G. D. Phillies, G. S. Ullmann, K. Ullmann and T. H. Lin, J. Chem. Phys. **82** (11), 5242-5246 (1985).

22. T. Odijk, Biophys. J. **79** (5), 2314-2321 (2000).

23. T.-H. Fan, J. K. Dhont and R. Tuinier, Phys. Rev. E **75** (1), 011803 (2007).

24. R. Tuinier and T.-H. Fan, Soft Matter **4** (2), 254-257 (2008).

25. A. Ogston, J. Chem. Soc. Faraday Trans **54**, 1754-1757 (1958).

26. G. Ogston Alexander, B. N. Preston, J. D. Wells and J. M. Snowden, Proc. Royal Soc. Lond **333** (1594), 297-316 (1973).

27. A. R. Altenberger and M. Tirrell, J. Chem. Phys. **80** (5), 2208-2213 (1984).

28. L. Johansson, C. Elvingson and J. E. Loefroth, Macromolecules **24** (22), 6024-6029 (1991).

29. B. Amsden, Macromolecules **32** (3), 874-879 (1999).

30. P. De Gennes, Macromolecules **9** (4), 594-598 (1976).

31. H. Fricke, Phys. Rev. **26** (5), 678 (1925).

32. F. B. Wyart and P.-G. de Gennes, Eur. Phys. J. E **1** (1), 93-97 (2000).

33. G. D. Phillies, Macromolecules **20** (3), 558-564 (1987).

34. G. D. Phillies and D. Clomenil, Macromolecules **26** (1), 167-170 (1993).

35. G. D. Phillies, J. Phys. Chem. **93** (13), 5029-5039 (1989).

36. G. D. Phillies, Macromolecules **21** (10), 3101-3106 (1988).

37. G. D. Phillies, C. Richardson, C. A. Quinlan and S. Ren, Macromolecules **26** (25), 6849-6858 (1993).

38. Y. B. Mel'nichenko, in *Hydrogen Bond Networks* (Springer, 1994), pp. 433-439.

39. V. Klepko, Y. Mel'nichenko and V. Shilov, Polym. Gels and Netw. **4** (4), 351-361 (1996).

40. J. Liu, D. Cao and L. Zhang, J. Phys. Chem. C **112** (17), 6653-6661 (2008).

41. V. Ganesan, V. Pryamitsyn, M. Surve and B. Narayanan, J. Chem. Phys. (2006).

42. G. H. Koenderink, S. Sacanna, D. G. Aarts and A. Philipse, Phys. Rev. E **69** (2), 021804 (2004).

43. Y. Cheng, R. K. Prud'Homme and J. L. Thomas, Macromolecules **35** (21), 8111-8121 (2002).

44. R. Poling-Skutvik, R. Krishnamoorti and J. C. Conrad, ACS Macro Lett. **4** (10), 1169-1173 (2015).

45. O. Krichevsky and G. Bonnet, Rep. Prog. Phys **65** (2), 251 (2002).

46. J. Ries and P. Schwille, BioEssays **34** (5), 361-368 (2012).

47. E. Haustein and P. Schwille, Annu. Rev. Biophys. Biomol. **36**, 151-169 (2007).

48. R. A. Murray, Y. Qiu, F. Chiodo, M. Marradi, S. Penadés and S. E. Moya, Small **10** (13), 2602-2610 (2014).

49. G. Brakenhoff, M. Müller and R. Ghauharali, J. Microsc. **183** (2), 140-144 (1996).

50. C. D. Chapman, K. Lee, D. Henze, D. E. Smith and R. M. Robertson-Anderson, Macromolecules **47** (3), 1181-1186 (2014).

51. S. Egorov, J. Chem. Phys. **134** (8), 084903 (2011).

52. T. Frick, W. Huang, M. Tirrell and T. Lodge, J. Polym. Sci. B **28** (13), 2629-2649 (1990).

53. H. Guo, G. Bourret, R. B. Lennox, M. Sutton, J. L. Harden and R. L. Leheny, Phys. Rev. Lett. **109** (5), 055901 (2012).

54. R. Holyst, A. Bielejewska, J. Szymański, A. Wilk, A. Patkowski, J. Gapiński, A. Żywociński, T. Kalwarczyk, E. Kalwarczyk and M. Tabaka, Phys. Chem. Chem. Phys **11** (40), 9025-9032 (2009).

55. J. T. Kalathi, U. Yamamoto, K. S. Schweizer, G. S. Grest and S. K. Kumar, Phys. Rev. Lett. **112**, 108301 (2014).

56. P. Nath, R. Mangal, F. Kohle, S. Choudhury, S. Narayanan, U. Wiesner and L. A. Archer, Langmuir **34** (1), 241-249 (2018).

57. J. C. Reina, R. Bansil and C. Koňák, Polymer **31** (6), 1038-1044 (1990).

58. S. Seiffert and W. Oppermann, Polymer **49** (19), 4115-4126 (2008).

59. U. Yamamoto and K. S. Schweizer, Macromolecules **48** (1), 152-163 (2015).

60. A. Pluen, P. A. Netti, R. K. Jain and D. A. Berk, Biophys. J. **77** (1), 542-552 (1999).

61. E. Geissler, F. Horkay and A. M. Hecht, Macromolecules **24**, 6006−6011 (1991).

62. R. G. Larson, *The Structure and Rheology of Complex Fluids*

(*Topics in Chemical Engineering*. (Oxford University Press: New York, 1999).

63. A. H. Clark and S. B. Ross-Murphy, presented at the Biopolymers, Berlin, Heidelberg, 1987 (unpublished).

64. T. Narita, A. Knaebel, J.-P. Munch and S. J. Candau, Macromolecules **34** (23), 8224-8231 (2001).

65. S. Rose, A. Marcellan, D. Hourdet, C. Creton and T. Narita, Macromolecules **46** (11), 4567-4574 (2013).

66. A. Michelman-Ribeiro, F. Horkay, R. Nossal and H. Boukari, Biomacromolecules **8** (5), 1595-1600 (2007).

67. J. M. Petit, X. X. Zhu and P. M. Macdonald, Macromolecules **29** (1), 70-76 (1996).

68. M. Tokita, T. Miyoshi, K. Takegoshi and K. Hikichi, Phys. Rev. E **53** (2), 1823-1827 (1996).

69. C. A. Grabowski and A. Mukhopadhyay, Macromolecules **41** (16), 6191-6194 (2009).

70. B. Amsden, Polymer **43** (5), 1623-1630 (2002).

71. U. Yamamoto and K. S. Schweizer, J. Chem. Phys. **135** (22), 224902 (2011).

72. C. A. Grabowski and A. Mukhopadhyay, Macromolecules **47** (20), 7238-7242 (2014).

73. Z. E. Dell and K. S. Schweizer, Macromolecules **47** (1), 405-414 (2014).

74. D. G. H. Phillies, Adv. Chem. Phys. Rev. Lett. **161**, 277−358 (2016).

75. Z. Bu and P. S. Russo, Macromolecules **27** (5), 1187-1194 (1994).

76. H.-W. Gao, R.-J. Yang, J.-Y. He and L. Yang, J. Appl. Polym. Sci. **116** (3), 1459-1466 (2009).

77. A. Michelman-Ribeiro, H. Boukari, R. Nossal and F. Horkay, Macromolecules **37** (26), 10212-10214 (2004).

78. S. Alam and A. Mukhopadhyay, J. Phys. Chem. C **118** (47), 27459-27464 (2014).

79. M. Weiss, H. Hashimoto and T. Nilsson, Biophys. J. **84** (6), 4043-4052 (2003).

80. N. Fatin-Rouge, K. Starchev and J. Buffle, Biophys. J. **86** (5), 2710-2719 (2004).

81. P. A. Netz and T. Dorfmüller, J. Chem. Phys. **103** (20), 9074-9082 (1995).

82. G. A. Hurst, M. Bella and C. G. Salzmann, J. Chem. Educ. **92** (5), 940-945 (2015).

83. J. F. Vega, A. Santamaría, A. Muñoz-Escalona and P. Lafuente, Macromolecules **31** (11), 3639-3647 (1998).

84. M. Bercea, S. Morariu and D. Rusu, Soft Matter **9** (4), 1244-1253 (2013).

85. M. Doi and S. F. Edwards, *The Theory of Polymer Dynamics; Oxford*. (1988).

86. C.-S. Wu, *Handbook of Size Exclusion Chromatography and Related Techniques: Revised and Expanded*. (CRC Press, 2003).

87. H. Li, W. Zhang, X. Zhang, J. Shen, B. Liu, C. Gao and G. Zou, Macromol. Rapid Commun **19** (12), 609-611 (1998).

88. D. Langevin and F. Rondelez, Polymer **19** (8), 875-882 (1978).

89. J. C. Dyre, Rev. Mod. Phys. **78** (3), 953-972 (2006).

90. G. Modesti, B. Zimmermann, M. Börsch, A. Herrmann and K. Saalwächter, Macromolecules **42** (13), 4681-4689 (2009).

91. K. K. Senanayake and A. Mukhopadhyay, Langmuir (2019).

92. F. Babayekhorasani, D. E. Dunstan, R. Krishnamoorti and J. C. Conrad, Soft Matter **12** (40), 8407-8416 (2016).

93. C.-C. Lin, E. Parrish and R. J. Composto, Macromolecules **49** (16), 5755-5772 (2016).

94. Y. Luo and Q. Wang, Int. J. Bio. Macromol. **64**, 353-367 (2014).

95. *Xanthan gum Book*. (CP Kelco US., Inc.,, 2001).

96. G. Cuvelier and B. Launay, Carbohydr. Polym. **6** (5), 321-333 (1986).

97. M. Milas, M. Rinaudo, M. Knipper and J. L. Schuppiser, Macromolecules **23** (9), 2506-2511 (1990).

98. T. Moschakis, B. S. Murray and E. Dickinson, Langmuir **22** (10), 4710-4719 (2006).

99. V. Ganesan, L. Khounlavong and V. Pryamitsyn, Phys. Rev. E **78** (5), 051804 (2008).

100. A. V. Dobrynin, R. H. Colby and M. Rubinstein, Macromolecules **28** (6), 1859-1871 (1995).

101. K. Kang, J. Gapinski, M. Lettinga, J. Buitenhuis, G. Meier, M. Ratajczyk, J. K. Dhont and A. Patkowski, J. Chem. Phys. **122** (4), 044905 (2005).

102. T. Shimada, M. Doi and K. Okano, J. Chem. Phys. **88** (4), 2815-2821 (1988).

103. P.-G. De Gennes and P.-G. Gennes, *Scaling concepts in polymer physics*. (Cornell university press, 1979).

104. T. K. Piskorz and A. Ochab-Marcinek, J. Phys. Chem. B **118** (18), 4906-4912 (2014).

105. C. Xue, X. Zheng, K. Chen, Y. Tian and G. Hu, J. Phys. Chem. Lett. **7** (3), 514-519 (2016).

106. D. W. de Kort, W. H. Rombouts, F. J. Hoeben, H. M. Janssen, H. Van As and J. P. van Duynhoven, Macromolecules **48** (20), 7585-7591 (2015).

107. J. D. Jones and K. Luby-Phelps, Biophys. J. **71** (5), 2742-2750 (1996).

108. B. Amsden, Polym. Gels Netw **6** (1), 13-43 (1998).

109. R. Tuinier, J. Dhont and T.-H. Fan, EPL **75** (6), 929 (2006).

110. K. Kang, A. Wilk, J. Buitenhuis, A. Patkowski and J. K. Dhont, J. Chem. Phys. **124** (4), 044907 (2006).

111. A. R. Altenberger, M. Tirrell and J. S. Dahler, J. Chem. Phys. **84** (9), 5122-5130 (1986).

112. H. Brinkman, Flow Turbul. Combust **1** (1), 27 (1949).

113. A. Jamieson, J. Southwick and J. Blackwell, J. Polym. Sci. B **20** (9), 1513-1524 (1982).

114. P. Ahlrichs, R. Everaers and B. Dünweg, Phys. Rev. E **64** (4), 040501 (2001).

115. D. Richter, K. Binder, B. Ewen and B. Stühn, J. Phys. Chem. **88** (26), 6618-6633 (1984).

116. P. Wiltzius, H. R. Haller, D. S. Cannell and D. W. Schaefer, Phys. Rev. Lett. **53** (8), 834 (1984).

117. K. Zhang, M. Briggs, R. Gammon, J. Sengers and J. F. Douglas, J. Chem. Phys. **111** (5), 2270-2282 (1999).

118. Y. Dong, X. Feng, N. Zhao and Z. Hou, J. Chem. Phys. **143** (2), 024903 (2015).

119. K. Sozanski, A. Wisniewska, T. Kalwarczyk, A. Sznajder and R. Holyst, PloS one **11** (8), e0161409 (2016).

120. A. Tuteja, M. E. Mackay, S. Narayanan, S. Asokan and M. S. Wong, Nano Lett. **7** (5), 1276-1281 (2007).

121. M. Muthukumar, J. Chem. Phys. **107** (7), 2619-2635 (1997).

122. A. Takahashi, N. Kato and M. Nagasawa, J. Phys. Chem. **74** (4), 944-946 (1970).

123. A. Yethiraj and C.-Y. Shew, Phys. Rev. Lett. **77** (18), 3937 (1996).

124. C. Holm, J. Joanny, K. Kremer, R. Netz, P. Reineker, C. Seidel, T. A. Vilgis and R. Winkler, in *Polyelectrolytes with defined molecular architecture II* (Adv Polym Sci 2004), pp. 67-111.

125. G. Migliorini, V. G. Rostiashvili and T. A. Vilgis, Eur Phys J E **4** (4), 475-487 (2001).

126. T. Odijk, Macromolecules **12** (4), 688-693 (1979).

127. M. Rubinstein, R. H. Colby and A. V. Dobrynin, Phys. Rev. Lett. **73** (20), 2776 (1994).

128. T. H. Lin and G. D. Phillies, J. Phys. Chem. **86** (20), 4073-4077 (1982).

129. J. Choi and M. F. Rubner, Macromolecules **38** (1), 116-124 (2005).

130. D. Reith, B. Müller, F. Müller-Plathe and S. Wiegand, J. Chem. Phys. **116** (20), 9100-9106 (2002).

131. W. Cox and E. Merz, J. Polym. Sci. **28** (118), 619-622 (1958).

132. P. J. Flory and J. E. Osterheld, J. Phys. Chem. **58** (8), 653-661 (1954).

133. M. Beer, M. Schmidt and M. Muthukumar, Macromolecules **30** (26), 8375-8385 (1997).

134. Z. Wang, H. Kriegs, J. Buitenhuis, J. K. Dhont and S. Wiegand, Soft Matter **9** (36), 8697-8704 (2013).

135. S. L. G. Bell, L. McCartney, , Adv. Colloid Interface Sci. **33**, 335 (1970).

## ABSTRACT


**DYNAMICS OF GOLD NANOPARTICLES IN POLYMER, BIOPOLYMER SOLUTIONS AND GELS**

by

**KAVINDYA K. SENANAYAKE**

**August 2019**

**Advisor:** Dr. Ashis Mukhopadhyay

**Major:** Physics

**Degree:** Doctor of Philosophy

Soft matter is a subfield of condensed matter physics including systems, such as polymers, colloidal dispersions, liquid crystals, surfactants. Understanding their interaction and dynamics is essential for many interdisciplinary fields of study as well as important for technological advancements. We used gold nanoparticles (AuNPs) to investigate the length-scale dependent dynamics in dilute, semidilute, entangled polymer solutions and gels. Two-photon fluctuation correlation spectroscopy (FCS) technique was used to investigate the translation diffusion coefficient of AuNPs. For polymer solutions, we found that existing hydrodynamic and obstruction models are inadequate to describe the size dependence of the particle diffusion coefficient. Within entangled Poly (vinyl) alcohol solutions, our results qualitatively agreed with the scaling theory prediction of 'hopping motion'. In semidilute xanthan solutions, we observed that polymer network relaxation is much slower compared to the diffusive time-scale of particles, and AuNP diffusion could not be explained by a single theory. The system was better explained by additionally considering the modified Darcy flow with the hydrodynamic screening. In the

semidilute polyelectrolyte solution, measured diffusion coefficients (D) showed a scaling relation, $D \sim (R/\xi)^{-1}$ in the range of $2R/\xi$ between 0.05 and 0.85, where R is the particle radius and $\xi$ is the correlation length.

## AUTOBIOGRAPHICAL STATEMENT

## KAVINDYA K. SENANAYAKE

**Education:**

- 2014-2019, Wayne State University, Detroit, MI: Ph.D. in Condensed Matter Physics
- 2014-2018, Wayne State University, Detroit, MI: MSc in Physics
- 2009-2014, University of Peradaniya, Peradeniya, Sri Lanka: BSc in Physics

**Publications:**

1. **Kavindya K. Senanayake**, E. A. Fakhrabadi, M. W. Liberatore, A. Mukhopadhyay, *et al.* Diffusion of Nanoparticles in Entangled Poly(vinyl alcohol) Solutions and Gels. Macromolecules. 2019 Jan 11; 10.1021/acs.macromol.8b01917

2. **Kavindya K. Senanayake** and A. Mukhopadhyay, *et al.* Nanoparticle Diffusion within Dilute and Semidilute Xanthan Solutions. May 2019; Langmuir 10.1021/acs.langmuir.9b01029 (2019)

3. Kavindya Senanayake, N. Shokeen, E. A. Fakhrabadi, M. W. Liberatore, and A. Mukhopadhyay et al. Diffusion of Nanoparticles within a semidilute polyelectrolyte solution", under review, softmatte, ID: SM-ART-07-2019-001313 (2019).

**Presentations:**

1. **Kavindya K. Senanayake**, Ashis Mukhopadhyay; "Study of interaction of Bovine Serum Albumin with gold nanoparticles", APS March meeting 2019". (March 2019), Oral presentation.

2. **Kavindya K. Senanayake**, Ashis Mukhopadhyay; "Diffusion of Nanoparticles in Entangled Poly(vinyl alcohol) Solutions and Gels", APS March meeting". (March 2019).

3. **Kavindya K. Senanayake**, and Ashis Mukhopadhyay; "Diffusion of charged gold nanoparticles in Poly(acrylic acid) solutions", Condensed matter physics seminar, Department of physics, Wayne State University, Detroit. (January 2018).

4. **Kavindya K. Senanayake**, and X. Q. Chu; "Role of antifreeze glycoproteins (AFGP) in preventing Ice-formation", "Summer School on Methods and Applications of Neutron Spectroscopy" National Institute of Standards and Technology (NIST) Center for Neutron Research, (June 2015).